NTNU
Norwegian University of
Science and Technology

Evaluation of Industry Practice for Buckling Analysis in Well Design

Trine Remmen

Preface

This thesis was carried out during the spring semester of 2018, and completes my Master of Science in Petroleum Engineering with a specialization in Drilling Technology. This thesis is carried out at the Norwegian University of Science and Technology at the Department of Geoscience and Petroleum.

The thesis was developed with background from the fall project "Analysis of the Industry Standard and Practice for Casing and Tubing Design". The fall project was written together with Eilen Bauge and Kristian Wilhelmsen.

Buckling is a relevant subject within casing and tubing design, but the available models are challenging to present. This thesis includes a comprehensive literature study and two buckling models for installation and operational cycles respectively.

Trondheim, 2018-06-11

Trine Remmen

Acknowledgement

First of all, I would like to thank my supervisor Bjørn Astor Brechan for his guidance and good discussions. The technical support and feedback provided during this thesis are gratefully appreciated. Your constructive feedback and enthusiasm have given me energy throughout this spring semester.

I would also like to pay my gratitude to Bernt Sigve Aadnoy. Thank you for the good discussions and for always being available when I needed it. Your motivation for the subject has been truly inspiring.

I would also like to thank Sigbjørn Sangesland. Thank you for providing me with supporting material and for guiding me towards the right path in the beginning. Your knowledge of the buckling subject has been motivating.

My project partners from fall 2017, Eilen Bauge and Kristian Wilhelmsen, also deserves my gratitude. I have learned so much from our good discussions, and the comprehensive understanding I got from the fall project gave me a head start on the master thesis.

Finally, I want to thank my fellow students for all the good times through these years at NTNU. For the friendships, for supporting each other through the tough subjects, and for all the laughs. These years would never have been the same without you.

T.R.

Summary

The development of horizontal drilling technology have enabled the production of oil and gas from thin layers. With the development of shallow, horizontal subsea wells, new challenges arises. The occurrence of compressive forces affects horizontal reach and tubing movement. These challenges can be seen in direct relation to buckling. The consequences of buckling can be costly work-overs and even loss of integrity.

The integrity of a well construction is essential, and design factors are included in the stress analysis to ensure safe and profitable hydrocarbon recovery. The highest design factor is used for axial loads, as they are subject to the highest uncertainty. Exceeding the buckling limit can introduce local bending forces. The tubing will permanently deform, if yield strength is exceeded by triaxial stress due to buckling. Deformation of the tubing can lead to loss of drift, or even loss of integrity and discharge to the environment as a worst case scenario. A better understanding of buckling can reduce the risk of severe axial failures.

Compressive forces are introduced early in the completion process. When the tubing is lowered, the compressive forces are mainly induced by friction. The occurrence of compression and geometrical imperfections can buckle the string, and affect the limit of reach in horizontal wells. A model is therefore developed to predict buckling during tubing installation. The model is applied on a generic well design for a shallow subsea field to investigate the tubing integrity for producers and injectors.

Post installation, the tubing is anchored between the wellhead and the production packer. Cyclic temperature and pressure loads induces tubing movement. Initiation of buckling causes additional tubing movement. A second model is developed to evaluate load cases and ensure that buckling does not affect the well integrity.

Literature review show that preexisting industry standard buckling models were developed at a time without widespread use of digital calculation aids. Consequently, the models are developed by simplifying assumptions enabling use of only hand calculations. These models have further been implemented in industry software, and are still in use today, despite these simplifying assumptions.

The digital aids are rapidly developing, and this opens the possibility of a new buckling model with no simplifying assumptions. When the simulations matches a real scenario, the model becomes more reliable. This thesis is the first step of achieving this long-term objective.

Sammendrag

Brønnteknologiske utviklinger har gjort det mulig å bore horisontalt for å produsere olje og gass fra tynne lag. Med utviklingen av grunne, horisontale undervannsfelt kommer nye utfordringer. Kompresjonskrefter påvirker både horisontal rekkevidde og rørbevegelse. Dette kan sees i direkte relasjon til bøying elle bukling av rør. Konsekvenser av bukling kan være kostbar brønnservice og tap av brønnintegritet.

Brønnintegritet er essensielt, og sikkerhetsfaktorer er inkludert i analysen for å sikre en trygg og lønnsom utvinning av hydrokarboner. Den høyeste sikkerhetsfaktoren brukes på aksielle laster, da det er knyttet høy usikkerhet til disse. Bøyning eller bukling er en konsekvens av kompresjon og geometriske ufullkommenheter. Hvis bukling oppstår, vil det skape lokale bøyespenninger. Produksjonsrøret deformeres hvis spenningene øker utover styrken på materialet. Permanent deformering av røret kan føre til at man ikke kommer gjennom med intervensjonsverktøy. Deformasjon kan også gå på bekostning av brønnintegritet, samt i verste fall føre til miljøutslipp. En økt forståelse av bukling kan redusere risikoen for alvorlig aksiell svikt.

Kompresjonskrefter introduseres tidlig i kompletteringsprosessen. Når produksjonsrøret senkes ned i brønnen er kompresjonskreftene i hovedsak skapt av friksjon. Forekomsten av høy kompresjon og geometriske ufullkommenheter kan føre til at røret bukles, og dette påvirker rekkevidden, spesielt i horisontale brønner. En modell er utviklet for å forutse når og hvor bukling skjer under installasjon av produksjonsrøret. Modellen er anvendt på et generisk brønndesign for et grunt undervannsfelt for å undersøke rørintegritet for produsenter og injektorer.

Etter installasjon vil produksjonsrøret være fastspent mellom brønnhodet og produksjonspakningen. Syklisk temperatur og trykk vil skape bevegelse i røret. Bukling vil føre til ekstra bevegelse. Ytterligere en modell er utviklet for å evaluere laster, og for å sørge for at bukling av produksjonsrøret ikke går på bekostning av brønnintegriteten.

En gjennomgang av tilgjengelig litteratur viser at industriens buklingmodell ble utviklet på en tid uten utbredt bruk av digitale hjelpemidler. Følgelig har modellene blitt utviklet på grunnlag av forenklende antagelser for å kunne gjøre beregningene for hånd. Disse modellene har videre blitt implementert i industriens programvare, og de er fortsatt i bruk, på tross av endringer i forutsetningene.

Digitale verktøy utvikles stadig, og dette åpner muligheten for å lage en ny buklingmodell uten forenklede antagelser. Når simuleringene ligner et realistisk scenario, blir modellen mer pålitelig. Denne avhandlingen er det første steget mot å oppnå dette langsiktige målet.

Contents

List of Figures

List of Tables

Nomenclature

α	=	Well inclination
β	=	Coefficient that determines buckling regime
$\Delta\rho_i$	=	Change in density inside tubing
$\Delta\rho_o$	=	Change in density outside tubing
ΔL	=	Section length in Adnoy's model
ΔL	=	Total length change by Lubinski
ΔL_1	=	Length change due to Hooke's law
ΔL_2	=	Length change due to helical buckling
ΔL_3	=	Length change due to radial pressure
ΔL_4	=	Length change due to thermal effects
ΔP_i	=	Change in inner pressure at packer level
Δp_i	=	Change in inner pressure at surface
ΔP_o	=	Change in outer pressure at packer level
Δp_o	=	Change in outer pressure at surface
ΔT	=	Change in temperature
δ	=	Drop of pressure per unit length due to flow
λ	=	Helix angle
λ'	=	Helix angle as a function of length
λ'_{max}	=	Maximum helix angle as a function of length for sinusoidal buckling
μ	=	Friction factor
μ	=	Poisson's ratio
ϕ	=	Azimuth
ρ_i	=	Fluid density inside tubing
ρ_o	=	Fluid density outside tubing
θ	=	Dog leg angle
a_ϕ	=	Azimuth build rate
A_i	=	Inner area
a_i	=	Inclination build rate
A_o	=	Outer area
A_p	=	Packer bore area
A_s	=	Cross-sectional area
C	=	Curvature of the helix
C_t	=	Coefficient of thermal expansion
E	=	Young's modulus
E_f	=	Final energy in the system
E_i	=	Initial energy in the system

F_a	=	True axial force
F_f	=	Fictitious force
F_{1nbc}	=	Normal contact force including curvature effects
$F_{buoyancy}$	=	Hydrostatic pressure acting on the bottom of the tubing
F_{cr}	=	Critical buckling limit
$F_{dynamic}$	=	Dynamic hook load
F_{eff}	=	Effective axial force
F_{icr}	=	Improved critical buckling force
F_{static}	=	Static hook load
F_{weight}	=	Weight of tubing
h	=	Height of well section
H_1	=	Vertical line subscript 1, for curved section length calculations
H_2	=	Vertical line subscript 2, for curved section length calculations
I	=	Moment of inertia
L	=	Tubing length
L_h	=	Length of the helix measured along its axis
L_p	=	Tubing length
n	=	Euler's end conditions
P	=	Pitch
P_i	=	Inner pressure at packer level
p_i	=	Inner pressure
P_o	=	Outer pressure at packer level
p_o	=	Outer pressure
$p_{i,TVD}$	=	Inner pressure at bottom of tubing
$p_{i,TVD}$	=	Outer pressure at bottom of tubing
R	=	Radius of curvature, for curved section length calculations
R	=	Ratio, OD/ID, of tubing
r_c	=	Radial clearance
U_b	=	Strain energy of bending
U_c	=	Strain energy of compression
U_f	=	Potential energy from a subjected force
U_{strain}	=	Strain energy
V	=	Volume
w	=	Weight defined by Lubinski
w_b	=	Buoyed weight
w_i	=	Weight of fluid inside tubing
w_l	=	Weight per unit length
w_o	=	Weight of fluid outside tubing
z	=	Vertical depth
z_{TVD}	=	Vertical depth at bottom of tubing

Abbreviations

CT Coiled Tubing

EDM Engineers Data Model

KOP Kick-Off Point

MD Measured Depth

NSP Neutral Stability Point

PBR Polished Bore Receptacle

SIWHP Shut-in Wellhead Pressure

TD Total Depth

TVD Total Vertical Depth

WDP Well Design Pressure

Chapter 1

Introduction

The development of horizontal drilling technology have enabled the production of oil and gas from thin layers. This technology has been practiced on the Norwegian continental shelf since the 1990's and especially the Troll field. Some recent fields are shallow and deviated, which means that the drill pipe during drilling and casing/tubing during installation will be in compression. Knowing the operational limits for buckling to understand where failure may occur and to know the limit of reach is important in life cycle integrity well design.

Frictional drag is a concern when the tubing is lowered in a long-reach horizontal well. If these drag forces becomes high, buckling can be initiated, and in the worst case cause lock-up before reaching the desired depth. Consequences of not reaching the desired depths can be lack of zone isolation. It is evident that the completion phases are very time-consuming amounting to nearly half of the total well construction time (Aadnoy, 2010, 241). An evaluation of the completion strategy can therefore be valuable for the company.

Forces during production is another aspect. Cycles of temperature and pressure on a tubing in compression may cause buckling post installation. Buckling length changes and the packer force must be calculated to evaluate where the neutral stability point is located. The packer force can both induce or reduce compressive stresses, thus it can be able to buckle a tubing more severely or even unbuckle it. It is important to predict buckling shape and severity for future intervention. As the effective inner area is reduced in a buckled tubing, tool passage can be a problem. Deformation of tubing can lead to loss of integrity and discharge to the environment in a worst case scenario.

Lack of knowledge have caused costly failures in the past (Lubinski et al., 1962, 659). It is therefore important to understand the theoretical foundation behind design software programs used in the industry. A better understanding can mitigate potential errors and wrong simulations.

A frictional drag model have been proposed by Aadnoy et al. (2010). These equations are applicable for running completion in a well with both inclination and azimuth. The

drag forces are calculated by dividing the well into a 3D well path, i.e. ideal sections. A limitation of the model is that it is derived from a soft-string model, i.e. bending stresses are neglected. The predicted contact force will therefore be underestimated. Another limitation is that the well is divided into large sections, and the uncertainty arises when a point of interest lies within a section. A consequence is that dog leg variations within each section are not accounted for. Dog leg variations will give a higher frictional force than expected.

Lock-up in coiled tubing is a topic frequently discussed. Lock-up occurs when the applied surface force exceeds the tubings capacity to move further into the horizontal well. This analogy is used to explain how compressive forces adds up when a long-reach horizontal well is developed.

1.1   Industry

WellCat is part of the landmark EDM, and it is the most used soft ware tool for advanced tubing and casing design in the industry. The fall project (Remmen et al., 2017) revolved around the industry standards and practices for casing and tubing design. Load cases were evaluated in detail, and the software WellCat was used to analyze the importance of all input parameters for the casing design of a subsea well in the Norwegian sector.

The remaining challenge is to clarify the theoretical foundation behind the buckling calculations performed in WellCat. The WellCat manual (Halliburton, 2001) states that Bellarby (2009) and Mitchell et al. (1999) are the sources for buckling analysis.

The main limitation of full understanding of how the software performs design, is the lack of technical details in the engineering performed. It is therefore challenging to understand the theoretical basis behind the calculations.

1.2   Literature

A comprehensive literature study on buckling was conducted, and the most acknowledgedged theory and methods are presented.

Lubinski et al. (1962) provided a model for helical buckling for tubing sealed in packers. The model is mainly developed for a vertical well with no friction. Mitchell et al. (1999) developed a theoretical understanding of the previous mentioned model, and developed equations for application of the model in deviated wells. It is challenging to understand and reproduce the Lubinski et al. (1962) model. Some of the assumptions taken does not apply for modern wells, and modifications needs to be done.

The main limitations of the theoretical foundations is the basic assumptions. Uncertainty arises when the assumptions does not match the realistic scenario.

Axial forces are subject to the greatest uncertainty. Since they are dependent on pressure, temperature, bending and drag. The consequences associated with axial failure can be serious, whether it is a tensile or compressive failure. As axial failure could cause considerable damage on people and surface equipment, a relatively high design factor is used (Bellarby, 2009, 521-522).

1.3 Objective and Approach

The aim of this thesis is to investigate and reduce some of the uncertainties by developing a buckling model combining installation of the completion and operational cycles with critical buckling limits. The initial compression and buckling present in the string after installation will also be useful for simulation of the operational cycles. A remaining challenge will then be to create a visual representation of buckling, when and where it occurs. Numerical aids can improve axial load analysis by dividing the tubing into indefinite small cross-sections.

This thesis can contribute to better understanding of when and where buckling occurs, and the importance of a thorough investigation of this matter throughout the entire lifetime of a completion. By a better understanding of the load limits, costly work-overs and time consuming interventions can be avoided. Numerical aids improves the drag analysis by dividing the tubing into indefinite small cross-sections.

Two models were developed in MatLab. The first model is a representation of a scenario where a tubing is installed in a shallow, horizontal well. Buckling induced by drag forces are presented by implementing buckling limits. Lock-up scenarios are then predicted. The second model is an implementation of the buckling analysis used in WellCat. Both models are generalized to apply for both vertical and deviated wells, and results for a shallow, horizontal well are presented.
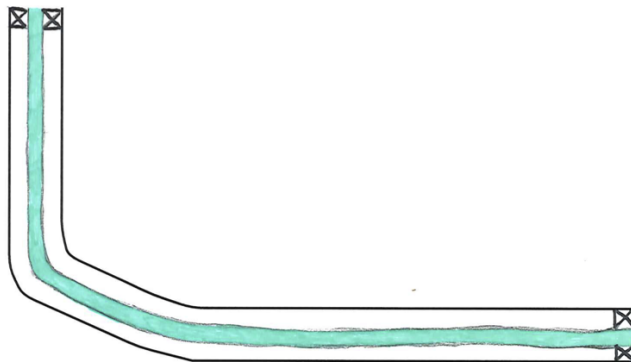
Figure 1.1: Sketch of well profile used in buckling analylsis

Chapter 2

State of the Art

When a structure is subjected to a compressive force, it can be forced to take another shape than it originally holds. It is said that the structure has buckled if it suddenly deflects sideways. Buckling is a structural instability that can lead to failure, and it is a subject of discussion in several areas of engineering. In petroleum engineering, buckling is a relevant subject within casing and tubing design, drilling, coiled tubing and snubbing.

2.1 Critical Buckling Limit

Imagine that a tubing is subjected to an increasing compressive force. The critical buckling limit is found at the instant moment when the tubing snaps into a buckled shape. Buckling can be categorized in sinusoidal buckling and helical buckling, thus there are one limit for sinusoidal buckling and another for helical buckling. The critical buckling limit has been derived by a range of authors:

2.1.1 Vertical well

The first critical buckling limit for a weightless rod in a vertical section was derived by Euler in 1757. (Hearn, 1997).

Lubinski et al. (1950) and Wu et al. (1995) included weight in the derivation of the critical sinusoidal and helical buckling limit, respectively, in a vertical well.

2.1.2 Deviated well

Dawson et al. (1984) considered the effect of well deviation on the critical buckling limit for sinusoidal buckling. This limit is well established, and still used in the industry, even for helical buckling (Halliburton, 2001) (Horgen, 2010).

Mitchell et al. (1999) found that a helical buckling limit could be derived by multiplying the limit developed by Dawson et al. (1984) with a constant. The region between these limits was defined as a transition where either sinusoidal or helical buckling can occur.

Dawson et al. (1984) neglected well curvature in the derivation of the critical buckling limit.

He et al. (1995) showed that the established equation by Dawson et al. (1984) was conservative in curved sections. It was therefore developed a new critical buckling limit, including the curvature effects. Their model indicated that curvature stabilizes the pipe, hence resulting in a higher critical buckling limit than previously expected.

Aasen et al. (2002) did a thorough investigation of the available models, to find that many buckling limits only varied by the coefficients.

2.2   Buckling During Operations

Lubinski et al. (1962) published a well known model regarding helical buckling of a tubing in a vertical well. The main focus of Lubinski et al. (1962) was to calculate the effective axial force by investigating length changes due to pressure and temperature changes. The slack-off force from the installation phase was also included in the analysis. A triaxial analysis was performed to investigate permanent deformation due to the increased bending stress, a consequence known as *permanent corkscrewing.*

When Lubinski et al. (1962) presented the model for helical buckling in a vertical well, Mitchell et al. (1988) investigated the foundation of the model. The solution was put in a more theoretical context to make the model applicable for deviated wells.

The model presented by both Lubinski et al. (1962) and Mitchell et al. (1988) was based on the assumption that the pipe instantly took a helical shape when reaching the critical buckling limit. It was however recognized by Mitchell et al. (1997) that sinusoidal buckling could occur before helical buckling, hence a new theoretical model was developed.

A fourth order differential equation for the helix angle was derived by Mitchell et al. (1997). The solution of the differential equation was found to be very useful when predicting the effect of well deviation on buckling shape, tubing length change, contact force and bending stress.

Mitchell et al. (1999) presented a more practical applicable model based on the equations in Mitchell et al. (1997). Correlations were developed to match the complex models. The correlations was compared to the results (Lubinski et al., 1962) presented, and it was shown that the buckling length change depended on the buckling shape. A convincing discovery was that the result presented by Lubinski et al. (1962) predicted an increase in tubing length for an increase in deviation angle, while Mitchell et al. (1999) predicted the opposite. Lateral gravity forces is proven to prevent buckling, and it was

concluded that Mitchell et al. (1999) predicted a more realistic scenario. Another finding was that (Lubinski et al., 1962) over predicted tubing movement. For a fixed tubing, the axial loads would by this method be underestimated, and this could lead to a non-conservative design. The model presented by (Mitchell et al., 1999) was proven to be better when designing a tubing in a deviated well.

Mitchell et al. (1999) gave a better understanding of the consequences of helical buckling versus sinusoidal buckling in a deviated well. The bending stress, buckling strain and length change is depending on whether the buckling is sinusoidal or helical shaped. The contact force is the last main factor affected by the buckling shape. When the buckling shape changes from sinusoidal to helical, the contact force increases significantly.

2.3 Buckling During Installation

The contact force is an important part of the torque and drag analysis. A coiled tubing operation can be strongly affected by friction. The friction forces will add up to the compression forces, and when the tubing snaps in to a helical shape, the contact force will increase even more. At one certain point, this can cause lock-up, and we will not be able to push the coiled tubing further into the well by applying a higher force on the surface. This analogy can also be used for tubing installation, as the tubing diameter is significantly small compared to the tubing length.

Aadnoy et al. (2010) presented a three-dimensional friction model for the drag analysis. This model includes contact force, dogleg angle and the capstan effect. The string was considered to be either tension- or weight-dominated, depending on whether the wellbore section is straight or curved. This assumption simplified the drag equations significantly, and a set of only two equations could be used to calculate drag in a wellbore with both inclination and azimuth. One can further use this drag force to calculate the hook load on surface and the axial load throughout the entire completion.

2.4   Timeline of Previous Work

Figure 2.1 presents a timeline of present state of the art.
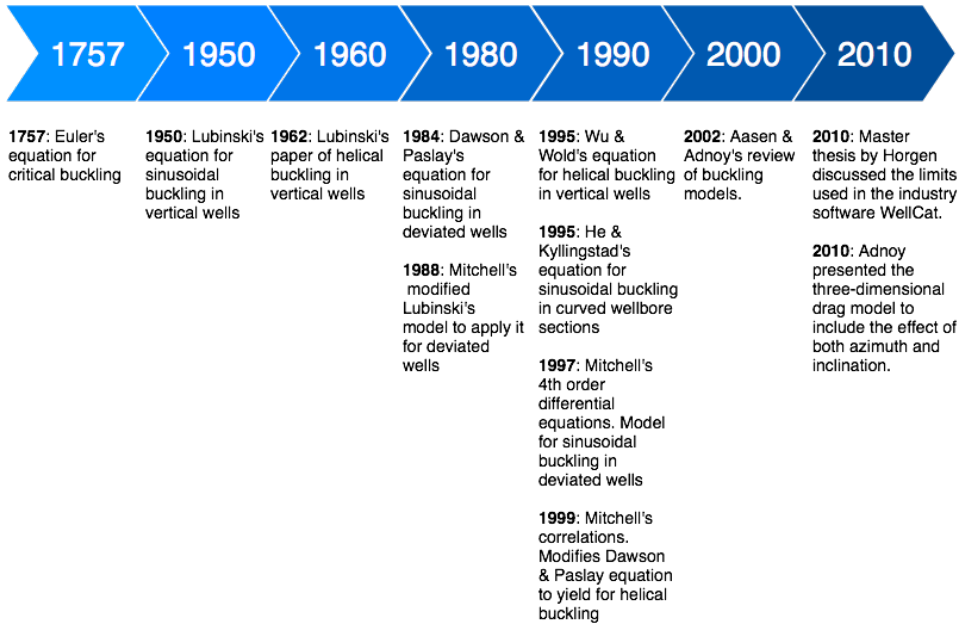
Figure 2.1: Timeline of previous work presented in state of the art

Chapter 3

Literature Study

A study of critical buckling limits for vertical and deviated well sections has been conducted. The effective axial force is defined, and its importance in buckling analysis is justified.

Finally, the theoretical foundation behind two models was investigated:

1. Buckling during installation

2. Buckling during operations (i.e. production, injection and other load cases)

The model of buckling during installation is based on the three-dimensional friction model developed by Aadnoy et al. (2010).

The model of buckling during operations is the existing model used for buckling analysis in the industry leading software WellCat. This model is developed by Lubinski et al. (1962) and Mitchell et al. (1999).

The aim of this chapter is to obtain a better understanding of failures related to sinusoidal or helical buckling, and to prevent potential failures in the future.

3.1   True Axial Force vs. Effective Axial Force

This section is written to clarify the difference between the true axial force and the effective axial force. The term "buckling force" is also frequently used in the literature , while the term "fictitious force" has contributed to more confusion around this subject (Lubinski et al., 1962) (Aasen et al., 2002) (Mitchell et al., 1999) (Aadnoy et al., 2009).

Tension is defined as a positive force, while compression is defined as negative.

3.1.1   Tubing string without packer

The axial force at the top of the string includes the weight of the string and the hydrostatic pressure acting on the bottom of the string.

3.1.1.1   True Axial Force

Aadnoy et al. (2009) presents the true axial force as:

$$F_a = (z_{TVD} - z)w_l + p_{i,TVD}A_i - p_{o,TVD}A_o \tag{3.1}$$

where z is the vertical depth of interest. At the top of the string, $z = 0$, the entire string weight is included. At the bottom of the string, $z = z_{TVD}$, the string weight equals zero, and the only forces acting are the hydrostatic pressure. The pressure terms are evaluated at the bottom of the tubing, regardless of depth of interest. A_i and A_o is the inner and outer area of the tubing respectively. At the bottom of the string, the true axial force becomes:

$$F_a = p_{i,shoe}A_i - p_{o,shoe}A_o \tag{3.2}$$

3.1.1.2   Effective Axial Force

The inner and outer pressure will affect the structural stability, so one can not rely on the compressive forces alone when buckling is calculated. The axial force combined with inner and outer pressure is summed up to make buckling calculation more convenient. The resulting force is called the effective axial force. When this effective force exceeds a certain limit, buckling will occur. The effective axial force is not a true force that can be measured, but it is useful to predict buckling tendencies. The effective axial force is defined as:

$$F_{eff} = F_a - p_i A_i + p_o A_o \tag{3.3}$$

These pressure terms are evaluated along the string.

Every long completion will be subjected to geometrical imperfections, and bends or irregularities will be present. Figure 3.1 illustrates a typical bend. The inner side of the bend will be in compression, while the outer side of the bend will be in tension. The part in tension will have a bigger inside area than the part in compression. The pressure will therefore act on a larger area on the tensile side, and the pipe will become

more unstable. At a certain point it can snap into a buckled shape, even though the entire pipe is in tension.
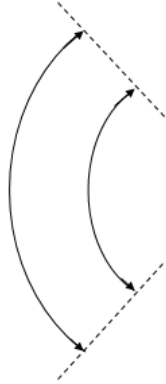
Figure 3.1: Geometrical imperfections induces bends in the tubing. The inside of the bend has a smaller area than the outside of the bend.

Compression and internal pressure will therefore promote buckling, while tension and external pressure reduces the chance of buckling (Bellarby, 2009, 492). Also note that a sufficiently high internal pressure can cause the effective axial load to be negative, although the true axial force is positive.

3.1.2 Tubing string with packer

3.1.2.1 True Axial Force

The hydrostatic pressures acting on the bottom of the tubing will now act on cross-sections of both the tubing and the packer. The true axial force are presented by Lubinski et al. (1962) as:

$$F_a = (A_p - A_o)P_o - (A_p - A_i)P_i \tag{3.4}$$

To calculate the axial force at surface, the string weight is simply added to equation (3.4).

3.1.2.2 Effective Axial Force

Lubinski et al. (1962) introduced the term "fictitious force" as the "effective force" at the bottom of the string. The equation for fictitious force is:

$$F_f = A_p(P_o - P_i) \tag{3.5}$$

Equation (3.5) is obtained by inserting equation (3.4) in to (3.3). If the inner and outer area is carefully expressed as the cross-sectional area in which the pressures are acting,

equation (3.1) and (3.3) can be correctly used for any general case. The string weight must be included to find the effective force at surface.

When the tubing is fixed, and loads affect tubing movement, the packer will act with an opposing force. This is presented in detail in section 3.4.

The true and effective axial force is plotted towards depth in figure 3.2. Note that the effective axial force equals zero at the bottom of the string. The reason for this is that the pressure terms cancels each other out at this point. This can be easily seen if the equation for true axial force is inserted in the equation for effective axial force.

Where the true axial force crosses the z-axis, the string is neither in compression nor tension. This is the point of zero axial load, and it is frequently denoted as the *neutral point*. The *neutral point* will not give us useful information on whether the string buckles or not. Buckling analysis requires knowledge of the effective axial force. This point where the effective axial force crosses the z-axis is defined as the *neutral stability point* (NSP).
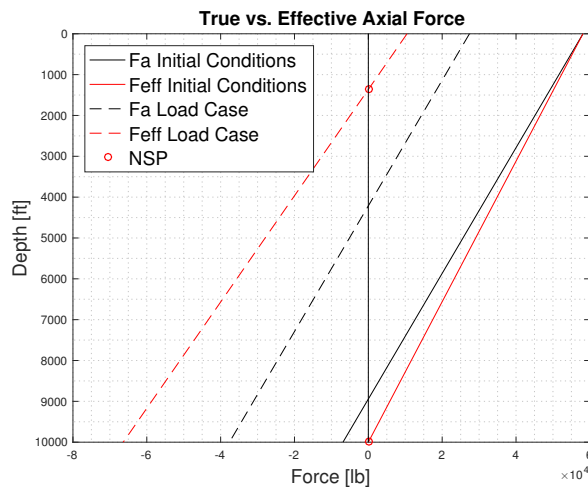
Figure 3.2: True and effective axial force from initial conditions and the squeeze cementing load case presented in Lubinski et al. (1962). The packer configuration enables free movement of the tubing.

Bellarby (2009) defines the neutral stability point as the boundary where buckling cannot occur and where it may occur, and one can therefore use the effective buckling force to evaluate at which depth the string buckles. This method is convenient, but utterly conservative. It is therefore developed critical buckling forces to make realistic predictions of buckling initiation.

3.2 Critical Buckling Limit

The critical buckling limit determines when and where buckling is initiated. When the buckling limits are presented, it is convenient to consider compression as a positive force. Buckling will not occur if the effective axial force is below the critical buckling limit. The sinusoidal buckling limit is the lowest buckling limit, then follows the helical buckling limit. In this section, the different buckling limits are presented, and the assumptions are clearly stated.

3.2.1 Euler's equation

Euler was the first to present a second order differential equation to represent buckling in a weightless rod Hearn (1997). The following assumptions forms the basis of this theory:

1. The column is subjected to axial loading

2. Material of the column is homogeneous and isotropic

3. The material of column is elastic and obeys Hooke's law

4. The length of the column is very large compared to the other dimensions

5. Self-weight of the column is neglected

6. The column is straight before loading

Equation (3.6) is a solution of this differential equation, and indicates the buckling limit, F_{cr}:

$$F_{cr} = n\frac{\pi^2 EI}{L^2} \tag{3.6}$$

where EI is the bending stiffness, and L is the tubular length. The coefficient, n, is dependent on the end conditions. For fixed-free end conditions, $n = \frac{1}{4}$. For fixed-fixed end conditions, $n = 4$ (Hearn, 1997, 28).

Euler's equation is fundamental for understanding elastic stability theory, but it does not consider tubulars confined within another circular cylinder. Laterally constrained pipes also presents more complex characteristics, and the equation has to be modified for application in well configurations (Cunha et al., 2003).

3.2.2 Pitch

Lubinski et al. (1962) derived an expression for the pitch, P, of a helix within a confining cylinder. The assumption of a vertical suspended weightless pipe was the basis of this theory. A helix geometry is displayed in figure 3.3.
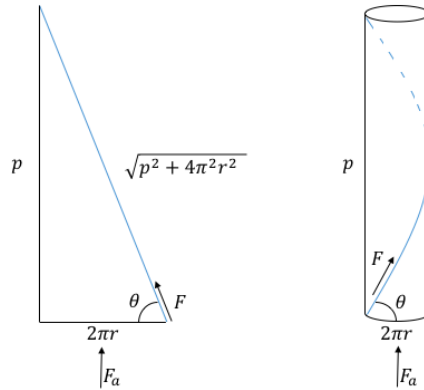
Figure 3.3: Visualization of helix geometry within a confining cylinder

The derivation of the pitch is included in Appendix A. By rearranging equation (A.14), Lubinski's equation for the pitch is obtained:

$$P = \sqrt{\frac{8\pi^2 EI}{F_f}} \tag{3.7}$$

where the force, F_f, is the fictitious force (Lubinski et al., 1962), also known as effective axial force at the bottom of the string. Equation (3.7) describes the pitch at the very bottom of the tubing string.

3.2.3 Vertical well

Both Euler and Lubinski et al. (1962) assumed a weightless rod when deriving equation (3.6) and (3.7) for critical buckling.

Buckling limits were also derived by considering tubular weight. Lubinski et al. (1950) derived the following solution for sinusoidal buckling in a vertical well:

$$F_{cr} = 1.94(EIw_b^2)^{1/3} \tag{3.8}$$

where w_b is the buoyed weight in [lb/in].

Wu et al. (1995) presented the following solution for helical buckling in a vertical well:

$$F_{cr} = 5.55(EIw_b^2)^{1/3} \tag{3.9}$$

Aasen et al. (2002) revisited several buckling models, and came to the conclusion that the different sources had presented similar coefficients to determine the critical buckling limit for vertical wells. The practical relevance of these coefficients are limited, as the buckling limit is generally low for vertical wells.

3.2.4 Deviated well

Inclination needs to be considered for deviated wells. Well inclination will stabilize the tubular, and a higher axial force will be required for buckling to be initiated. Dawson et al. (1984) presented an expression for sinusoidal buckling in inclined wells:

$$F_{cr} = 2\sqrt{\frac{EIw_b\sin\alpha}{r_c}} \tag{3.10}$$

where α is the well inclination and r_c is the radial clearance.

This equation is called the Paslay-Dawson equation. The equation is based on the assumption that the radial clearance, r_c, is small in comparison with the pitch length, P. That is, $\frac{2\pi r_c}{P} << 1$. Another assumption is that the well curvature is negligibly small. Hence, the equation applies for straight, inclined wellbores.

Mitchell et al. (1999) used the Paslay-Dawson equation to define the critical limits and the transition between sinusoidal and helical buckling. The buckling force must exceed the Paslay-Dawson force to initiate sinusoidal buckling. The following equation defines a region where the buckling may be either sinusoidal or helical:

$$F_{cr} = 1.4 \sim 2.8 \times 2\sqrt{\frac{EIw_b\sin\alpha}{r_c}} \tag{3.11}$$

The variation between 1.4 and 2.8 reflects uncertainty of when sinusoidal buckling switch to helical buckling while loading, and visa versa while unloading. The buckling force must exceed 1.4 to initiate helical buckling, and when it exceeds 2.8, only helical buckling occurs.

3.2.5 He and Kyllingstad's model for curved sections

He et al. (1995) derived an improved formula for critical buckling loads in curved wells. They saw one significant limitation with one specific assumption the Paslay-Dawson equation is based on. Derivations of the Paslay-Dawson equation is based on the assumption that the well curvature is negligibly small. He et al. (1995) generalized this equation by substituting $w_b\sin\alpha$ with a normal contact force which includes curvature effects. They called this normal contact force F_{1nbc}, and obtained the following equation:

$$F_{icr} = \frac{\beta F_{1nbc}EI}{r_c} \tag{3.12}$$

where F_{icr} is the improved critical buckling force and F_{1nbc} is the normal contact force including curvature effects. β is a coefficient that determines whether the buckling regime becomes sinusoidal or helical. $\beta=4$ is used for sinusoidal buckling and $\beta=8$ for helical buckling.

The normal contact force including curvature effects is given by:

$$F_{1nbc} = \sqrt{(w\sin\alpha + F_a a_\alpha)^2 + (F_a \sin\alpha\, a_\phi)^2} \qquad (3.13)$$

where F_a is the axial force, a_α is the inclination build rate and a_ϕ is the azimuth build rate.

He et al. (1995) conducted a small-scale experiment with a string within a transparent tube. The tube had a vertical part, a curved part and a horizontal part. When the string was located in the curve, it became more resistant to buckling. I.e. the critical buckling limit was higher than expected in the curved section, while the pipe buckled in both the straight vertical and horizontal section. It was therefore shown that the established equation by Dawson et al. (1984) was conservative in curved sections.

3.2.6   Summary of critical buckling limits

Table 3.1 presents the critical buckling limits presented in this chapter.

Table 3.1: Critical buckling limits for vertical, straight deviated and curved well sections.

TYPE	VERTICAL	STRAIGHT DEVIATED	CURVED
Sinusoidal	$F_{cr} = 1.94(EIw_b^2)^{1/3}$	$F_{cr} = 2\sqrt{\frac{EIw_b\sin\alpha}{r_c}}$	$F_{icr} = \frac{4F_{1nbc}EI}{r_c}$
Helical	$F_{cr} = 5.55(EIw_b^2)^{1/3}$	$F_{cr} = 1.4 \sim 2.8 \times 2\sqrt{\frac{EIw_b\sin\alpha}{r_c}}$	$F_{icr} = \frac{8F_{1nbc}EI}{r_c}$

3.2.7   Limitations of theory

Both Euler and Lubinski et al. (1962) assumed that the tubing was straight before loading. This is not the case in real well completions.

Dawson et al. (1984) neglected the curvature effects when deriving the equation for sinusoidal buckling in deviated wells. As curvature effects will stabilize the tubing, the critical buckling limit by Lubinski et al. (1962) is conservative in curved sections.

He et al. (1995) show that curvature effects stabilizes the tubing, but the results were only conducted from one small-scale experiment.

3.3 Buckling During Installation

3.3.1 Hook load

The hook load is the actual weight of a pipe measured at surface. Generally, this force includes the weight of the string in air, reduced by any force that tend to reduce that weight. The most commonly known opposing force to the hook load, is the buoyancy force. Another opposing force is friction, also known as the drag force.

$$F_{static} = F_{weight} - F_{buoyancy} \tag{3.14}$$

$$F_{dynamic} = F_{weight} - F_{buoyancy} \pm F_{drag} \tag{3.15}$$

F_{static} is the hook load when no movement is induced and $F_{dynamic}$ is the hook load after induced movement. The drag force will be negative when lowering the string, and positive when hoisting the string.

3.3.2 Tubing-to-casing drag

Bellarby (2009) defined tubing-to-casing drag as a contact force that derives from three main sources:

1) Forces due to gravity. This will be the normal force, which is the component of the tubing weight that acts perpendicular to the casing. The normal force will increase as the inclination increases.

2) Frictional forces from buckling. When the tubing takes the form of a sinusoidal or helical buckling shape, it will immediately contact the casing. If buckling is initiated, it causes an increase in locally generated forces.

3) Frictional forces from the capstan effect. This effect occurs when the tubing passes through doglegs. If the tubing is in tension, it will be pulled to the high side of the bend. If the tubing is in compression, it will be pushed to the low side of the bend.

Figure 3.4 shows how all three contributions to the contact force can occur at the same time. In this figure, the neutral stability point is located below the first build section.
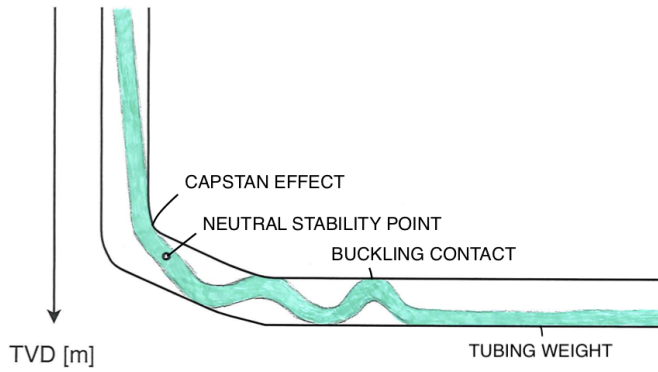
Figure 3.4: Illustration of how the capstan effect, buckling contact and tubing weight contributes to the drag force Bellarby (2009).

If the drag force becomes sufficiently high, it causes tubing lock-up when running on hole. If the compressive forces exceeds the buckling limit, the contact force induced by buckling will be added. The drag forces are especially important for extended-reach wells with high inclination.

3.3.3   Three-dimensional drag analysis

A two-dimensional analysis considers the curvature by inclination. Hereby the friction, including the capstan effect, plays a significant role. By considering azimuth, the drag force can be modelled in three dimensions. The three-dimensional analytic drag model by Aadnoy et al. (2010) can be applied for all wellbore shapes. The model is based on soft-string theory (Aadnoy, 2010, 244).

The drag analysis can be modeled by only two sets of equations, whereas they each represent the gravitational and tensional friction effects. The first equation is developed for straight, inclined wellbore sections:

$$F_2 = F_1 + \Delta L w \Big(\cos\alpha - \mu \sin\alpha \Big) \tag{3.16}$$

where ΔL is the section length and μ is the friction factor.

The second equation is developed for curved wellbore sections:

$$F_2 = F_1 e^{\mu|\theta_2 - \theta_1|} + \Delta L w \left(\frac{\sin\alpha_2 - \sin\alpha_1}{\alpha_2 - \alpha_1} \right) \tag{3.17}$$

The first part of equation (3.17) is known as the capstan effect. The magnitude of this effect depends on the dogleg angle, which is calculated in the following manner:

$$\theta = \cos^{-1} \Big[\sin\alpha_1 \sin\alpha_2 \cos(\phi_1 - \phi_2) + \cos\alpha_1 \cos\alpha_2 \Big] \tag{3.18}$$

where α is the inclination, ϕ is the azimuth and θ is the dog leg angle in radians. The capstan effect is derived from the assumption that the pipe is weightless, hence weight is added at the end of the bend.

Subscript 1 is the deepest position, 2 is the highest.

3.3.4 Limitations of theory

Soft string model neglects the bending stiffness, EI. Neglecting bending stiffness implies that the bending moment and bending stress is neglected, and that the calculated contact force will be lower than in reality. By not predicting the correct axial load, the buckling severity can be under estimated.

When the string is located in a straight section, it is assumed that the friction contribution solely comes from the gravitational normal force. It is therefore said that equation (3.16) is "weight-dominated". When the string is located in a curved section, it is assumed that the tension is much higher than the weight of the pipe in the bend. The string is assumed to be weightless. Equation (3.17) is therefore said to be "tension-dominated".

The purpose of these assumptions was to simplify the equations. The equations are easier to use, and easier to understand. When tension or compression dominates, equation (3.17) is correct. However, the "tension-dominated" equation can lead to errors at the parts of the string where tension and compression does not dominate (Aadnoy et al., 2010, 34). In a highly inclined build section, the weight can be the dominating effect. The exact equation in App. E in Aadnoy et al. (2010) should therefore be applied.

The end-condition F_1 is assumed to be zero. This is correct if the hole is clean, and no initial force pushes the string backwards when it is run in hole.

3.4 Buckling During Operations

To understand the concept regarding tubing movement, length changes and packer forces, one can start by imagining a tubing configuration where the packer permits free motion. When the tubing is subjected to an operation, (i.e. any load case), the pressure and temperature change will lead to changes in the axial force. The change in axial force implies that the tubing length will change. The effects causing length changes are known as buoyancy, ballooning, thermal expansion, drag and slack-off (Remmen et al., 2017). When all length changes are calculated, one imagines the same tubing being anchored in a packer. Tubing movement is now restricted, thus are the length changes transformed to a packer force. This method is developed by Lubinski et al. (1962), and used in the industry software WellCat (Halliburton, 2001). The method can be confusing. The purpose of this chapter is to explain the procedure presented by Lubinski et al. (1962) and to enhance the understanding of this topic. A graphical representation is added at the end of this section.

3.4.1 Lubinski's model

The theory in this section is mainly based on the model presented by Lubinski et al. (1962), but Bellarby (2009) and Aadnoy et al. (2010) are also used for further understanding of the aforementioned model.

Lubinski et al. (1962) presented compression as a positive force and tension as a negative force. The opposite is more commonly used. In the following section, compressive is considered negative, while tension is considered positive.

Lubinski et al. (1962) used the notation F_a for the direct piston force acting on the tubing, and F_f for the fictitious piston force that promotes buckling. This implies that F_a is the true axial force and F_f is the effective axial force at the bottom of the string. The fictitious force F_f is replaced by F_{eff} for consistency.

3.4.1.1 Packer that permits free motion

A freely hanging tubing only supported by pressure was imagined. Pressure acted on the cross-sectional area of both the tubing and the packer. This opposing force caused the tubing to shorten. This physical shortening in the tubing was expressed by Hooke's law:

$$\Delta L_1 = \frac{L_p}{EA_s}F \qquad (3.19)$$

where L_p is the tubing length, and F is the true axial force. When the outer and inner pressure changed, the length change was obtained:

$$\Delta L_1 = \frac{L_p}{EA_s}\Big[(A_p - A_o)\Delta P_o - (A_p - A_i)\Delta P_i\Big] \qquad (3.20)$$

It is assumed that helical buckling occurs when $F_{eff} < 0$. There will be a physical length change due to the buckling itself, and this length change will always be negative, as the

tubing shortens when it snaps into a helical shape. The length change is promoted by the effective force acting on the bottom of the tubing. Any length change due to helical buckling is calculated by a non-linear equation:

$$\Delta L_2 = -\frac{r_c^2}{8EIw} F_{eff}^2 \tag{3.21}$$

where the weight, w, was defined as:

$$\begin{aligned} w &= w_l + w_i - w_o \\ &= w_l + \rho_i A_i - \rho_o A_o \end{aligned} \tag{3.22}$$

and ρ_i is the fluid density in the tubing, and ρ_o is the fluid density in the annulus. w_s, w_i and w_o is the weight of tubing in air, weight of liquid inside tubing and weight of liquid outside tubing respectively. The unit for w is [lb/in]. Equation (3.22) equals the equation for buoyancy factor when two different fluids are present on the inside and the outside of the pipe, times the weight of string in air (Aadnoy et al., 2010, 25).

The effective force, F_{eff}, was calculated with equation (3.5). When the outer and inner pressures changed, the length change due to buckling was expressed as:

$$\Delta L_2 = -\frac{r_c^2}{8EIw} \left[A_p^2 (\Delta P_o - \Delta P_i)^2 \right] \tag{3.23}$$

Equation (3.23) is valid under the assumption that the initial inner pressure equals the initial outer pressures.

Change in pressure and temperature causes indirect elongation or shortening of the tubing. When the change in inner pressure is larger than the change in outer pressure, the radial force will promote ballooning. This radial pressure will cause the tubing to contract, and visa versa will reverse ballooning cause the tubing to elongate. The length change due to radial pressure and flow inside tubing was expressed by Lubinski et al. (1962) as:

$$\Delta L_3 = -\frac{\mu}{E} \frac{\Delta \rho_t - R^2 \Delta \rho_a - \frac{1+2\mu}{2\mu}\delta}{R^2 - 1} L_p^2 - \frac{2\mu}{E} \frac{(\Delta p_i - R^2 \Delta p_o) L_p}{R^2 - 1} \tag{3.24}$$

where μ is Poisson's ratio. R is the ratio between OD and ID of the tubing, $\Delta \rho$ is the change in density from initial conditions to load case conditions and δ is the drop of pressure per unit length due to flow.

Note that Δp is the change in surface pressure.

Fluid drag induced axial loads are often ignored in hand calculations and in many software packages (Bellarby, 2009, 489-490). For ballooning in static conditions, the following equation can be used:

$$\Delta L_3 = \frac{-2\mu L}{E(A_o - A_i)} (\Delta \overline{p_i} A_i - \Delta \overline{p_o} A_o) \tag{3.25}$$

In equation (3.25), $\Delta \overline{p}$ is the average change in pressure between surface and packer.

A positive temperature change will cause thermal expansion, and a negative temperature change will cause thermal contraction. The length change due to temperature changes is expressed by (3.26) by both Lubinski et al. (1962) and Bellarby (2009).

$$\Delta L_4 = L_p C_t \Delta T \tag{3.26}$$

where C_t is the coefficient of thermal expansion.

The total operational length change, ΔL will then be the sum of these:

$$\Delta L = \Delta L_1 + \Delta L_2 + \Delta L_3 + \Delta L_4 \tag{3.27}$$

The freely suspended tubing will now have changed its physical length by ΔL.

3.4.1.2   Packer that permits limited motion

The same tubing was then configured with a packer that permitted limited motion. The tubing can be installed in compression on purpose. Lubinski et al. (1962) explained that a shoulder on the tubing is removed, so the tubing can be elongated with the length corresponding to this compressive force, F_{so}. The length elongation is ΔL_5. This explanation is confusing because it does not apply for a practical well installation.

A more practical example to explain the procedure behind "slack-off" is attempted. To install a tubing in compression, a stick-up length is required. The stick-up length is an additional length that we denote ΔL_5. When this additional length is slacked off and the tubing is installed in the tubing hanger, this results in an additional force. This force is called the "slack-off"-force, F_{so}. The opposite of a slack-off force, is a "pick-up"-force. Due to Hooke's law of deformation, this elongation will be cancelled when the tubing is landed. The sum of all length changes will after installation equal zero:

$$\begin{aligned}
\Delta L &= \Delta L_1 + \Delta L_2 + \Delta L_5 = 0 \\
\Delta L_5 &= -\left(\Delta L_1 + \Delta L_2\right) \\
&= -\left(\frac{L_p}{EA_s} F_{so} - \frac{r_c^2}{8EIw} F_{so}^2\right)
\end{aligned} \tag{3.28}$$

When the tubing is subjected to loading, the total operational length change will be:

$$\Delta L = \Delta L_1 + \Delta L_2 + \Delta L_3 + \Delta L_4 + \Delta L_5 \tag{3.29}$$

This length change will apply to the limited motion of the tubing, and the seal length must be within this ΔL.

3.4.1.3   Packer that permits no motion

The final scenario was to imagine a tubing configuration where the packer permits no motion. There will then be no physical length changes in the tubing, because it can not physically move from its position. Instead of physically change its length, the packer

will subject an opposing force to this calculated length change.

The problem was explained as a sequence.

The effective force was earlier defined as the force defining the neutral stability point. The fictitious force is consecutive. The fictitious force was plotted towards length change, where the negative part of F indicated buckling, while the positive part of F indicated no buckling.

Lubinski et al. (1962) simulated a squeeze cementing load case. The effective axial force at packer depth was calculated and plotted as if the packer permitted free motion. The case considered however, was a packer permitting no tubular movement. The force associated with the calculated length changes would therefore be transferred to the packer. The packer force were shown to be tensile, thus it reduced the compressive effective force at the packer depth.

$$F_{eff}^* = F_{eff} + F_p \tag{3.30}$$

The corresponding axial force for an anchored tubing is:

$$F_a^* = F_a + F_p \tag{3.31}$$
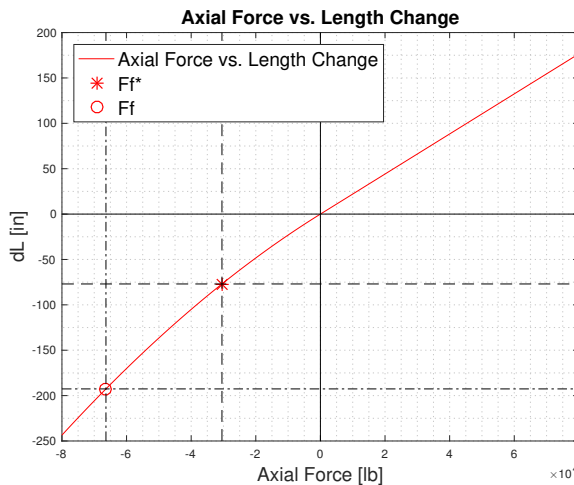
Figure 3.5: Reproduction of the length change and packer force calculation in the model proposed by Lubinski et al. (1962)

A new coordinate system was presented with F_{eff} as the origin. The shortening of the tubing ΔL was plotted, and it was clear that the packer force was located at the positive side of the x-axis in the new coordinate system. A flow chart is presented for further understanding of this method:

The Lubinski Method
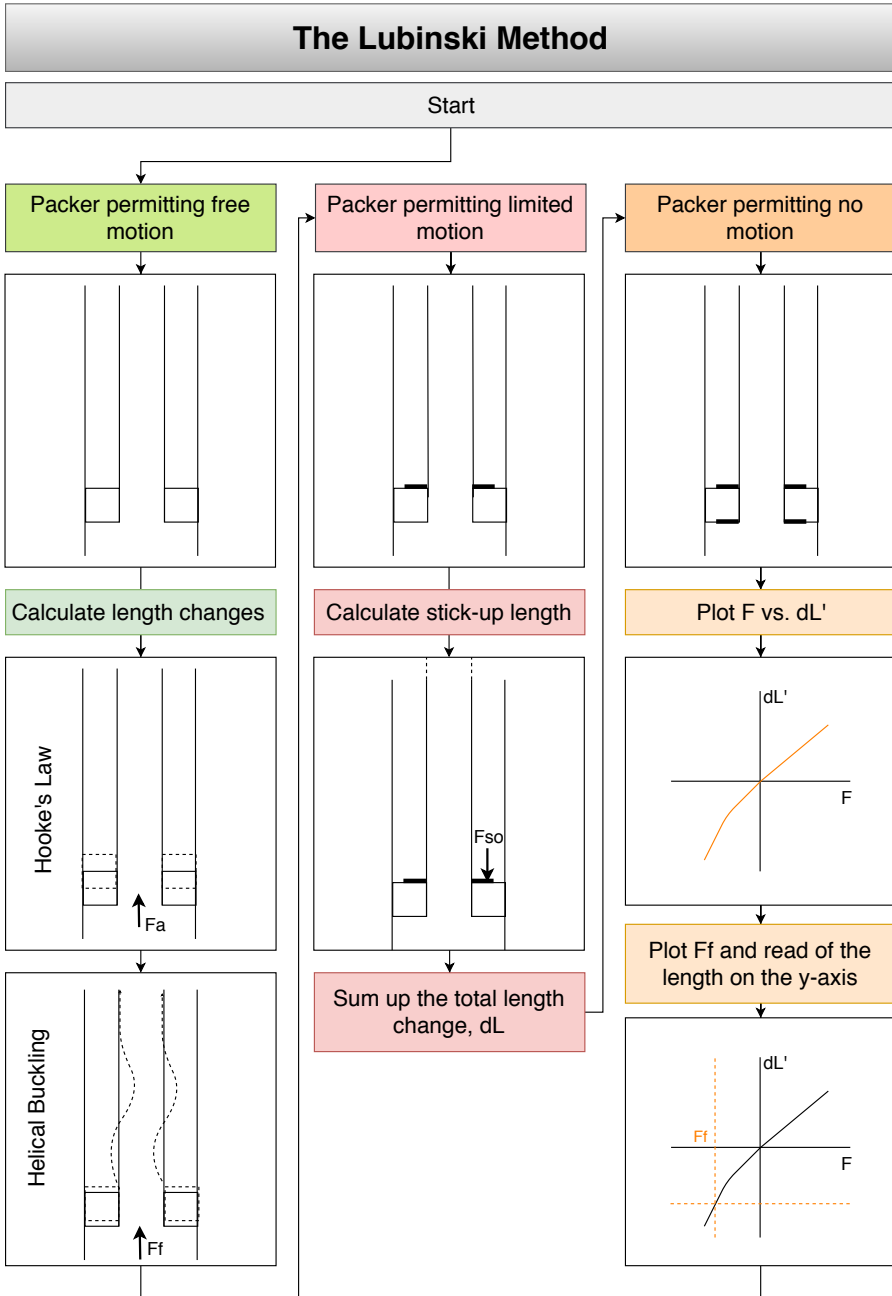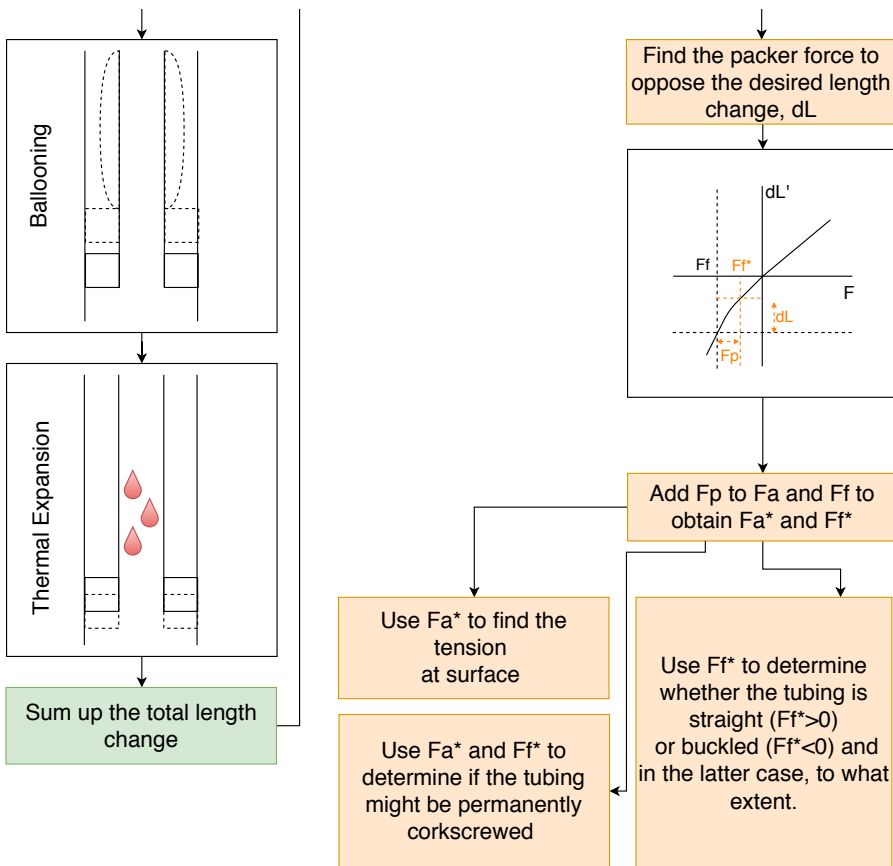
3.4.2 Mitchell's non-linear differential equation

One of the main limitations of the model developed by Lubinski et al. (1962) is that it was limited to helical buckling in vertical wells. Mitchell et al. (1988) investigated the derivation of helical buckling by Lubinski et al. (1962) and developed an approximate analytic solution of non-linear buckling equations for arbitrary well deviation. The solutions were developed to solve sinusoidal and helical buckling problems in a tubing with weight.

Mitchell et al. (1999) presented the lateral displacements as:

$$u_1 = r_c \cos(\lambda)$$
$$u_2 = r_c \sin(\lambda)$$

$$(3.32)$$

where the helix angle, λ, is given by a differential equation:

$$\left[-EI\lambda'''' + 2EI(\lambda')^3 - F\lambda' \right] + \left(w_l/r_c \right)\sin(\lambda) = 0 \tag{3.33}$$

F is the value of the axial force in the buckled state, also known as the effective axial force or fictitious force.

According to Mitchell et al. (1999), general solutions to equation (3.33) are difficult to obtain. The Galerkin method with cubic interpolation was used to calculate λ as a function of z. This method is too complex and slow for use in casing and tubing design, so Mitchell et al. (1999) presented approximate *correlations* to make the model more practical.

3.4.3 Mitchell's correlations

3.4.3.1 Helix Angle

Mitchell et al. (1999) presented correlations for the non-linear differential equations developed for buckling in deviated wells. By identifying that there can be both sinusoidal and helical buckling regime, parameters like helix angle, bending stress and bending strain were conditionally developed.

When a string is buckled like a sinusoidal, the bend of the helix, λ, will change through the S-shape. Thus, the maximum helix angle was found for sinusoidal buckling. The maximum helix angle, λ_{max}, for sinusoidal buckling was given by Mitchell et al. (1999) as:

$$\lambda'_{max} = \frac{1.1227}{\sqrt{2EI}} F_{eff}^{0.04}(F_{eff} - F_{cr})^{0.46} \tag{3.34}$$

For helical buckling, the helix angle is assumed to be constant (Bellarby, 2009, 496). The helix angle was given as:

$$\lambda' = \sqrt{\frac{F_{eff}}{2EI}} \tag{3.35}$$

3.4.3.2 Buckling Strain

The buckling strain, ϵ_b, was defined as the buckling length change per unit length, thus the elongation is unitless. Lubinski et al. (1962) followed the weightless string principle and derived an expression for the ϵ, using the geometry of a helix configuration (Figure 3.3). For the case of sinusoidal buckling, Mitchell et al. (1999) developed a correlation of the average strain. It was assumed that sinusoidal buckling occurs up to $2.8 \times F_{cr}$. The buckling strain was conditionally determined:

$$\epsilon_b = \begin{cases} 0 & F_{eff} < F_p \\ -0.7285 \frac{r_c^2}{4EI} F_{eff}^{0.08} \Big(F_{eff} - F_p\Big)^{0.92} & F_p < F_{eff} < 2.8F_p \\ -\frac{r_c^2}{4EI} F_{eff} & F_{eff} > 2.8F_p \end{cases} \tag{3.36}$$

In figure 3.6, it is clear that the amount of buckling strain is significantly reduced for values of F below the helical buckling limit.
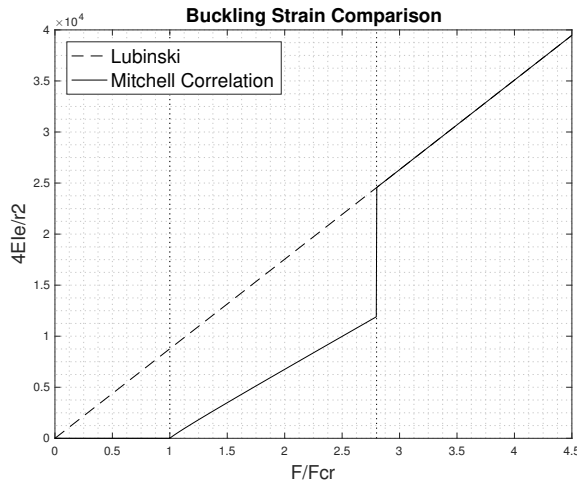
Figure 3.6: Comparison of buckling strain by Lubinski et al. (1962) and Mitchell et al. (1999).

To find the buckling length change, ΔL_b ($= \Delta L_2$), the buckling strain was integrated with respect to z. z was integrated between the bottom of the string and the neutral stability point. It was assumed that the neutral stability point was located within the string.

$$\Delta L_z = \int_0^n \epsilon_z dz \tag{3.37}$$

Further,

$$\frac{F_z}{z} = \frac{F_{eff}}{n} \tag{3.38}$$

Inserting the equation for helical buckling strain in equation (3.37), and integrating from 0 to n gives:

$$
\begin{aligned}
\Delta L_z &= \int_0^n -\frac{r_c^2}{4EI} F_z dz \\
&= \left[-\frac{r_c^2}{8EI} F_z^2 \right]_0^n \\
&= -\frac{r_c^2}{8EI} n F_{eff}
\end{aligned}
\tag{3.39}
$$

The neutral stability point, n, can be calculated by:

$$
n = \frac{F_{eff}}{w}
\tag{3.40}
$$

where w has to be defined as in equation 3.22. Inserting equation (3.40) for (3.39), gives the final equation for sinusoidal and helical buckling length changes. The same procedure is performed with the correlations for buckling strain, and the conditional buckling length changes are given as:

$$
\Delta L_b = \begin{cases}
0 & F_{eff} < F_p \\
-\frac{r_c^2}{4EI}(F_{eff} - F_{cr})[0.3771 F_{eff} - 0.3668 F_{cr}] & F_p < F_{eff} < 2.8 F_p \\
-\frac{r_c^2}{8EIw} F_{eff}^2 & F_{eff} > 2.8 F_p
\end{cases}
\tag{3.41}
$$

The length change correlation for sinusoidal and helical buckling is presented in figure 3.7.
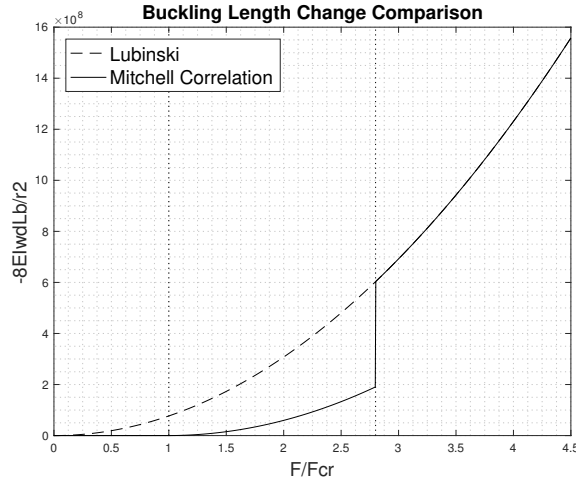
Figure 3.7: Comparison of buckling length change by Lubinski et al. (1962) and Mitchell et al. (1999).

Applying the buckling length change by Mitchell et al. (1999) into the Lubinski et al. (1962) model, the packer force reduces slightly. The result is seen in figure 3.8.
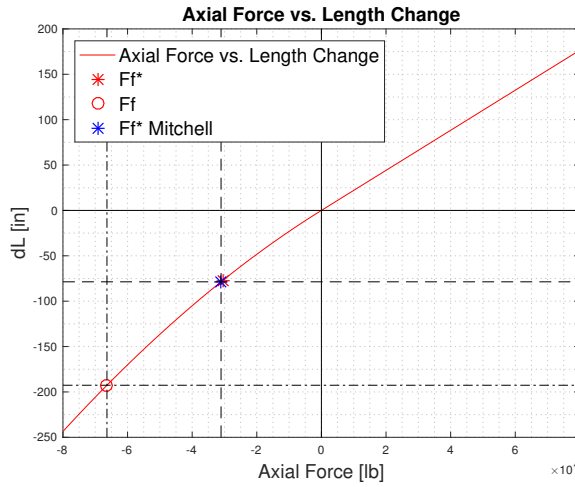
Figure 3.8: The effective axial force is compared when buckling length change by Mitchell et al. (1999) is used instead of Lubinski et al. (1962).

3.4.3.3   Bending moment and stress

The buckling severity depends on whether the tubing is sinusoidal or helically buckled. The pitch will also vary along the string. When buckling first is initiated, the pitch is expected to be high. The more severely the tubing buckled, the smaller the pitch gets.

The dog leg curvature of the helix in [rad/in] was given as:

$$\kappa = \begin{cases} r_c \lambda_{max}'^2 & \text{Sinusoidal Buckling} \\ r_c \lambda'^2 & \text{Helical Buckling} \end{cases} \tag{3.42}$$

The higher dog leg curvature, the higher bending moment. Bending moment, M, was generally given as:

$$M = EI\kappa \tag{3.43}$$

The bending moment was further given for the different buckling regimes:

$$M = \begin{cases} 0 & F_{eff} < F_{cr} \\ 0.6302 r_c F_{eff}^{0.08}\left(F_{eff} - F_{cr}\right)^{0.92} & F_{cr} < F_{eff} < 2.8 F_{cr} \\ 0.5000 r_c F_{eff} & F_{eff} > 2.8 F_{cr} \end{cases} \tag{3.44}$$

The bending moment is directly related to the bending stress, σ_b.

$$\sigma_b = \frac{M \times OD}{2I} \tag{3.45}$$

Conditionally:

$$\sigma_b = \begin{cases} 0 & F_{eff} < F_{cr} \\ 0.3151 \frac{ODr_c}{I} F_{eff}^{0.08} \left(F_{eff} - F_{cr} \right)^{0.92} & F_{cr} < F_{eff} < 2.8 F_{cr} \\ 0.2500 \frac{ODr_c}{I} F_{eff} & F_{eff} > 2.8 F_{cr} \end{cases} \tag{3.46}$$

3.4.4   Limitations of theory

A limitation of Lubinski et al. (1962) is that the method is developed for vertical wells. Friction between tubing and casing is not included. In horizontal wells, friction will be of importance and should not be neglected.

Lubinski et al. (1962) assumes that the tubing buckles when the tubing is subjected to an effective axial force. This is a conservative buckling limit.

When applying the change in effective force in equation (3.23), it is assumed that the initial inner pressure equals the initial outer pressure. Equation (3.23) has to be modified to apply for cases where the initial inner pressure does not equal the initial outer pressure.

Another assumption is that the neutral stability point is within the string. This is often true for vertical wells, but for multiple completions or shallow, horizontal wells, the neutral stability point can be shifted to a location above the string of interest (Lubinski et al., 1962).

It was challenging to compare the results from Lubinski et al. (1962) and Mitchell et al. (1999), as the entire example in Lubinski et al. (1962) is developed to work for a vertical well. To compare the results, Mitchell et al. (1999) assumed a kick-off point (KOP) at 2000 ft, and constructed a well path consisting of one vertical section and one sail section. This is not a realistic scenario, and considerations regarding build-sections is therefore not included.

Mitchell et al. (1999) assumed sinusoidal buckling for $F_{cr} < F_{eff} < 2.8 F_{cr}$. It is an uncertainty of whether helical or sinusoidal buckling occurs between $1.4 F_{cr}$ and $2.8 F_{cr}$. In theory, the maximum limit of stable sinusoidal buckling occurs at $2.8 F_{cr}$. In practice however, helical buckling will occur before reaching that limit. This is because of irregularities in the actual geometry. This assumption can lead to under-estimation of buckling length changes.

3.5   Permanent Corkscrewing

Casing and tubing design is planned within the elastic regime. When the yield point, σ_{yield}, is exceeded, a plastic regime is reached. When a pipe buckles and enters the plastic regime, the pipe goes through a permanent deformation. This is defined as an axial failure.

It is important to be aware of the correlations by Mitchell et al. (1999) when investigating post-buckling behavior. Permanent corkscrewing damages the tubing string, and it should therefore be carefully considered which buckling regime that might be present at the time of each load. As bending stress occurs on both the inside and outside of the bend, the positive and negative bending stress should be accounted for. Severe bending stress could cause the string to yield at the outermost fiber instead of the innermost fiber. Bending stress is included in the total axial stress implemented in the von Mises equation in section 3.5.

The permanent corkscrewing limit be obtained by the von Mises criterion:

$$2\sigma_{VME}^2 = \sqrt{(\sigma_\theta - \sigma_r)^2 + (\sigma_r - \sigma_z)^2 + (\sigma_z - \sigma_\theta)^2} \tag{3.47}$$

As an industry practice, it is established that casing and tubing strings are limited to the elastic stress-strain regime. For thick-walled cylinders, Lame's equations can be applied for the radial and tangential stress components, σ_r and σ_θ respectively, as a function of pressure (Bellarby, 2009, 515):

$$\begin{aligned}
\sigma_r &= \frac{r_i^2 r_o^2 (p_o - p_i)}{r_o^2 - r_i^2} \frac{1}{r^2} + \frac{p_i r_i^2 - p_o r_o^2}{r_o^2 - r_i^2} \\
\sigma_\theta &= -\frac{r_i^2 r_o^2 (p_o - p_i)}{r_o^2 - r_i^2} \frac{1}{r^2} + \frac{p_i r_i^2 - p_o r_o^2}{r_o^2 - r_i^2}
\end{aligned} \tag{3.48}$$

When Lame's equations are inserted in the von Mises criterion, one can express one relation for permanent corkscrewing at the outer wall, and another relation for permanent corkscrewing and the inner wall.

Permanent corkscrewing at the outer wall is given by equation (3.49):

$$\sigma_o = \sqrt{3 \left[\frac{P_i - P_o}{R^2 - 1} \right]^2 + \left[\frac{P_i - R^2 P_o}{R^2 - 1} + \sigma_a \pm \sigma_b \right]^2} \le \sigma_{yield} \tag{3.49}$$

Permanent corkscrewing at the inner wall is given by equation (3.50):

$$\sigma_i = \sqrt{3 \left[\frac{R^2 (P_i - P_o)}{R^2 - 1} \right]^2 + \left[\frac{P_i - R^2 P_o}{R^2 - 1} + \sigma_a \pm \frac{\sigma_b}{R} \right]^2} \le \sigma_{yield} \tag{3.50}$$

where R is the ratio between the outer and inner diameter of the tubing. The pressures, P_i and P_o are the pressures at the packer after the relevant load. The total axial stress is given as:

$$\sigma_z = \sigma_a \pm \frac{\sigma_b}{r_o} r_c \qquad (3.51)$$

The axial stress, σ_a, is the total axial load divided on cross-sectional area, A_s.

The bending stress, σ_b, is given depending on the buckling type and well deviation. The sign in front of the bending stress, $\pm$, is chosen as the one that gives the highest σ_o or σ_i.

Lubinski et al. (1962) used bending stress for helical buckling exclusively when calculating how permanent corkscrewing relates the the initial slack-off or pick-up force, and figure 3.9 is a reproduction of this:
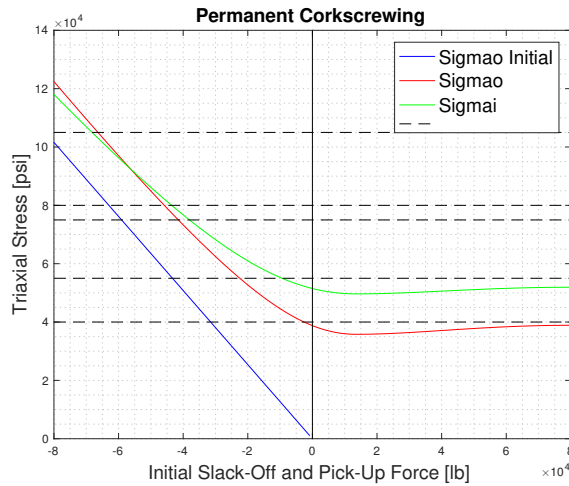
Figure 3.9: Triaxial stress plotted towards initial slack-off or pick-up force. This is a reproduction of the results presented in Lubinski et al. (1962).

$\sigma_{o,initial}$ is the initial yield after slack-off but before any pressures or temperatures have changed. The dotted lines represents the available grades for this tubing. When the triaxial stress exceeds a line, the line above should be chosen, and the available grade can be read of at the y-axis.

Chapter 4

Results

Tubing design is determined by analyzing load cases and investigating critical parameters. In this chapter, the critical parameters are clarified and evaluated, a drag analysis is performed to predict lock-up situations, and operational load cases are run to calculate the packer force and to locate the neutral stability point. Both models investigated whether buckling affects the well integrity by permanent corkscrewing.

The theories are tested on a shallow, horizontal well path with a dry x-mas tree. Figure 4.1 presents a simple sketch. The purpose of using this design, is to observe how pressure and temperature affects the axial force in a tubing installed in a horizontal well.
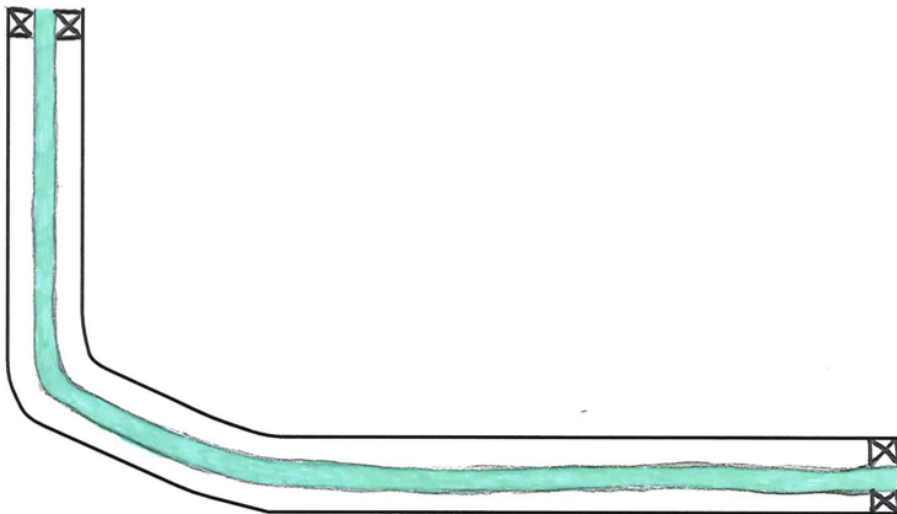
Figure 4.1: Sketch of well profile used in buckling analysis

4.1 Critical Buckling Limit

The critical buckling limit was plotted as a function of relevant parameters. Relevant parameters in buckling analysis are bending stiffness, weight, inclination and radial clearance. By evaluating these parameters, the tubing configuration can be optimized. The critical buckling limit was evaluated for a vertical well section, a deviated straight well section and a horizontal well section.

4.1.1 Effect of relevant parameters

A large radial clearance implies that the tubing is small relative to the confining casing. The tubing will tend to lean towards the sides of the casing to reach the equilibrium position. When the tubing has significant radial space, the buckling severity will increase due to reduced stability. The critical buckling limit for a vertical well is independent of radial clearance. Radial clearance affects the critical buckling limit for deviated wells. A well inclination of 45° is used. Figure 4.2a shows a correlation between radial clearance and the critical buckling limit. The opposite effect will be seen for bending stiffness and weight. A higher weight implies a larger tubing thickness. If the thickness increases, bending stiffness increases accordingly because of the definition of moment of inertia. It is evident that the trend will be positive for increasing values of bending stiffness and weight.

Increased inclination will provide support and stability to the tubing. Figure 4.2b shows how the critical buckling limit increases with inclination. A horizontal section will provide more stability than a section with a smaller inclination. Note that these are strictly a simulation of sail sections with different inclinations. As equation 3.10 does not include curvature effects, the plot will not apply for curves sections. For a vertical well, i.e. no inclinations, the limits presented in equation (3.8) and (3.9) should be used.
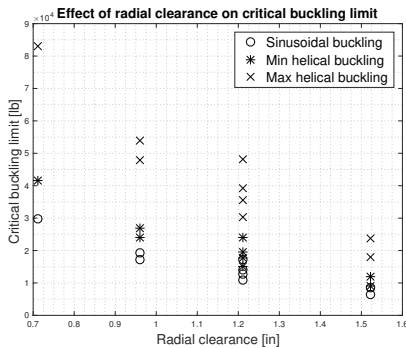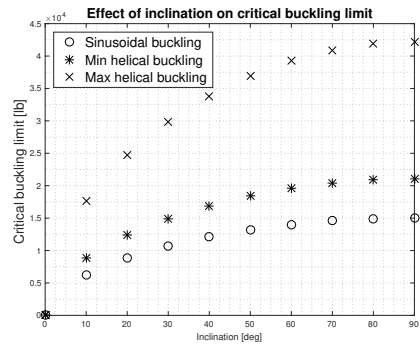
(a) Radial clearance   (b) Inclination

Figure 4.2: Effect of radial clearance and inclination on critical buckling limit in a deviated well section with 45°inclination.

4.1.2 D/t-ratio

The outer diameter to thickness ratio, D/t-ratio, will affect the geometric instability of the tubing. If this ratio is high, i.e. a thin-walled pipe, the instability naturally increases.

One of the failure modes in casing and tubing design is collapse. Buckling is previously stated to be suppressed by high external pressure. However, if the tubing is thin-walled, it is showed that the tubing fails because of buckling before it fails because of collapse.

One can categorize pipes with different D/t-ratios, in three collapse regimes. The first one is for low D/t-ratios. This is called yield collapse, and it is here Lame's equations are valid. The second region is plastic collapse, where the collapse limit is adapted to API empirical data. The last one, but most relevant to the buckling scenario, is the elastic collapse. Pipes within this D/t-category seems to collapse at a trend matching Euler's buckling equation. (Remmen et al., 2017)

Figure 4.3a presents a range of tubings with low D/t-ratio. The figure shows no correlation between D/t-ratio and the critical buckling limit. Only L80 pipes were chosen, and the D/t-ratios were calculated to be within yield or plastic collapse regime (Remmen et al., 2017). In figure 4.3b it is clearly a correlation between high D/t-ratios and the critical buckling limit. This result is expected for tubings in the elastic collapse region, where the thin-walled piped experiences buckling before collapse.
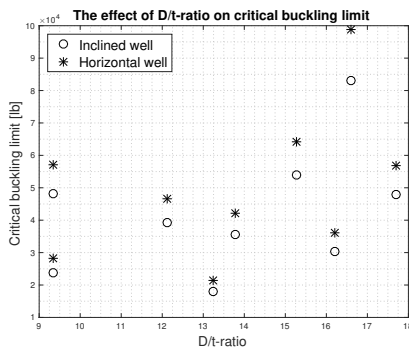
(a) Low D/t-ratios.
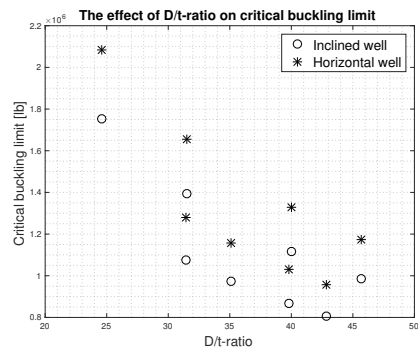
(b) High D/t-ratios.

Figure 4.3: Effect of D/t-ratio on the critical buckling limit in a deviated well section with 45°inclination and a horizontal well.

4.2   Critical Buckling Ratio

In this section, a set of API tubings are compared to a 3 1/2" #9.2 L80 tubing by deriving a critical buckling ratio. The ratio is the relation between an arbitrary API tubing and the initially chosen tubing. If the ratio is ≥ 1, the tubing will be better than the initially chosen one, and if the ratio is ≤ 1, the tubing is worse. This method can therefore be used to see if one choice of tubing is better than another with regards to buckling.

4.2.1   Vertical well

The critical limit is calculated by equation (3.8) for sinusoidal buckling, and equation (3.9) for helical buckling. The ratio for sinusoidal buckling will equal the ratio for helical buckling, as they only differ by coefficients. The critical buckling ratio, F_{cr}^* for a vertical well is:

$$F_{cr}* = \frac{1.94 \sim 5.55 \sqrt[3]{EIw_b^2}}{1.94 \sim 5.55 \sqrt[3]{EI_i w_{b,i}^2}} = \sqrt[3]{\frac{Iw_b^2}{I_i w_{b,i}^2}} \tag{4.1}$$

where the notation i is the tubing initially chosen. The variables in equation (4.1) is the moment of inertia, I, and the buoyed weight, w_b. Generally, one can increase the tubing weight to increase the critical buckling limit. One can also increase moment of inertia by increasing tubing OD, and even the lowest corresponding weight will increase the limit.

4.2.2   Deviated well

The critical buckling limit in a deviated well is calculated by equation (3.10) and (3.11). The ratio for sinusoidal buckling will equal the ratio of helical buckling. The critical buckling ratio for a deviated well is:

$$F_{cr}* = \frac{1.4 \sim 2.8 \times 2\sqrt{\frac{EIw_b\sin\alpha}{r_c}}}{1.4 \sim 2.8 \times 2\sqrt{\frac{EI_i w_{b,i}\sin\alpha}{r_{c,i}}}} = \sqrt{\frac{\frac{Iw_b}{r_c}}{\frac{I_i w_{b,i}}{r_{c,i}}}} \tag{4.2}$$

Note that the buckling ratio for a deviated well is independent of inclination. It can therefore be applied for both inclined and horizontal sections. The radial clearance will affect the buckling limit for deviated and horizontal wells. In an inclined or horizontal well, the radial clearance affects the critical buckling limit.

For the 4" #10.7 tubing marked with green, it can be seen that this tubing is a better choice than the 3 1/2" #12.7 tubing. The lower radial clearance in the deviated section will stabilize the tubing. The critical buckling limit for vertical wells is not depending on the radial clearance, hence other factors like bending stiffness and weight will be dominating. The results are presented in table 4.1.

Table 4.1: A set of tubing configurations from 2 7/8" to 4 1/2" is compared to the 3 1/2" #9.2 tubing. The tubings are sorted from best to worst with regards to buckling.

VERTICAL				INCLINED/HORIZONTAL			
OD [in]	w [lb/ft]	rc [in]	Fcr*	OD [in]	w [lb/ft]	rc [in]	Fcr*
4 1/2"	12.6	0.7105	1.64	4 1/2"	12.6	0.7105	2.34
3 1/2"	12.7	1.2105	1.36	4"	10.7	0.9605	1.52
4"	10.7	0.9605	1.29	3 1/2"	12.7	1.2105	1.35
4"	9.5	0.9605	1.14	4"	9.5	0.9605	1.35
3 1/2"	10.2	1.2105	1.11	3 1/2"	10.2	1.2105	1.11
3 1/2"	9.2	1.2105	1.00	3 1/2"	9.2	1.2105	1.00
3 1/2"	7.7	1.2105	0.85	3 1/2"	7.7	1.2105	0.86
2 7/8"	8.6	1.5230	0.81	2 7/8"	8.6	1.5230	0.67
2 7/8"	6.4	1.5230	0.61	2 7/8"	6.4	1.5230	0.51

4.2.3 Moment of inertia and radial clearance

Figure 4.4a presents how moment of inertia affects the critical buckling ratio. A clear correlation is seen for both the vertical and deviated section.

Figure 4.4b presents how radial clearance affects the critical buckling ratio. Even though the critical buckling ratio in the vertical section is not directly proportional to the radial clearance, a correlation is seen. Radial clearance is calculated from the outer diameter, and the outer diameter will strongly affect the moment of inertia. Hence, a correlation will still be present here.
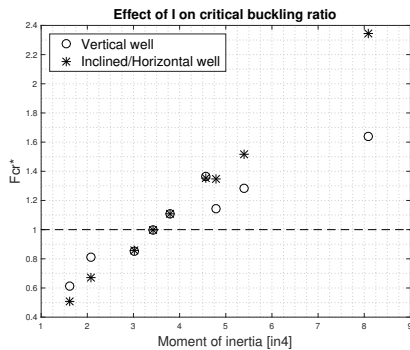
(a) Moment of inertia
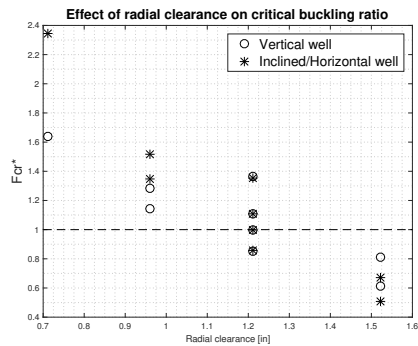
(b) Radial clearance

Figure 4.4: Effect of moment of inertia and radial clearance. The markers above "1" indicates the range of tubings that can withstand buckling better than the initially chosen tubing.

4.3   Buckling During Installation

The installation of a completion string in a long horizontal well is often one of the most critical operations. The purpose of investigating this subject is to predict lock-up situations and permanent corkscrewing due to helical buckling.

The friction model by Aadnoy et al. (2010) was developed for two well configurations. One was compiled from the traditional ideal well path theory, while the other was compiled in the Landmark software Compass. Drag calculations in two dimensions are presented for a range of friction coefficients, and the effective force is calculated and compared to the critical buckling limit.

4.3.1   Construction of ideal well path

The traditional way of hand-calculating torque and drag is by dividing the well path into ideal sections. The well path is presented in figure 4.5.
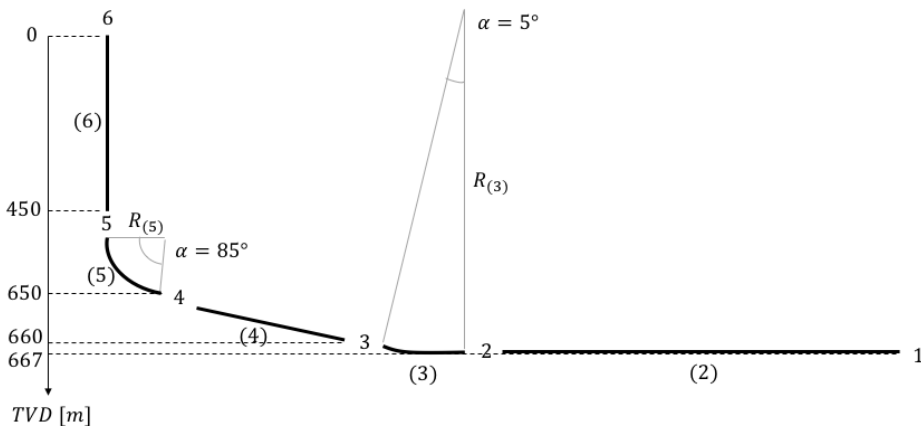
Figure 4.5: The ideal well path divided in sections. Each well section is indexed from 1 to 6. The subscripts between each section represents the order of drag-calculation. Subscript 1 is before subscript 2 and so on.

The curved sections was calculated as if the build angle was constant throughout the entire curve. The curved well length was then calculated by knowing the radius of curvature. Figure 4.6 illustrates this technique.
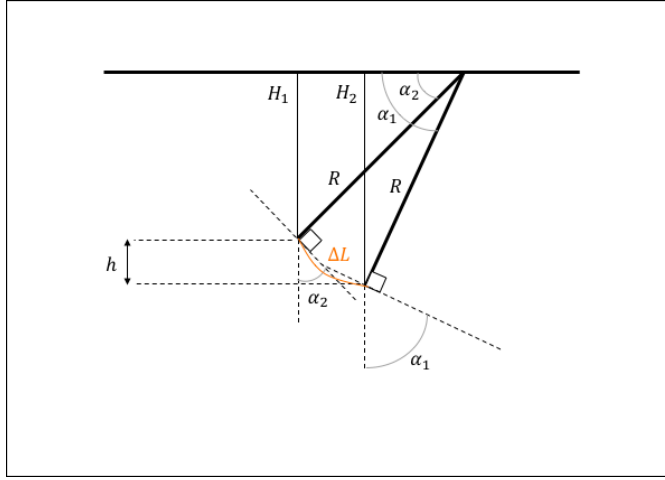
Figure 4.6: Illustration of an arbitrary build section to show the technique of calculating section length in an ideal well path curve.

Consider the two vertical lines, H_1 and H_2. These lines can be expressed by trigonometry:

$$H_1 = R\sin\alpha_1 \tag{4.3}$$
$$H_2 = R\sin\alpha_2 \tag{4.4}$$

The height of the section will now be the difference between these lines:

$$h = H_1 - H_2 = R\left(\sin\alpha_1 - \sin\alpha_2\right) \tag{4.5}$$

The radius of curvature is then found to be:

$$R = \frac{h}{\sin\alpha_1 - \sin\alpha_2} \tag{4.6}$$

The measured length of the section is now calculated using the arc length equation:

$$\Delta L = R \times \alpha \tag{4.7}$$

For each build section, the section length is calculated by equation (4.7). The technique is illustrated for the first and second build section in Appendix C. The height and angle of the sail section is known, and the section length is easily found by trigonometry. The vertical and horizontal section lengths are given.

During drag-calculations, one begin with the lowermost section and calculate upwards. It is convenient to use the ideal well path method for hand-calculations due to the reduced amount of iterations.

4.3.2   Construction of real well path

The equivalent well path is compiled in the Landmark software Compass. The well path was then exported to excel as 99 data points, and further was measured depth, total vertical depth and inclination easily exported to MatLab. 99 iterations were conducted to calculate the radius of curvature and the remaining parameters. In the ideal well path, the radius of curvature naturally had to be constant throughout the bend. The real well path provides a set of radius of curvature similar to the ideal well path. There is a slight difference in radius of curvature from the ideal and real well path. The real well path shows dog leg variation. This is not found in the ideal well path.

Figure 4.7a presents the ideal well path, and figure 4.7b presents the real well path.

(a) Ideal well path   (b) Real well path
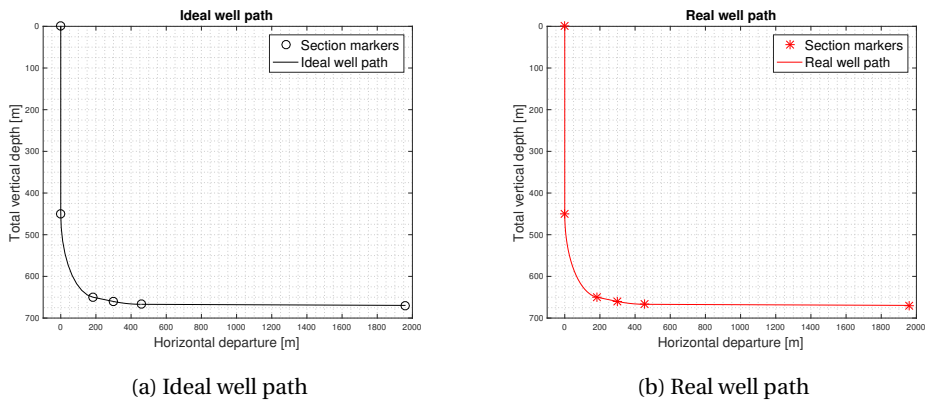
Figure 4.7: Presentation of ideal well path and real well path.

Figure 4.8a shows the ideal and real well path in the same graph, while figure 4.8b shows the deviations in the curved section.

(a) Ideal and real well path plotted in the same   (b) Ideal and real well path plotted in the same
graph   graph. Zoomed in on the curved section.
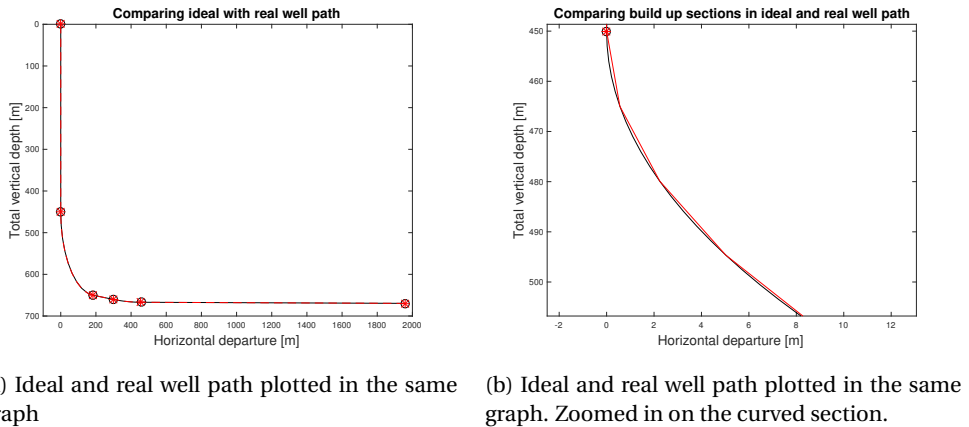
Figure 4.8: Comparison of the ideal well path and real well path.

4.3.3 Verification of static hook load

The program is verified by comparing the static hook load to the dynamic hook load with coefficient of friction equal to zero. The vertical projected height principle is used to calculate the static hook load (Aadnoy, 2010).
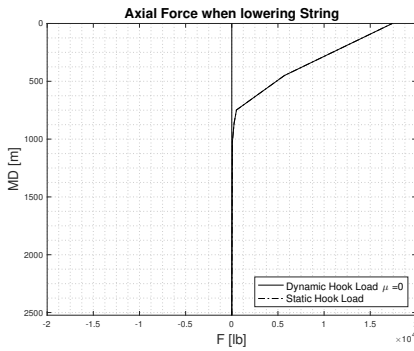
(a) μ=0 for the ideal well path
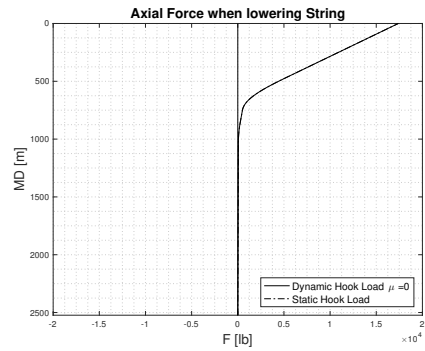
(b) μ=0 for the real well path

Figure 4.9: Dynamic hook load and static hook load overlaps at μ=0

4.3.4 Results from drag analysis

Figure 4.10, 4.11, 4.12 and 4.13 present the results from the drag analysis.

Notice how the hook load changes when the friction factor increases, and also notice the difference between the ideal and the real well path.
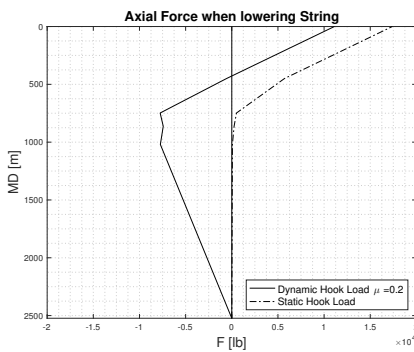
(a) μ=0.2 for the ideal well path
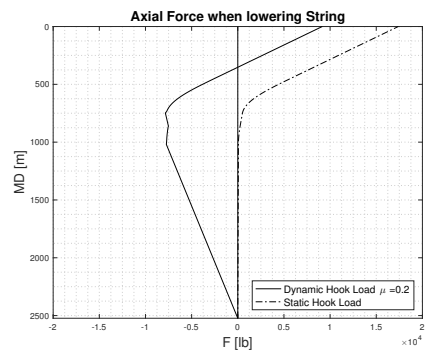
(b) μ=0.2 for the real well path

Figure 4.10: Dynamic and static hook load for μ=0.2
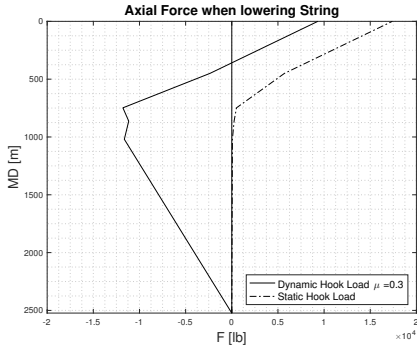
(a) μ=0.3 for the ideal well path
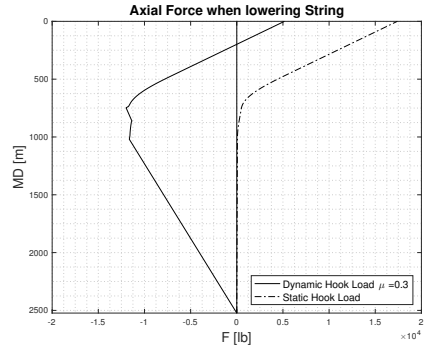
(b) μ=0.3 for the real well path

Figure 4.11: Dynamic and static hook load for μ=0.3
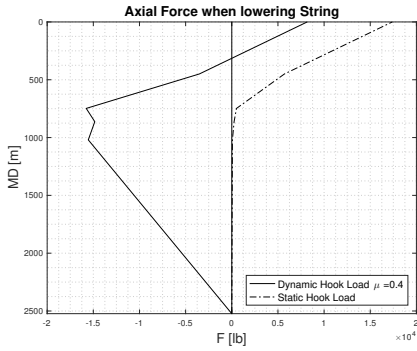
(a) μ=0.4 for the ideal well path
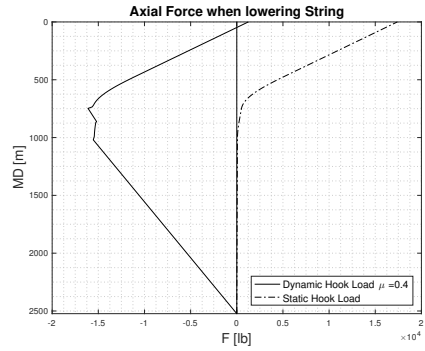
(b) μ=0.4 for the real well path

Figure 4.12: Dynamic and static hook load for μ=0.4
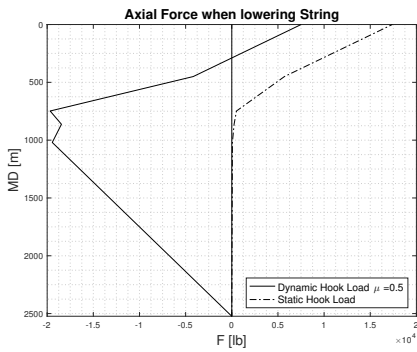
(a) μ=0.5 for the ideal well path
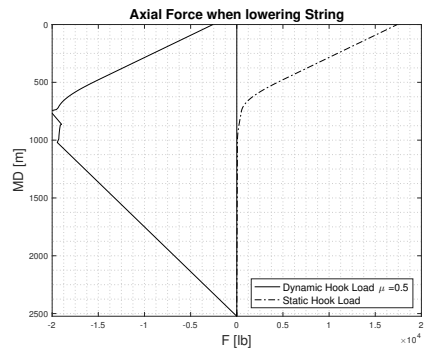
(b) μ=0.5 for the real well path

Figure 4.13: Dynamic and static hook load for μ=0.5

4.3.5 Implementation of critical buckling limits

The effective axial force is calculated. Well fluids will be present when running in hole, and this will create an opposing force when lowering the string. This effect is included when the true axial forces is calculated. Further, the effective axial force is calculated and compared to the critical buckling limit.

Figure 4.14, 4.15 and 4.16 present the results after implementation of the critical buckling limits. Sketches are included for a clear visualization of each buckling regime.

(a) μ=0.25 for the real well path

(b) Sketch of buckling scenario when μ=0.25
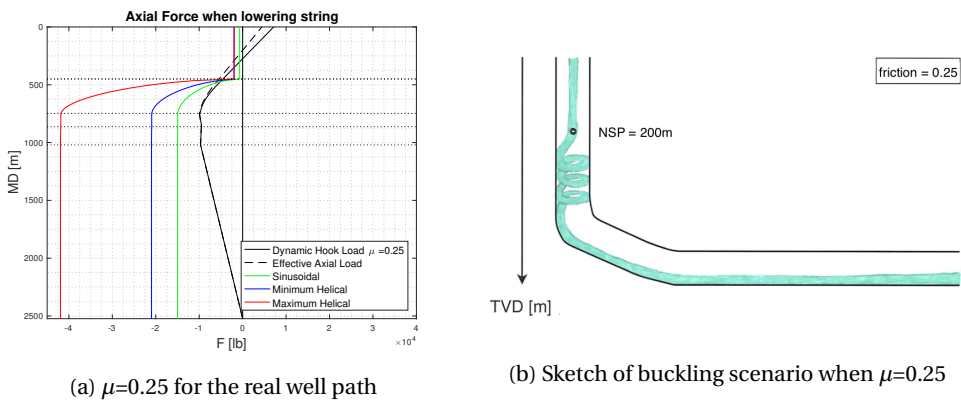
Figure 4.14: Buckling during installation when μ=0.25

(a) μ=0.35 for the real well path

(b) Sketch of buckling scenario when μ=0.35
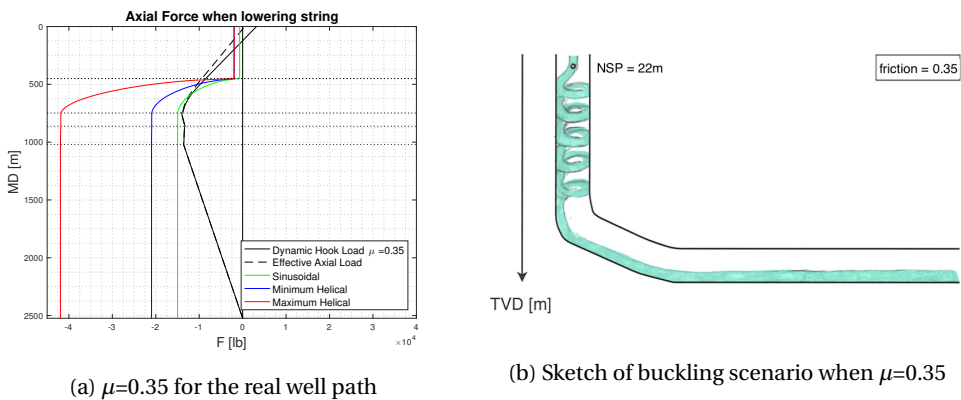
Figure 4.15: Buckling during installation when μ=0.35

(a) μ=0.45 for the real well path

(b) Sketch of buckling scenario when μ=0.45
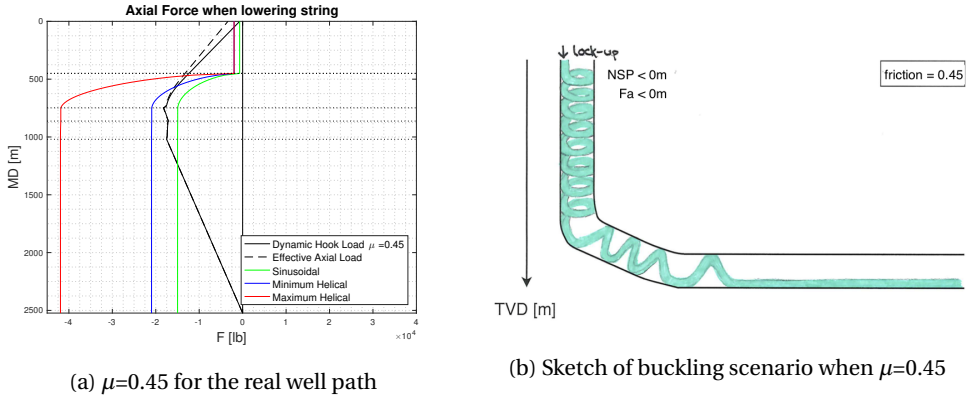
Figure 4.16: Buckling during installation when μ=0.45

4.3.6   Permanent corkscrewing

When pressure and temperature is not changed in the well, i.e. during lowering of the completion, permanent corkscrewing occurs when the bending stress at the outer wall exceeds the yields strength. The derivation is conducted from the outer stress in equation (3.49). $P_i=P_o$ gives:

$$
\begin{aligned}
\sigma_o &= |\frac{P_i(1-R^2)}{R^2-1} + \sigma_a \pm \sigma_b| \\
&= |-P_i + \sigma_a \pm \sigma_b| \\
&= |-P_i + \frac{-P_i(A_i-A_o)}{A_s} \pm \sigma_b| \\
&= |\pm \sigma_b| \\
&= \sigma_b \leq \sigma_{yield}
\end{aligned}
\tag{4.8}
$$

Figure 4.17 shows a plot of triaxial stress versus the effective axial force. The triaxial stress on the outer wall has been reduced to the bending stress. The relation between bending stress and effective axial stress is linear.

If the bending stress exceeds the available grades, permanent corkscrewing will occur. The effective axial force required to permanently deform the pipe is calculated and marked in the plot. The minimum effective axial force required is ≈130000 psi, and this force is not encountered in any of the drag scenarios. The lowest grade available is therefore applicable for buckling scenarios during installation.
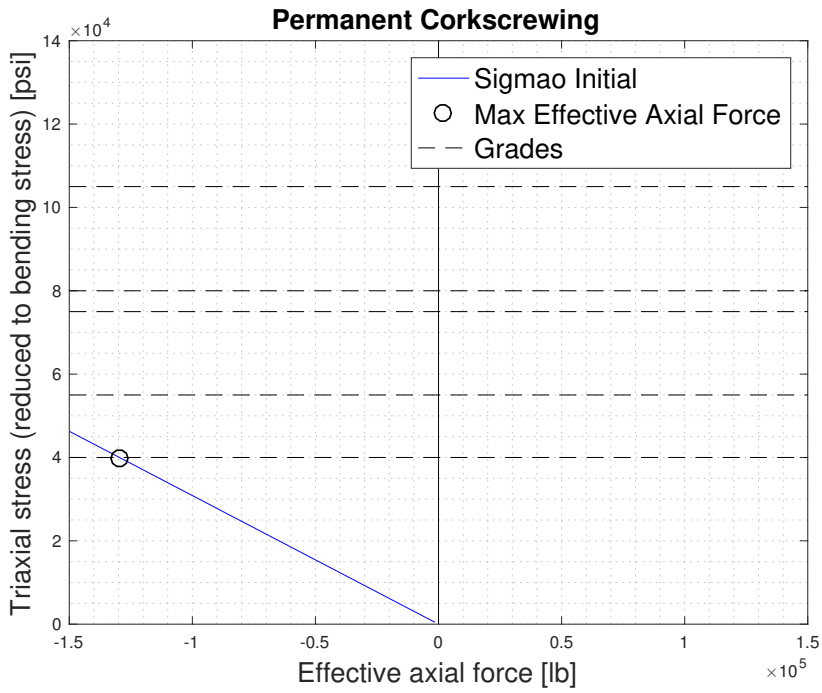
Figure 4.17: The relation between effective axial stress and bending stress is linear. When the bending stress exceeds the yield strength, i.e. grade, of the tubing, permanent corkscrewing will occur.

4.4   Buckling During Operations

Theoretical models for buckling during operations are developed and used in the industry. The models are modified and applied for a shallow, horizontal well.

It is assumed that the completion fluid has the density equivalent to sea water, reservoir pressure is 70bar and reservoir temperature is 17°C.

4.4.1   Packer force and neutral stability point

The packer force is calculated using the Lubinski et al. (1962) method.

The neutral stability point is found by calculating the true and effective axial force for an anchored tubing, thus including the packer force (B.S. Aadnoy, personal communication, May 27, 2018). The vertical projected height principle is used to calculate tubing weight (Aadnoy, 2010). Inserting equation (3.30) and (3.31) in equation (3.40) results in the following expression:

$$n = \frac{F_f^*}{w} = \frac{F_{eff}}{w} \tag{4.9}$$

The calculation procedure for axial forces at surface is presented:

$$F_a^* = \text{TVD} \times w_l + P_o(A_p - A_o) - P_i(A_p - A_i) + F_p = F_a + F_p$$

$$F_{eff}^* = F_a^* - p_i A_i + p_o A_o = F_{eff} + F_p$$

Further, the calculation procedure for axial forces at the packer is presented:

$$F_a* = P_o(A_p - A_o) - P_i(A_p - A_i) + F_p = F_a + F_p$$

$$F_{eff}* = F_a * - p_i A_i + p_o A_o = F_{eff} + F_p$$

Capital P is the pressure at packer level, and lowercase p is the pressure at surface. Note how the pressures are used in each equation. A flow chart for further understanding of F_{eff}^* is presented.

Packer force and neutral stability point

Start

Packer permitting no motion

Ballooning

Calculate length changes

Thermal Expansion

Calculate packer force

Hooke's Law

Fa

Sum up the total length change

dL

Fp

Calculate Ff* = Ff + Fp

Helical Buckling

Ff

Find the neutral stability point with the new Ff*

Fp

Ff*

dL

Ff
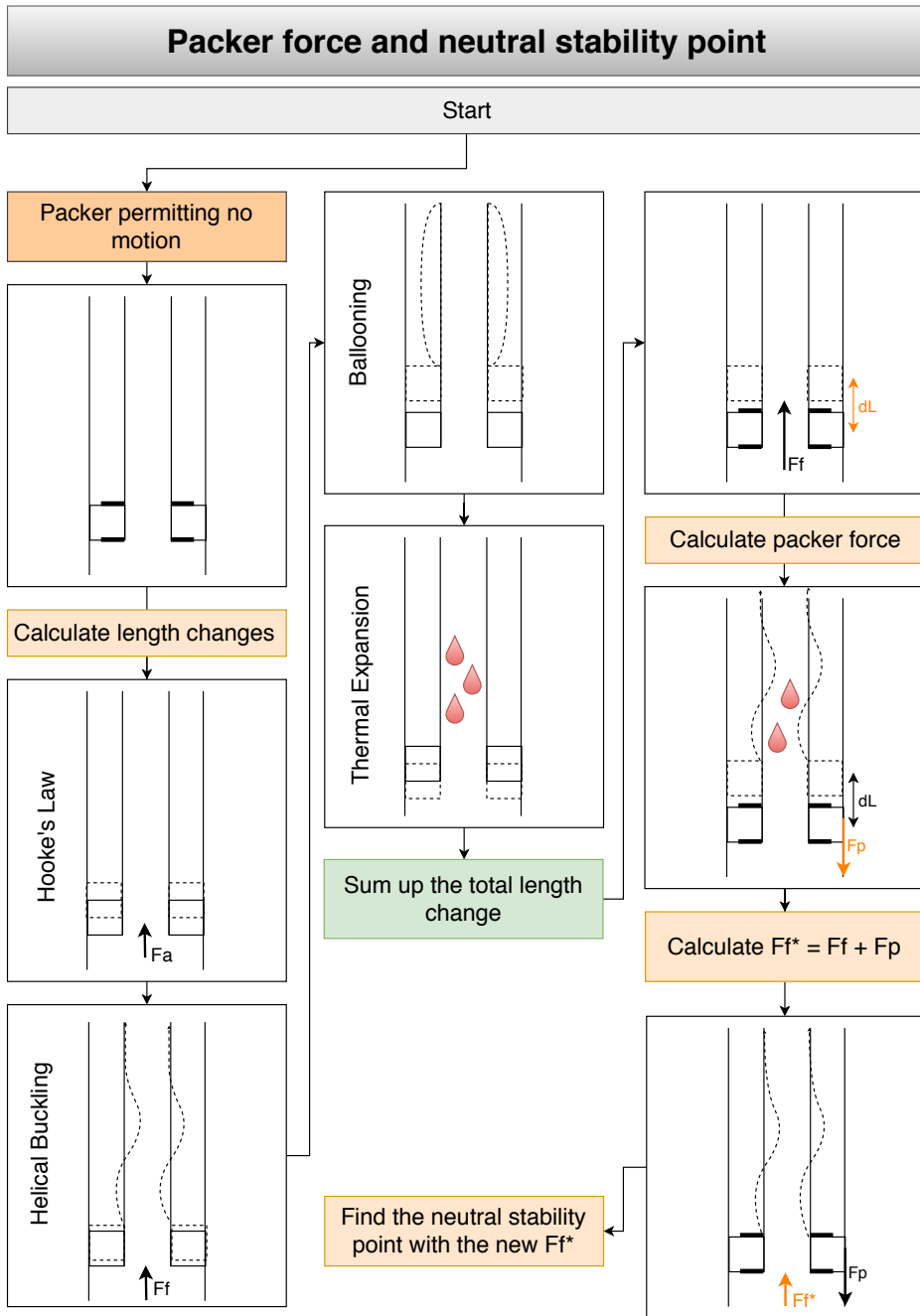
4.4.2   Buckling in thermal environments

Buckling will get more severe with a combination of high temperatures and high inner pressure. Thermal expansion is often a dominating length change effect that can greatly affect the packer force. The model is therefore run for two load cases, one cold and one hot for comparison:

1. Shut-in

2. Start bullheading

Figure 4.18 presents the temperature cycles for the load cases shut-in and start bullheading. It is assumed that this well is installed while circulating fluid with a temperature of 10 °C. The temperature cycle for start bullheading equals the temperature cycle for production.
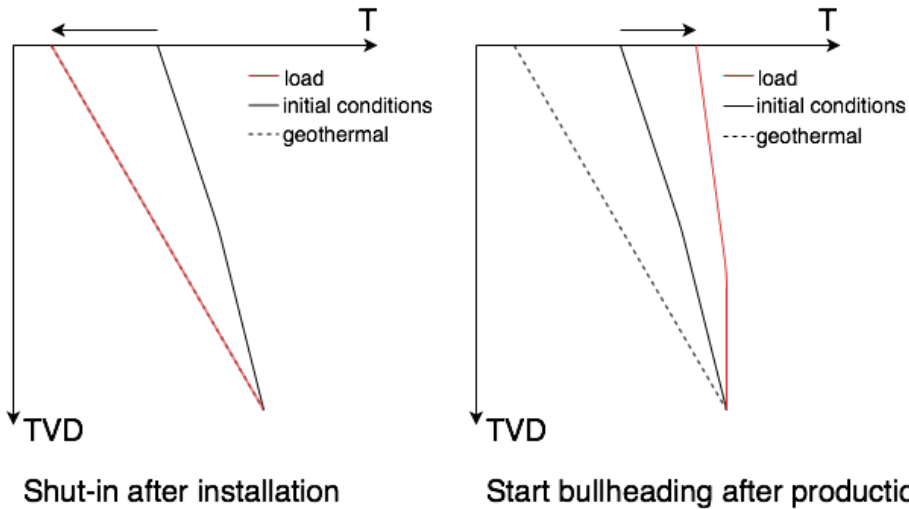
Figure 4.18: Temperature cycles for shut-in after installation and start bullheading after production.

The initial condition is the temperature after installation. After shut-in, the temperature will approach the geothermal gradient. After production, the temperature will increase at wellhead. bullheading is initiated by applying a high surface pressure.

4.4.2.1 Shut-in

The tubing will shorten due to ballooning and the negative thermal effect, and this causes the packer to act with a tensile force. The packer force is now located within the tensile region on the plot, and it means that the tensile force causes the tubing to unbuckle. Figure 4.19 shows that the neutral stability point is located below the string.
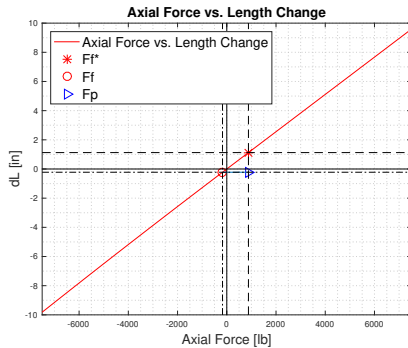
(a) $F_f^* > F_f$, thus tensile packer force
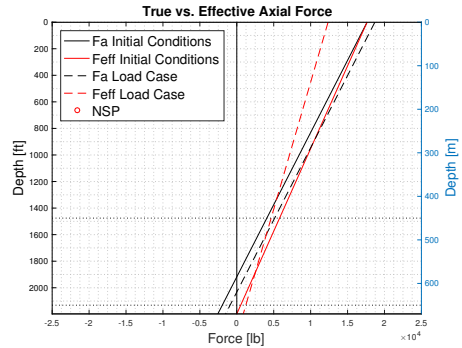
(b) Neutral stability point due to shut-in

Figure 4.19: Packer force and neutral stability point during shut-in

4.4.2.2 Start bullheading

A bullheading operation can be subsequent to a clean-up operation, and the pump pressure is determined as if the well is gas filled. If the fluid contents is heavier, i.e. oil filled, the burst load will be higher than if the well actually contains gas. The tubing will in both cases elongate due to the positive thermal effect, and this causes the packer to act with a compressive force.

Both scenarios were simulated to illustrate the effect. Figure 4.20a present the start bullheading procedure in a gas filled well. Figure 4.20b show that the neutral stability point was located within the build section.

Figure 4.20c show that the packer force was larger for the oil filled well than the gas filled well. Figure 4.20d show that the neutral stability point was now located in the vertical section.
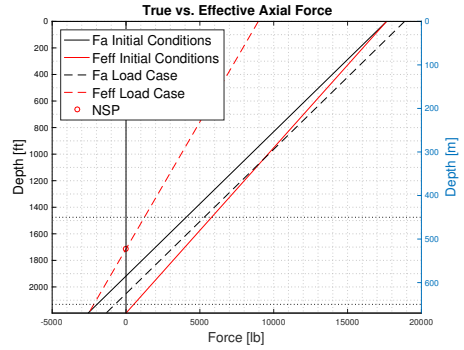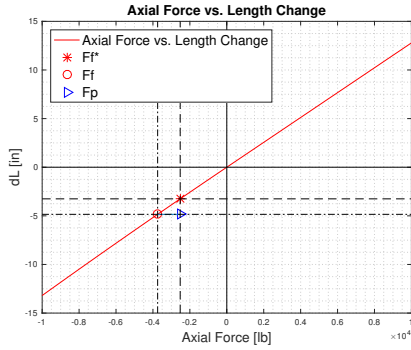
(a) Simulation of packer force in gas filled well

(b) Neutral stability point in the gas filled well
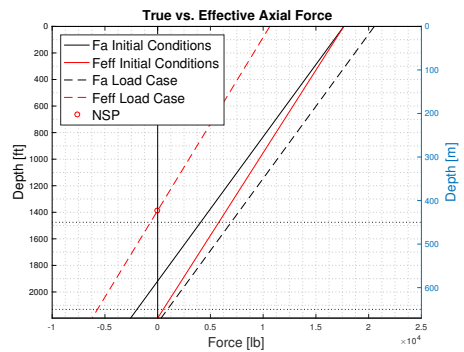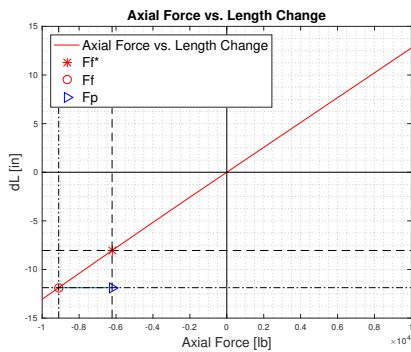
(c) Simulation of packer force in oil filled well

(d) Neutral stability point in the oil filled well

Figure 4.20: Packer force and neutral stability point for start bullheading.

4.4.3 Set packer procedure

When the tubing is installed, pressure needs to be applied to set the packer. As the reservoir pressure in a shallow well is low, this is the the highest pressure the tubing will experience. Figure 4.21 shows that the high inner pressure will cause the tubing to buckle, even though it is in complete tension.
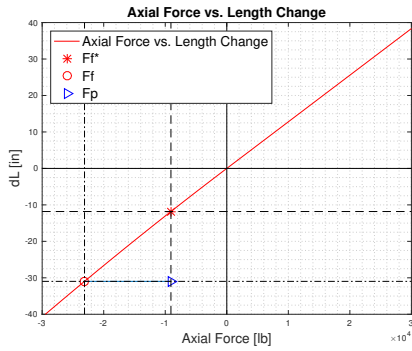
(a) $F_f^* > F_f$, thus tensile packer force
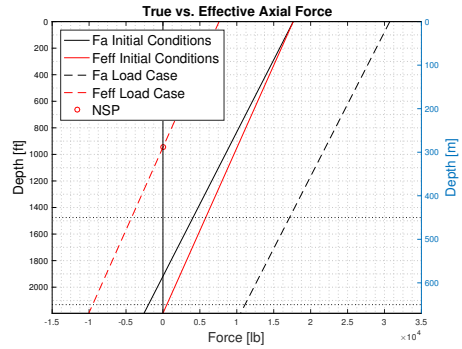
(b) Neutral stability point when packer is set

Figure 4.21: Packer force and neutral stability point during set packer

4.4.4 Implementation of critical buckling limits

The critical buckling limits are implemented to be compared with the effective axial force. Different authors have presented a range of critical buckling limits, and the most acknowledged are included in the scripts to create a realistic scenario.

Buckling induces bending stress, and this will be locally superimposed to the true axial stress. A bend consists of both a tensile part and a compressive part. If the axial stress is tensile, the tensile stress from the outer bend will be added. If the axial stress is compressive, the compressive force from the inner bend will be added.

Figure 4.22 includes the bending stress when each buckling regime is clarified.

(a) Set packer

(b) Start bullheading with gas filled well

(c) Start bullheading with oil filled well

(d) Shut-in
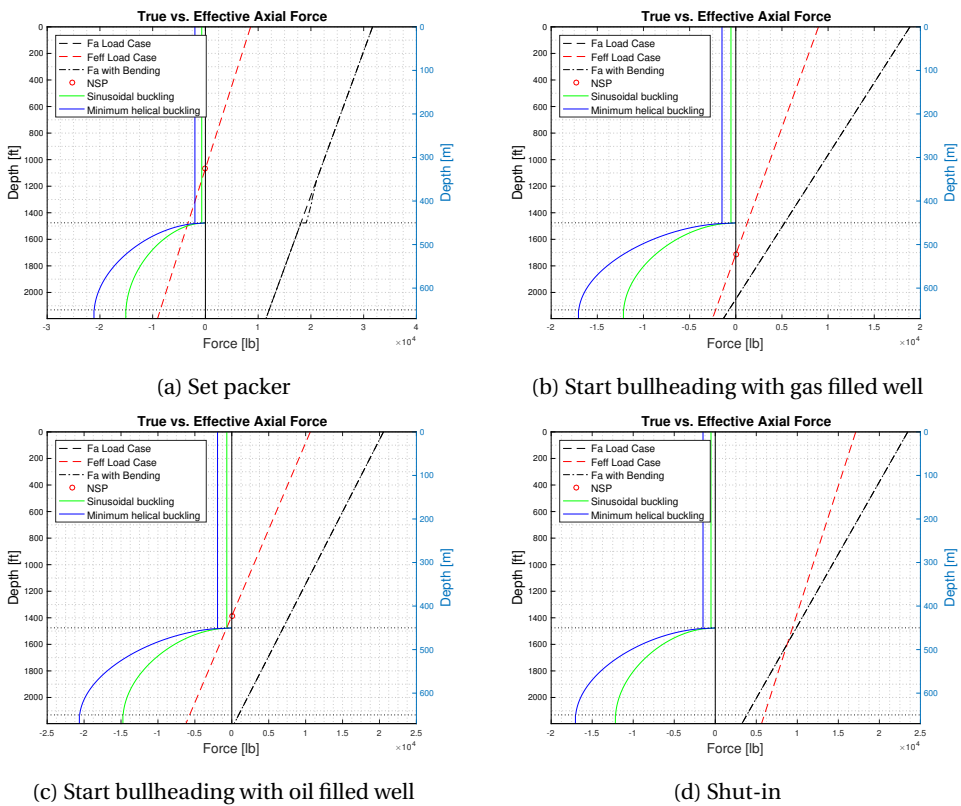
Figure 4.22: Implementation of critical buckling limits for operations.

Both sinusoidal and helical buckling will occur during the set packer load case. Both buckling regimes will cause extra bending stresses, that locally superimpose to the true axial force.

4.4.5 Permanent corkscrewing

The completion can be initially installed in compression by purpose. Lubinski et al. (1962) investigated how different values of initial slack-off/pick-up can cause the pipe to permanently deform due to high bending stresses.

Figure 4.23 plots initial slack-off and pick-up versus triaxial stress.

(a) Start bullheading   (b) Set packer
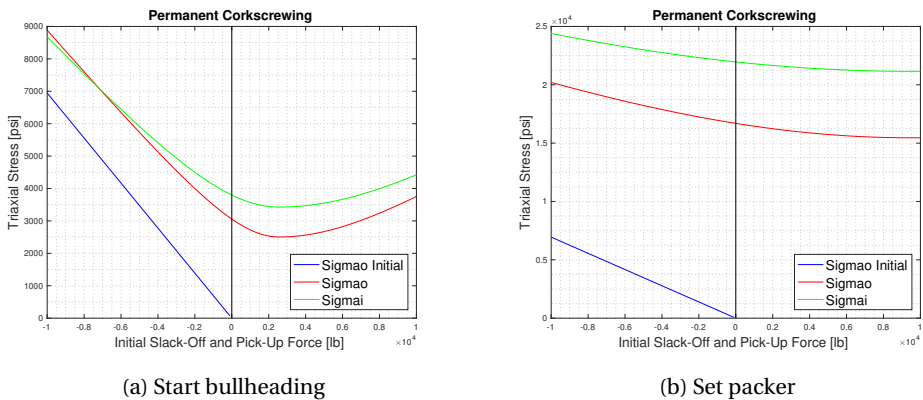
Figure 4.23: Triaxial stress in tubing during start bullheading and set packer

It is clear that the triaxial stress does not exceed the minimum grade available for this tubing, that is 40ksi. The tubing does not permanently corkscrew when slack-off/pick-up forces are between -10000 and 10000 lb. However, it should be noticed that for slack-off forces higher than 7500 lb, the bending stress induces higher triaxial stress at the outer wall than the inner wall for start bullheading.

It is not expected that permanent corkscrewing will be an issue during any operations.

Chapter 5

Discussion and Evaluation

5.1 Buckling During Installation

5.1.1 Evaluation of parameters

Friction factors between 0.0 and 0.5 was used in the analysis. When lowering the string, the friction factor mainly depends on the fluid type, and whether the tubing is in contact with a metal or non-metal surface. In most cases, it will be metal-to-metal. Table 5.1 presents a range of theoretical friction factors.

Table 5.1: A range of typical friction factors depending on lubrication and interfaces. (Mitchell et al., 1996)

MATERIALS	SURFACE CONDITIONS	μ STATIC	μ KINETIC
Metal on metal	Clean	0.40-1.00	0.30-1.00
Metal on metal	Unlubricated	0.20-0.40	0.15-0.30
Metal on metal	Lubricated	0.05-0.12	0.05-0.12
Metal on unmetal	Unlubricated	0.40-0.60	0.30-0.80
Metal on unmetal	Lubricated	0.05-0.12	0.05-0.12

By evaluating the friction factors, one can determine which completion fluid that should be used. It is evident that a completion fluid with lubrication is preferable.

When lowering the string, drag will occur due to the dynamic friction factor. If the compressive forces exceeds the buckling limit and causes the string to get stuck or even lock up, a static friction factor applies. The static friction factor is higher than the dynamic friction factor. A tubing should be designed based on the worst-case-scenario, and it can therefore a better choice to use the static friction factor to avoid potential lock-up. To predict a realistic scenario, a variation of friction factors should be used.

The string is normally not rotated during tripping. When rotating the string, the friction is reduced, thus it is common with lower friction factors in drilling operations. Dynamic friction factors experienced while drilling are between 0.1 and 0.3.

5.1.2   Lock-up conditions

Lock-up can be defined as the situation when the surface axial force turns from tension to compression. In this case, the additional surface weight will cause the tubing to buckle in the upper part of the well. If the compression is increased further at surface, the buckling severity will consequently increase. The lower part of the tubing will not be significantly affected by this, as the drag force will add as additional friction force in the first pitches (He et al., 1995, 13). Hence, the tubing can not be pushed any further into the horizontal section.

Some completions are designed for zone isolation. It is critical that the horizontal part of the completion gets installed at the correct depth. A buckled liner or tubing will be shorter than the initial length, and lack of predictions can cause tubing assemblies to be at wrong depth in relation to the reservoir. An intervention to get a proper overview of the tubing location can be costly, and is something that should be avoided.

It was expected that the both well paths would give similar curves. It was rather found that the real well path was very much affected by the coefficient of friction. When the coefficient of friction increases from 0.4 to 0.5, the tubing configuration locks-up for the real well path, while the hook load remains in tension for the ideal well path.

In the ideal well path, the dog leg angle is constant throughout the curved sections. This is not the case in the real well path. Since the real well path is adjusted to certain targets in Compass, small dog leg variations will occur. In Compass, this is seen as rapid changes in inclination, creating an incremental curve instead of a smooth curve. In real wells, dog leg variations will occur due to irregularities in the wellbore. This is called tortuosity, and causes friction to build up while the string is lowered. Qualitatively, one can assume that tortuosity is included in the friction factor (B.S. Aadnoy, personal communication, May 30, 2018). One can therefore reach higher values than expected. One should therefore carefully consider the dog leg variation and friction factors when installing a completion in a long-reach horizontal well.

This reasoning can be verified. A full-scale experiment was conducted on a research well, and it was found that local curvatures were significant, as they contributed to an earlier lock-up situation than expected from the ideal model. (Weltzin et al., 2009)

The critical limit for helical buckling is higher than the compressive force in the horizontal section. Drag in the straight section was calculated under the assumption that weight dominates. One will not expect any helical buckling here, as the buckling limit is high and the tubing is stable. However, the growth of sinusoidal buckling can be expected, and this causes associated increase in contact forces (Payne et al., 1996).

5.1.3 Evaluation of critical buckling limits

For the vertical section, the critical buckling limits are calculated by equation (3.8) and (3.9). It is clear that the buckling limit in the vertical section is low, and the transition between sinusoidal and helical buckling will not be of significant importance in these simulations.

For the deviated sections, equation (3.10) is used. The limit increases significantly in the build up from 0 to 85 degrees. The limit in the tangential section is constant before it increases slightly from 85 to 90 degrees.

According to Mitchell et al. (1999), there is a transition period between 1.4 and 2.8 times the Paslay Dawson equation where helical buckling can occur. Figure 5.1 illustrates how the limits are defined.
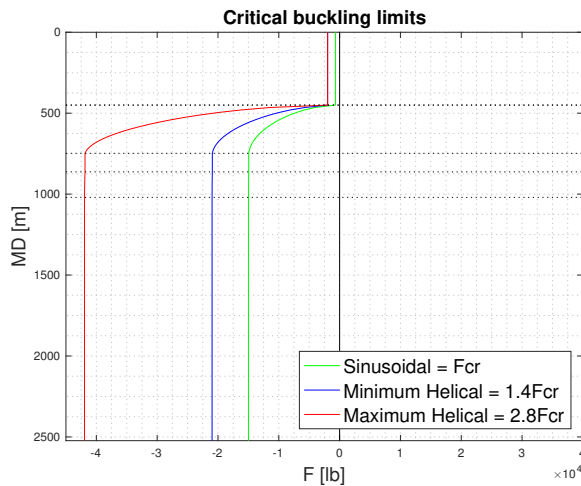
Figure 5.1: Sinusoidal buckling limit is defined by the Paslay Dawson equation. The transition between sinusoidal and helical buckling occurs between 1.4 and 2.8 times the Paslay Dawson limit.

5.1.3.1 Effect of curvature

For the highest friction considered, μ=0.45, one can not see any indications of helical buckling in the straight, deviated sections. Using the Paslay-Dawson equation in the curved sections, indicates a transitional region for helical buckling.

According to He et al. (1995), a curved section will provide additional support to a tubing in compression. If one includes the contact forces initiated by curvature effects like build-up/azimuth rate, the buckling limit can actually be higher than expected. If the limit for sinusoidal buckling is higher than expected in the first build up section, the pipe will remain straight at the low side of the bend.

The tangential section will not experience any buckling as it is below the sinusoidal buckling limit. Moving further down to the horizontal section in the well, the model proposed by He et al. (1995) does not apply. Hence buckling can be present in this straight section, even if it is suppressed in the build sections.

Figure 5.2 presents a graphical visualization of this scenario.
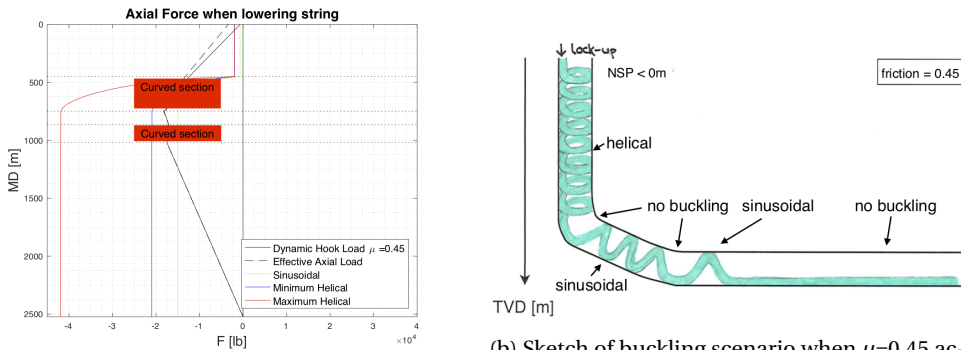
(a) μ=0.45 with the curved sections clearly illustrated

(b) Sketch of buckling scenario when μ=0.45 according to He et al. (1995)

Figure 5.2: Buckling during installation when μ=0.45. The effects of curvature is included in the sketch.

5.1.3.2 Hypothetical scenario of helical buckling in horizontal section

Consider a case where the effective axial force exceeds the helical buckling limit in the horizontal section.

To understand the consequences, a hypothetical scenario is analyzed. To get the effective axial force to exceed the minimum helical buckling limit in the horizontal section, the friction factor had to be set to $\mu = 0.6$. The effective axial force will now be within the helical transition zone in the horizontal section. If geometrical irregularities is present, helical buckling can occur in the horizontal section.

According to table 5.1, a friction factor of 0.6 matches the combination "clean surface, metal on metal" or "unlubricated, metal on unmetal". It can therefore theoretically be a scenario when running pipe in an open hole with water based mud.

If it is assumed that any curvature increases the buckling limit over the operational force, the following scenario is expected: The tubing will helically buckle in the vertical section. It will not be buckling in the curved section. Helical or sinusoidal buckling will be present in the tangential section, while there is no buckling in the next curved section. Finally, there will be either helical or sinusoidal buckling in the horizontal section. Figure 5.3 presents the hypothetical scenario of installation of the completion with a friction factor of 0.6.
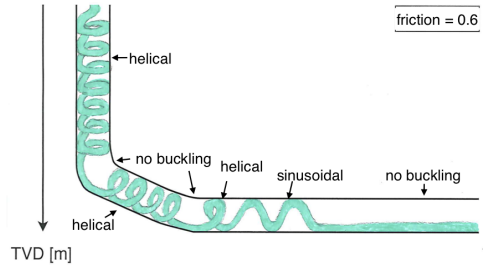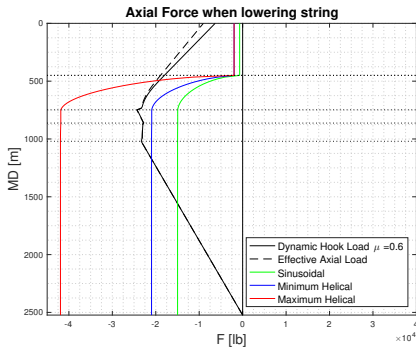
(a) μ=0.6 for tubing within 6 5/8" casing

(b) Sketch of buckling scenario when μ=0.6

Figure 5.3: Hypothetical scenario of buckling during installation when μ=0.6

Previous knowledge have shown that the tubing locks-up for a friction factor of 0.45. Adding more weight on surface, will only cause the vertical section to buckle more severely, without affecting the tubing in the horizontal section. Figure 5.3 is therefore an unrealistic scenario for this well path.

5.1.4 Quality and shortcomings

Analyzing a real well path had the advantage that it included the tortuosity effect in the build up sections. The dog leg variation caused friction to build up in the string, thus pushing the neutral stability point higher up than expected.

A shortcoming of the model is that it was simulated with a constant friction factor. In real well operations, the friction factor will vary due to fluid parameters like viscosity and density. If the well is not clean, remains could cause friction to build up.

In this analysis it was assumed that the tubing string was lowered within a casing that ensures a constant radial clearance. If the string was entering a section with a larger radial clearance, it would decrease the buckling limit in the deviated section, hence increasing the possibility of buckling. Figure 5.4 shows that the radial clearance affects whether there is a possibility for helical buckling in the horizontal section or not. A lower radial clearance will stabilize the tubing.

(a) μ=0.45 for tubing within 6 5/8" casing

(b) μ=0.45 for tubing within 9 5/8" casing
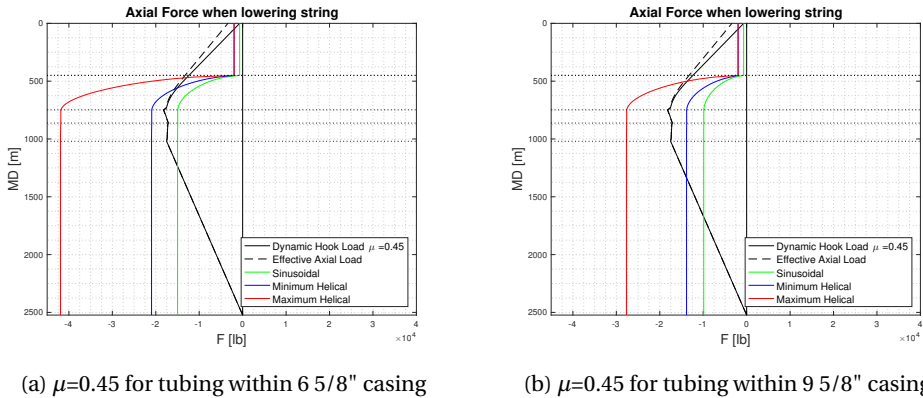
Figure 5.4: Comparison of critical buckling limits for a tubing inside a 6 5/8" casing and 9 5/8" casing

Radial clearance is shown to be of importance. The largest casing increases the possibility of buckling in the deviated sections. There are two situations that will cause the radial clearance to increase: a smaller tubing outer diameter, or a larger casing inner diameter.

If the tubing were to enter the open hole, both friction and radial clearance would increase. This is not accounted for in the model.

When analyzing drag forces while lowering the string, it was convenient to include the buckling limits in every section.

Contact force due to helical buckling was not included in the drag model. Weltzin et al. (2009) did a full-scale experiment where no friction where experienced in the vertical section, even though helical buckling was present. The theoretical model can therefore be correct when not including friction in the vertical part. Weltzin et al. (2009) concluded that friction from sinusoidal buckling could be of significance in deviated wells. The contact force from sinusoidal buckling is calculated in the same manner as the normal force from the tubing weight (Mitchell et al., 1999). The contact force induced by helical buckling would probably replace the normal force from the tubing weight.

5.1.5   Future improvements

The model is based on two equations where one is assumed to be tension-dominated, and the other weight-dominated. Numerical aids are beneficial for complex calculations, thus both tension and weight should be implemented in all sections.

An argument for simulating scenarios for high friction factors is to create a worst case scenario, as is common practice in tubing design. The program should be able predict the earliest possible time of a potential lock-up situation.

The model by He et al. (1995) should be implemented, to get a clear representation of buckling in the curved sections.

A future improvement is to implement vectors with exact measurements for each part of the well. A vector consisting of friction factors adjusted for the realistic scenario would give a more reliable result. A vector could also include different radial clearances. Variations could be due to wear, tubing connections or crossovers. An open hole will also have varying diameter due to washouts and other irregularities.

The contact force due to helical buckling in the deviated sections should be included if buckling is present. The induced contact force can make it more difficult to reach the desired depth. This is particularly important for perforation and zone-isolation.

There should be conducted full-scale experiments to be able to predict buckling in horizontal wells. Few full-scale experiments give a poor foundation for the analytic models.

5.2 Buckling During Operations

5.2.1   Implementation challenges

When implementing the model by Lubinski et al. (1962) on a shallow, horizontal subsea well, some considerations had to be done:

1. Lubinski et al. (1962) defines compression as a positive force and tension as a negative force. A complete review of the model had to be done to change compression to a negative force and tension to a positive force.

2. Well path configuration. Lubinski et al. (1962) uses a vertical well in the model. The correct measurements for TVD and MD had to be implemented in the script for accurate hydrostatic pressure calculation.

3. Packer configuration. Lubinski et al. (1962) uses a packer configuration that gives $A_p \neq A_i$. A polished bore receptacle (PBR) is assumed to be installed, hence the packer bore, A_p, equals the inner area, A_i.

4. The well design pressure (WDP) had to be considered. The wellhead on a shallow, horizontal well will have a lower tolerance for pressure than a deep, vertical well. The load cases therefore needed to be adjusted to WDP. For this well, WDP=1892psi.

5. The load cases involves fluids in static conditions. Equation (3.24) is therefore replaced by equation (3.25) in the model to evaluate the ballooning effect in static conditions.

5.2.2   Load cases that can induce buckling

According to theory, positive length changes in combination with a high inner pressure will give the worst buckling scenario. Tubing elongation leads to compressive packer forces, and when compression adds up in the bottom of the string, the neutral stability point will be located higher than it was.

Tubing elongation is caused by slack-off, thermal expansion and reverse ballooning. Slack-off is not recommended in a long horizontal well, as the weight applied on the surface can cause unwanted buckling in the vertical section. Reverse ballooning occurs when the change in outer pressure is higher than the change in inner pressure. An increase in outer pressure will stabilize the tubing, thus this is not the worst case with regards to buckling. This leaves thermal expansion as the critical effect.

Buckling was not associated with neither the shut-in or start bullheading load case. These are considered to be of secondary importance, and the discussion of these is therefore added to Appendix A.

5.2.3 Set packer procedure

Initially, the lower part of the tubing will be in compression due to the pressure acting on the bottom of the tubing. When the process of setting the packer is initiated, the inner pressure will increase. The ballooning effect will cause the tubing to contract. When the packer opposes this desired length change, it acts with a tensile force. The packer force is high enough to leave the entire tubing in tension. According to theory in section 3.1, the tubing can buckle even though it is completely in tension.

For the set packer situation, the neutral stability point is located in the vertical section. Figure 5.5 shows results of the simulation. The effective force at the bottom of the string is also higher than the effective force at the bottom of the vertical section.

in
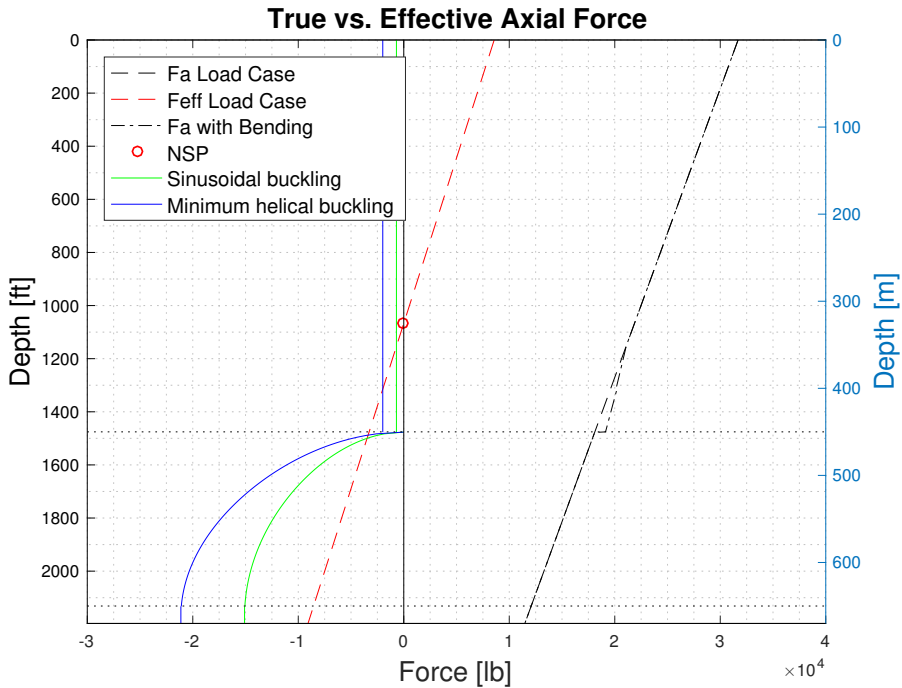
Figure 5.5: The effective axial force exceeded the critical buckling limits in the vertical section. No buckling is shown below the vertical section

5.2.4   Evaluation of buckling length changes

When buckling occurs, the tubing will have the desire to shorten due to the buckling itself. According to theory, the are two ways to calculate buckling length change. The method depends on the buckling shape and well deviation.

The Lubinski et al. (1962) method is developed for a vertical well. It was assumed that a fictitious force at the bottom of the tubing will induce helical buckling from the bottom of the string up to the neutral stability point. The length change is in other words calculated from the effective force at packer depth.

The buckling length change calculation is more complex when several buckling regimes are evaluated in a deviated well.

The critical buckling limit for the vertical section is compared with the effective axial force. The limits suggests that the vertical region below the neutral stability consists of three scenarios: first no buckling, then sinusoidal buckling and finally helical buckling. Figure 5.5 shows that buckling is suppressed in the build-up section. Due to the discussion in 5.1.3, the limits can be expected to be even higher. It is therefore confidently assumed that no buckling occurs within this region.

Let the vertical section in figure 5.5 be considered as an isolated system. The effective axial force acting on the bottom of the tubing in the vertical section will be the force that induces the helical buckling. It is therefore this force that should be used to give more accurate predictions for helical buckling length changes.

The vertical region consists of both sinusoidal buckling and helical buckling. Equation (3.21) for helical buckling will overestimate the length change, while equation (3.41) for sinusoidal buckling will underestimate the length change. The real length change is found between these solutions. A weighted average should be calculated to find an approximate length change over the vertical section.

5.2.4.1   Weakness in model

The model is set by default to calculate the buckling length change associated with helical buckling. One single iteration is required to calculate the length change associated by sinusoidal buckling instead. This is assumed reasonable for vertical well sections due to the uncertainty on the critical buckling limits in the vertical well. The transition zone between helical and sinusoidal buckling can be relatively small, and the helical buckling length change will give the worst-case scenario. Buckling length change is deviated sections should be modified, as the transition between sinusoidal buckling and helical buckling would be of significance.

However, the effective axial force used in the calculation is the force at packer depth. This is not correct, and a weakness in the model.

5.2.4.2 Future improvement

A future recommendation is to implement the following iterations if buckling occurs in the vertical section for a general well path:

1. Implement load case

2. Calculate the effective axial force as if the tubing was free to move

3. Assume helical buckling in entire tubing

4. Calculate buckling length change with the effective axial force at the bottom of the string

5. Find packer force and plot the effective axial force with the critical buckling limits

6. If buckling only occurs in the vertical section, find effective axial force at the bottom of the helical buckling region and sinusoidal buckling region

7. Return to the buckling length change calculation, and calculate the a new weighted average of the buckling length change using the force for helical and sinusoidal buckling respectively.

8. Repeat procedure. Calculate packer force and plot the effective axial force with the critical buckling limits.

9. Repeat until the buckling length change converges.

The length change associated with buckling is often the smallest length change. The consequences of over- or underestimating this length changes is not severe compared to the other effects. However, this contributes to the uncertainty that revolves around axial forces. A more accurate prediction of buckling length change will improve axial analysis.

5.2.5 Vertical depth sensitivity

The same well path was considered as a subsea well with wet x-tree, to see the effect of a reduced vertical section. 400 meters of the vertical section is now replaced with seawater, and the initial hydrostatic pressures will now be the weight of the water. The reservoir pressure and temperature is assumed to be the same as in the previous case. The neutral stability point is calculated for the same load cases as earlier. The main difference is that the tubing length is reduced by 400 meters, and the vertical section now equals 50 m. This subsea well is based on an existing well path under development known by the author.

Figure 5.6 shows where the neutral stability point was located during each load case.

(a) Set packer

(b) Start bullheading with gas filled well

(c) Start bullheading with oil filled well

(d) Shut-in
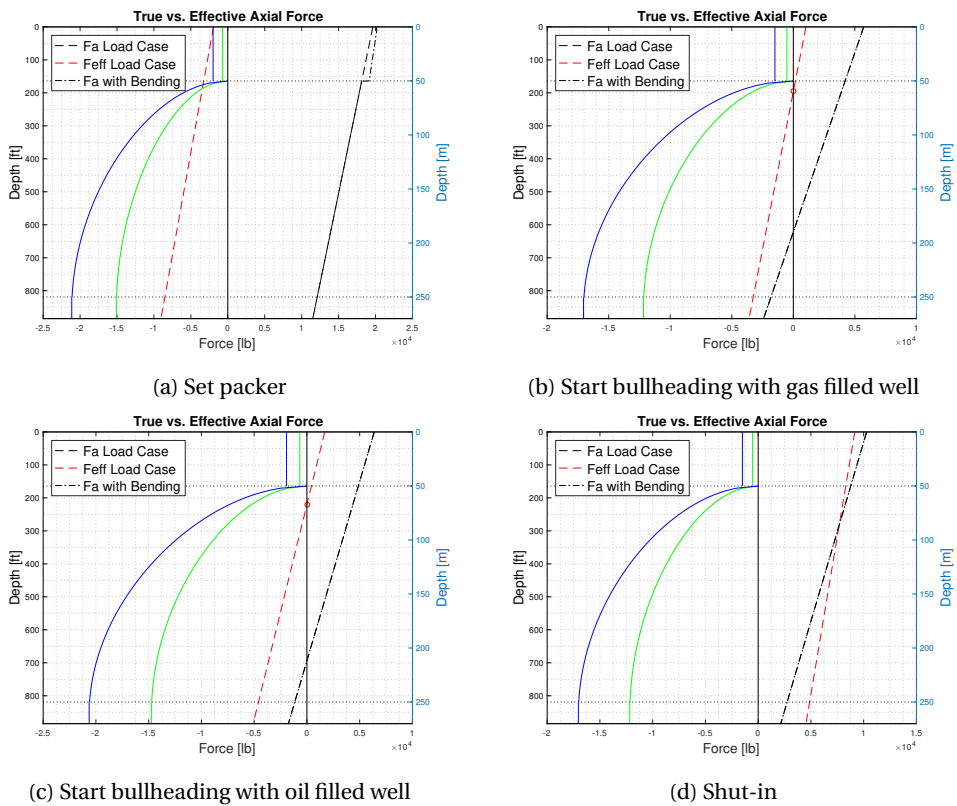
Figure 5.6: Location of neutral stability point in a shallow subsea well with wet tree

The set packer case causes the neutral point be located above the string. It means that compression will be expected at the wellhead. At the wellhead, the main concern is wellhead growth. This takes place when the tubing is under compression at the tubing hanger. As the wellhead is an important element in the primary barrier envelope, this should be carefully considered. To avoid this problem, a packer that require a lower set pressure should be considered.

5.2.6 Quality and shortcomings

5.2.6.1 Evaluation of parameters

Tubing and casing properties are defined as input. This makes it convenient to investigate whether the impact of radial clearance on buckling. The model is further generalized to work for any load case. The load cases can easily be implemented in the model by defining densities, pressures and temperatures.

It is assumed that the tubing is thick-walled when permanent corkscrewing is calculated. This is the same assumption used in the WellCat software. For the pipe considered in this thesis, this assumption is correct. If another tubing is desired, and it does not fall in under the definition "thick-walled", the analysis of permanent corkscrewing should be modified.

The model developed by Lubinski et al. (1962) does not account for couplings or connections. It is possible that high bending stresses causes the threads to deform, thus making connections the weak points in the completion. Failures related to connections might be both structural and leak failures (Bellarby, 2009, 544). A future improvement would be to include the effects of bending stress on connections.

The buckling models presented in this thesis does not include friction. Vibrations will most likely occur during production or injection, and cause the frictional forces to be negligible with regards to buckling severity. However, will vibration effects not necessarily mitigate friction in highly deviated wells. It is previously presented by Mitchell et al. (1996) that friction can affect the axial stress during production or injection. A future improvement would be to evaluate buckling by considering friction.

The entire model takes on average between 2 seconds to run. It is therefore a time efficient method to evaluate length changes, packer forces, neutral stability point, permanent corkscrewing and critical buckling.

5.2.6.2 Evaluation of the pitch

The theoretical expression for pitch is given by Lubinski et al. (1962) in equation (3.7). The pitch is defined as the length between to spirals. The pitch will decrease with increasing compression, and will the tubing buckle more severely at the bottom part of the string. However, assumptions behind this equation limits the application. The pitch in equation (3.7) is defined as the distance between spirals, just above the lower end of the tubing. The pitch is not included in this model due to its limited practical application.

A future improvement would be to estimate a variation of the pitch over an entire buckled interval. This would make it possible to determine the exact location of the string in the well. This technology could also be applied in drilling engineering when hole cleaning is a problem. While circulating the well, it will be beneficial that the pipe is located at high side. This will create a flow path below the pipe, and the accumulated mud or dirt can be flushed out. (S. Sangesland, personal communication, March 13, 2018)

5.2.6.3 Temperature and pressure implementation

Lubinski et al. (1962) developed the model from a vertical well, while Mitchell et al. (1999) added a sail section directly to the vertical section. Neither of those assumptions are valid when developing the model for a horizontal well. The main problems are the temperature and pressure calculations. A future improvement is to include exact measurements of pressure and temperatures in the entire well. In a deviated well, the hydrostatic pressure will be the same throughout the entire horizontal section, causing the mean pressure to be underestimated by the traditional arithmetic average. A weighted average of the pressure and temperature would give a better estimation.

5.2.6.4 Evaluation of geometrical imperfections.

The theory behind critical buckling limits suggests that the effective axial force needs to exceed a critical limit before sinusoidal buckling occurs. I.e. the tubing is assumed perfectly straight before the sinusoidal is developed. The critical buckling limits determined for a vertical well is debated (Cunha et al., 2003), and different coefficients to determine sinusoidal and helical buckling is suggested. A long tubing run in a well can be subjected to multiple defections. In a vertical well, the practical importance of the different coefficients is therefore limited.

An experimental and analytic study of sinusoidal buckling in vertical wells was conducted by Salies et al. (1994), and it was found that equation (3.8) by Lubinski et al. (1950) is a good approximation for a a tubing length equivalent to $7.94 \times (\frac{EI}{w_b})^{1/3}$. For strings with lengths greater than this, $\frac{L}{(\frac{EI}{w_b})^{1/3}} > 7.94$, the critical limit is less. A quick calculation shows that the length of the vertical section considered in this thesis is equivalent to $33 \times (\frac{EI}{w_b})^{1/3}$. Hence, the analytic limit for sinusoidal buckling can be less than expected according to Salies et al. (1994). Further, the experiments conducted in Salies et al. (1994) confirmed that the critical buckling limit was less. When the length was further increased, the critical limit decreased towards a constant value.

The author assumes that geometrical imperfections will determine when the real critical limit is reached. The longer the pipe is, the more deflections is present. It is therefore possible that sinusoidal buckling occurs between $F_{eff} = 0$ and $F_{eff} = 1.94(EI w_b^2)^{1/3}$ in a vertical well. Full-scale experiments should be performed to give a better foundation for the analytic models.

5.2.7 Evaluation of industry software

WellCat assumes that helical buckling occurs in vertical sections when F_{eff} is negative. This leaves no room to evaluate how different buckling regimes impacts the stress regime. This assumption affects length change calculations, packer force predictions,

contact force and bending stress.

WellCat uses equation (3.10) to determine whether the tubing buckles or not in straight deviated sections (Horgen, 2010). This critical buckling limit determines when stable sinusoidal buckling occurs. By using the Paslay Dawson equation to predict the onset of helical buckling, an implicit safety factor will be included. This is therefore a conservative method to predict buckling. It can be useful for critical well applications (Aasen et al., 2002), but it contributes to the uncertainty of axial force analysis.

The model presented in this thesis includes the critical buckling limits, thus opens the possibility to investigate this further. The simulation of a horizontal well gives a more complex result than a vertical well. The study of buckling during operations show that WellCat is conservative in its buckling analysis for both vertical and straight deviated wells.

Chapter 6

Conclusion

- A comprehensive study of the theoretical foundation behind buckling analysis is conducted, and the most acknowledged theory behind critical buckling limits are presented.

- A critical buckling ratio is suggested. This method can be used to see if one tubing is better than another with regards to buckling.

- A buckling model has been developed for installation of a completion. The model accounts for dog leg variations in all well sections, and predicts lock-up in the string. The drag forces were underestimated when dog leg variations was not included.

- WellCat is found to perform conservative buckling analysis for both vertical and straight, deviated wells.

- Buckling analysis is improved by supplementing the existing models with the latest of theory. These models were modified to be applicable for all well designs.

- The model developed for well operations is an integrated model that calculates the axial forces, the packer force and permanent corkscrewing. An initial installation strategy can also be chosen by implementing a variation of slack-off or pick-up forces.

- The calculation of buckling length change have contributed to uncertainty of the actual axial forces. A more accurate prediction of buckling length improves axial analysis.

- Compressive forces and geometrical imperfections affects the likelihood of buckling. It is found that buckling can occur even if the tubing is completely in tension.

- Transforming the subsea well from a dry tree to a wet tree causes significant difference because of the reduction in vertical extent. Wellhead growth is expected to be a problem for the subsea well during the set packer procedure.

- Buckling is not equivalent to failure. Permanent corkscrewing did not occur for installation nor critical operations.

Chapter 7

Further Work

7.1 Buckling During Installation

- Apply the weight- and tension equation in App. E from Aadnoy et al. (2010) for more accurate drag-analysis in the horizontal section.

- Include the critical buckling limit by He et al. (1995) for the curved sections.

- Implement vectors to account for a variation parameters like radial clearance and friction factor in the installation phase.

- Include contact force by helical buckling in drag calculations.

- The three-dimensional model presented by Bellarby (2009) neglects bending stiffness. The bending forces should be implemented in such a model to give a realistic view of the drag analysis. A recently published model (Mirhaj et al., 2016) presents a three-dimensional stiff-string model for torque and drag. Further work can be to compare these models and evaluate the effect of bending stress.

- Full-scale experiments should be conducted to predict accurate buckling scenarios in horizontal wells.

7.2 Buckling During Operations

- Implement the iterative process for buckling length changes

- Include measurements of exact pressure and temperatures during operations, or calculated a weighted average.

- Develop an equation for the pitch over the entire buckled interval.

- Include the effect of friction between the tubing and casing.

- Conduct full-scale experiments in horizontal wells to evaluate the importance of friction in temperature dominant operations.

- Include the effects of bending stress on connections.

7.3   General

Further work is to investigate the tubing condition from installation to further operations. This model will be able to account for tubing wear from the installation process.

Bibliography

Aadnoy, B. S. (2010). *Modern well design.* CRC Press.

Aadnoy, B. S., Cooper, I., Miska, S. Z., Mitchell, R. F., and Payne, M. L. (2009). *Advanced drilling and well technology.* SPE.

Aadnoy, B. S., Fazaelizadeh, M., Hareland, G., et al. (2010). A 3d analytical model for wellbore friction. *Journal of Canadian Petroleum Technology*, 49(10):25–36.

Aasen, J. A., Aadnøy, B. S., et al. (2002). Buckling models revisited. In *IADC/SPE Asia Pacific Drilling Technology.* Society of Petroleum Engineers.

Bellarby, J. (2009). *Well completion design*, volume 56. Elsevier.

Cunha, J. et al. (2003). Buckling of tubulars inside wellbores: a review on recent theoretical and experimental works. In *SPE Production and Operations Symposium.* Society of Petroleum Engineers.

Dawson, R. et al. (1984). Drill pipe buckling in inclined holes. *Journal of Petroleum Technology*, 36(10):1–734.

Halliburton (2001). *WellCat Manual.* Landmark Graphics Corporation.

He, X., Kyllingstad, A., et al. (1995). Helical buckling and lock-up conditions for coiled tubing in curved wells. *SPE Drilling & Completion*, 10(01):10–15.

Hearn, E. J. (1997). *Mechanics of Materials 2: The mechanics of elastic and plastic deformation of solids and structural materials.* Butterworth-Heinemann.

Horgen, T. (2010). Analysis of packer forces in vertical wells and frictionless sail sections. Master's thesis, University of Stavanger, Norway.

Kwon, Y. W. et al. (1988). Analysis of helical buckling. *SPE drilling engineering*, 3(02):211–216.

Lubinski, A., Althouse, W., et al. (1962). Helical buckling of tubing sealed in packers. *Journal of Petroleum Technology*, 14(06):655–670.

Lubinski, A. et al. (1950). A study of the buckling of rotary drilling strings. In *Drilling and Production Practice.* American Petroleum Institute.

Mirhaj, S., Kaarstad, E., Aadnoy, B., et al. (2016). Torque and drag modeling; soft-string versus stiff-string models. In *SPE/IADC Middle East Drilling Technology Conference and Exhibition*. Society of Petroleum Engineers.

Mitchell, R. et al. (1988). New concepts for helical buckling. *SPE Drilling Engineering*, 3(03):303–310.

Mitchell, R. et al. (1996). Comprehensive analysis of buckling with friction. *SPE Drilling & Completion*, 11(03):178–184.

Mitchell, R. et al. (1997). Effects of well deviation on helical buckling. *SPE Drilling & Completion*, 12(01):63–70.

Mitchell, R. et al. (1999). Buckling analysis in deviated wells: A practical method. *SPE Drilling & Completion*, 14(01):11–20.

Payne, M., Abbassian, F., et al. (1996). Advanced torque and drag considerations in extended-reach wells. In *SPE/IADC Drilling Conference*. Society of Petroleum Engineers.

Remmen, T., Bauge, E., and Wilhelmsen, K. (2017). Analysis of the industry standard and practice for casing and tubing design. In *Project Report*. NTNU.

Salies, J., Cunha, J., Azar, J., Soren Jr, J., et al. (1994). Experimental and analytical study of sinusoidal buckling in vertical wells. In *SPE Eastern Regional Meeting*. Society of Petroleum Engineers.

Weltzin, T., Aas, B., Andreassen, E., Lindland, M., et al. (2009). Measuring drillpipe buckling using continuous gyro challenges existing theories. *SPE drilling & completion*, 24(04):464–472.

Wu, J., Juvkam-Wold, H. C., et al. (1995). Coiled tubing buckling implication in drilling and completing horizontal wells. *SPE Drilling & Completion*, 10(01):16–21.

Appendix A

Additional Information

A.1 Derivation of Pitch

Figure A.1 displays the geometry of a helix confined within a cylinder.
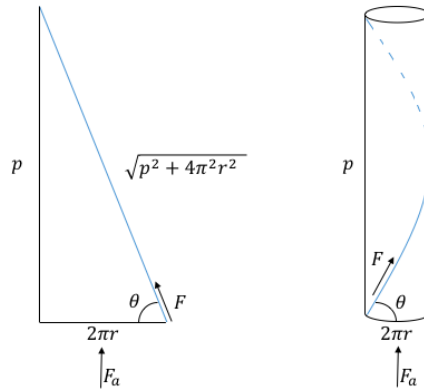
Figure A.1: Visualization of helix geometry within a confining cylinder

Basic trigonometry is used to obtain the following relations:

$$\sin\theta = \frac{F_a}{F} \tag{A.1}$$

$$\sin\theta = \frac{P}{\sqrt{P^2 + 4\pi^2 r^2}} \tag{A.2}$$

Combining equation (A.1) and (A.2) gives the expression for F_a:

$$F_a = F\frac{P}{\sqrt{p^2 + 4\pi^2 r^2}} \tag{A.3}$$

Conservation of energy is used to find the force required to buckle a string. The principle goes as following:

$$E_i = E_f \tag{A.4}$$

where E_i and E_f is the initial and final energy in the system, respectively.

Energy can not just occur nor disappear, hence we say that energy is conserved. The initial energy must equal the final energy. We consider the tubing string to be a static system, hence the kinetic energy is zero. Before the tubing is subjected to deformation, potential energy will build up in the system. The potential energy consist of strain energy of compression, strain energy of bending and the potential energy of a force subjected to the material.

Strain energy, U_{strain}, is the energy stored in a system undergoing deformation. For a cylinder, strain energy is defined as:

$$U_{strain} = \frac{1}{2} \frac{V}{E} \sigma^2 = \frac{1}{2} \frac{A_s L}{E} \frac{F_a^2}{A_s^2} = \frac{1}{2} \frac{L}{E} \frac{F_a^2}{A_s} \tag{A.5}$$

where V is volume, A_s is the cross-sectional area and σ is the axial stress.

By combining equation (A.3) and (A.5), the strain energy of compression, U_c is obtained:

$$U_c = \frac{F_a^2 L}{2 A_s E} = \frac{F^2 P^2 L}{2 A_s E (P^2 + 4\pi^2 r^2)} \tag{A.6}$$

When a string is bent, it will store energy from the bending. This is called the bending strain energy, U_b, and it is given by:

$$U_b = \frac{LEIC^2}{2} \tag{A.7}$$

where C is the curvature of the helix.

When the curvature of the helix is given by

$$C = \frac{4\pi^2 r}{p^2 + 4\pi^2 r^2} \tag{A.8}$$

the strain energy of bending becomes:

$$U_b = \frac{8\pi^4 r^2 EIL}{P^2 + 4\pi^2 r^2} \tag{A.9}$$

From geometric similarities, the potential energy from the subjected force is obtained:

$$U_f = FL_h = \frac{FPL}{\sqrt{P^2 + 4\pi^2 r^2}} - \frac{F^2 P^2 L}{A_s E (P^2 + 4\pi^2 r^2)} \tag{A.10}$$

where U_f is the potential energy from a subjected force, and L_h is the length of the helix measured along its axis.

The total potential energy, U, of the system is equal to the sum of strain energies U_c

and U_b and the potential energy from the subjected force, U_f. Equation (A.6), (A.9) and (A.10) is combined to give the final expression for U:

$$U = -\frac{F^2 P^2 L}{2 A_s E (P^2 + 4\pi^2 r^2)} + \frac{8\pi^4 r^2 EIL}{(P^2 + 4\pi^2 r^2)^2} + \frac{FPL}{\sqrt{p^2 + 4\pi^2 r^2}} \tag{A.11}$$

The equilibrium is obtained by minimizing the total potential energy.

$$\frac{dU}{dP} = 0$$

$$\frac{P(P^2 + 4\pi^2 r^2)}{A_s E} F^2 - (P^2 + 4\pi^2 r^2)^{3/2} F + 8\pi^2 EIP = 0 \tag{A.12}$$

The equation was the derivative of total potential energy with respect to the pitch with constant r. Once a helical buckled pipe contacts the wall, r is constant, and P is therefore the only variable (Kwon et al., 1988).

This expression results in two roots. The smallest root corresponds to the smallest potential energy, hence we solve the equation for the smallest root. The following expression is obtained:

$$F = \frac{A_s E \sqrt{P^2 + 4\pi^2 r^2}}{2P} \left[1 - \sqrt{1 - \frac{32\pi^2 IP^2}{A_s (P^2 + 4\pi^2 r^2)^2}} \right] \tag{A.13}$$

Two assumptions were made to simplify this expression. First, $P^2 \gg 4\pi^2 r^2$. This assumption is found reasonable, as it is backed up by other authors (Mitchell et al., 1988). The other assumption is that the second term in the square root will be small. For practical reasons, lets call this term a. Using Taylor expansion on $\sqrt{1-a}$, the expression can be simplified to $1 - \frac{a}{2}$. Equation (A.13) can then be reduced to:

$$F = \frac{A_s E}{2} \left[1 - (1 - \frac{16\pi^2 IP^2}{A_s P^4}) \right] = \frac{8\pi^2 EI}{P^2} \tag{A.14}$$

By rearranging equation (A.14), equation (3.7) in section 3.2.2 is obtained.

A.2   Construction of Build Sections

Figure A.2 and A.3 was used to calculate the length change of each curved section. The technique was described in section 4.3.1.
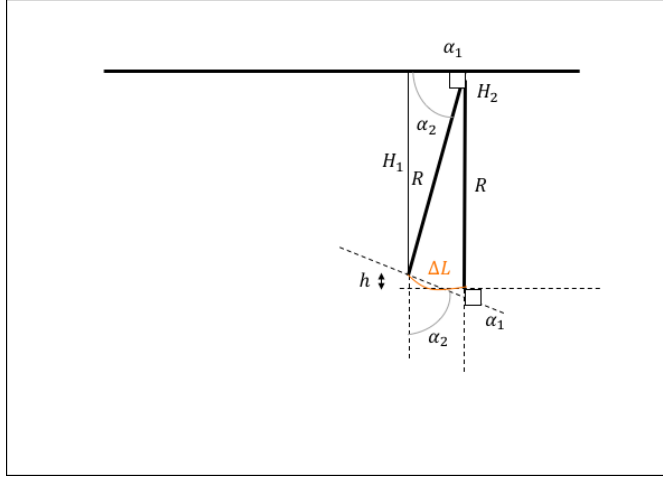
Figure A.2: Illustration of build to horizontal section
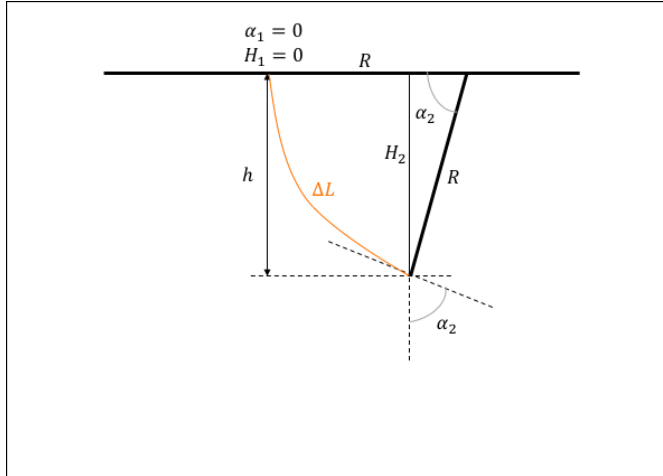
Figure A.3: Illustration of build from vertical section

A.3 Shut-in

During installation, fluids will be circulated in the well. The circulating fluid is affected by surface temperature, and it will be warmer than the sea water temperature. If shut-in is required, the fluids in the well will become static, and the heat will transfer to the surroundings. In practice, this means that the temperature will approach the geothermal gradient. The highest part of the tubing will experience the highest temperature decrease. This will make the tubing contract, and consequently will more tension build up in the tubing string.

It is assumed that gas fills up the well, and the inner pressure will increase. Figure A.4 shows the true and effective axial force when the well is shut in. The length changes associated with this load will only be negative, thus the neutral stability point consequently moves downwards. In this case, the point is located below the string. As the tubing is entirely in tension through the build sections, it is expected that it is located at the high side of the curvatures.

Buckling is definitely not associated with this load case.
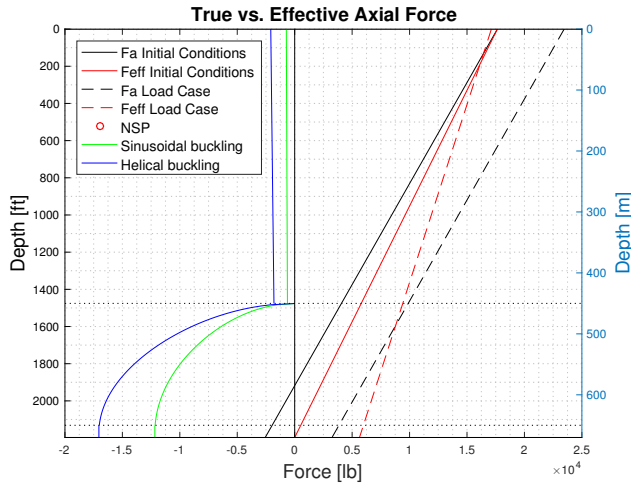
Figure A.4: The negative length changes causes the entire tubing to be in tension during the shut-in load case.

A.4   Start bullheading

The tubing has to be designed to withstand a kill-operation at any time. If there are reasons to kill the well, a surface pressure equivalent the shut-in wellhead pressure (SI-WHP) plus an additional safety margin will be applied. This is known as the well design pressure (WDP). The pressure needs to be this high to ensure the gas filled well is killed. If the well is oil filled when this pressure is applied, the pressure will consequently increase due to the hydrostatic column of oil.

The highest temperature difference in the well after production will be present at the tubing head. This thermal effect will cause the tubing to expand. This positive length change will contribute to a higher compressive load in the tubing.

Effects encountered due to increased inner pressure are ballooning and buckling. Ballooning will have a shortening effect on the tubing, thus reduce the compressive loads. Increasing inner pressure also causes structural instability due to geometrical imperfections, and consequently decreases the effective axial force. Buckling will also occur, and there will be a shortening associated with this effect.

Figure A.5 shows the true and effective axial force when start bullheading is initiated in a gas-filled well. The negative length changes causes the tubing above the horizontal section to be in tension. The inner pressure applied at surface will cause the effective axial force to be shifted to a more compressive state than it was initially, but it is still not enough to expect buckling to occur in any of the sections. The neutral stability point will be located in the build section, and the neutral point is located at the bottom of the build section. This indicates that most part of the tubing is located at the high-side of the curve.
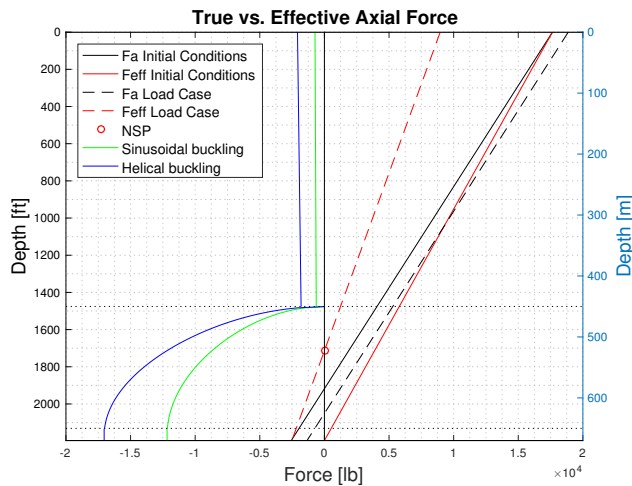
Figure A.5: Critical buckling for start bullheading in a gas filled well.

Figure A.6 shows the true and effective axial force when start bullheading is initiated in a oil filled well. The negative length changes are dominating, indicating that the tubing will be completely in tension. However, the high inner pressure will cause the effective axial force to shift towards a more negative state than it was initially. The neutral stability point will consequently move upwards, and be located in the vertical section. The effective axial force is not high enough to cause buckling in any of the lower sections.
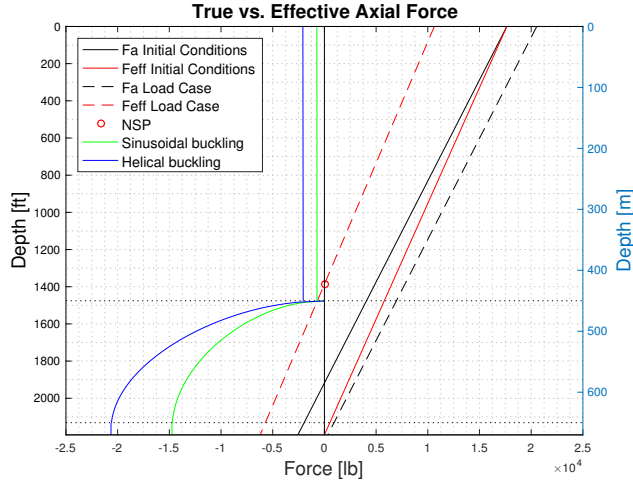
Figure A.6: Critical buckling for start bullheading in a oil filled well.

The start bullheading load case covers the production load case with regards to buckling. During production, the temperature increase will equal the start bullheading case. However, the surface pressure is forced to be very low to be able to produce from the low reservoir pressure. The inner pressure will thus be lower than in the start bullheading scenario.

Appendix B

Critical Buckling Limit

This appendix includes the MatLab scrips used for compiling results from critical buckling limit. The limit is compiled for sinusoidal and helical buckling in a vertical section, straight deviated section of 45 ° and a horizontal section.

Contents

```
clear
clc
```

Critical Buckling Limit

```
% Tubing inputs

% Casing sizes with high D/t-ratios:
%OD      = [18.625 18.625 18.625 18.625 20.000 20.00 20.00 20.000]; %in
%weight  = [87.5   94.5   106    117    94     106.5 133   169];    %lb/ft
%ID      = [17.755 17.689 17.563 17.439 19.124 19.00 18.73 18.376]; %in

% Tubing sizes with low D/t-ratios:
 OD      = [2.875 2.875 3.5   3.5   3.5   3.5   4     4     4.5  ]; %in
 weight  = [6.4   8.6   12.7  10.2  9.2   7.7   9.5   10.7  12.6 ]; %lb/ft
 ID      = [2.441 2.259 2.750 2.922 2.992 3.068 3.548 3.476 3.958]; %in

E       = 30*10^6;                      %psi   Young's modulus
I       = (pi/64)*(OD.^4-ID.^4);        %in4   moment of inertia
t       = (OD-ID)./2;                   %in    thickness

dtratio = OD./t;                        %      D/t-ratio

% Wellpath inputs for deviated well
incl    = 45*pi/180;                    %rad   inclination

% Fluid properties
rhosw   = 1.02;                         %sg    sea water density
rhosteel = 7.89;                        %sg    steel density
buoyedw = (1-rhosw/rhosteel).*weight/12; %lb/in buoyed weight

% Investigate collapse region for grade L80

% D/t-ratio is a vector.

for i = 1:length(dtratio)
    if dtratio(i) < 13.38
        % Thick-walled tubing: Yield collapse
        disp(['Yield Collapse for tubing ', num2str(OD(i)), ...
            'in and #', (num2str(weight(i)))]);
    elseif dtratio(i) < 22.47
        % Plastic Collapse
        disp(['Plastic Collapse for tubing ', num2str(OD(i)), ...
            'in and #', (num2str(weight(i)))]);
    else
        % Thin-walled tubing: Elastic collapse
```

```
        disp(['Elastic Collapse for tubing ', num2str(OD(i)), ...
            'in and #', (num2str(weight(i)))]);
    end
end

% Casing Inputs
%csgID = [32 32 32 32 32 32 32 32];
csgID = [5.921 5.921 5.921 5.921 5.921 5.921 5.921 5.921 5.921]; %in

% Radial Clearance
rc       = csgID/2-OD/2;                %in
```

```
Yield Collapse for tubing 2.875in and #6.4
Yield Collapse for tubing 2.875in and #8.6
Yield Collapse for tubing 3.5in and #12.7
Yield Collapse for tubing 3.5in and #10.2
Plastic Collapse for tubing 3.5in and #9.2
Plastic Collapse for tubing 3.5in and #7.7
Plastic Collapse for tubing 4in and #9.5
Plastic Collapse for tubing 4in and #10.7
Plastic Collapse for tubing 4.5in and #12.6
```

Critical Buckling Force in a vertical section

```
% Sinusoidal buckling is defined by Lubinski et. al (1950)
Fcsinv   = 1.94*(E*I.*buoyedw.^2).^(1/3); %lb

% Helical buckling is defined by Wu et. al (1995)
Fchelv   = 5.55*(E*I.*buoyedw.^2).^(1/3); %lb
```

Critical Buckling Force in an inclined section @ 45 deg

```
% Sinusoidal buckling is defined by Dawson et. al (1984)
Fcsinincl = sqrt((4*E*I.*buoyedw.*sin(45*pi/180))./rc);

% Minimum and maximum helical buckling is defined by Mitchell et. al (1996)
Fchelinclmin = 1.4*sqrt((4*E*I.*buoyedw.*sin(45*pi/180))./rc);
Fchelinclmax = 2.8*sqrt((4*E*I.*buoyedw.*sin(45*pi/180))./rc);
```

Critical Buckling Force in a horizontal section

```
% Sinusoidal buckling is defined by Dawson et. al (1984)
Fcsinhor = sqrt((4*E*I.*buoyedw.*sin(90*pi/180))./rc);

% Minimum and maximum helical buckling is defined by Mitchell et. al (1996)
Fchelhormin  = 1.4*sqrt((4*E*I.*buoyedw.*sin(90*pi/180))./rc);
Fchelhormax  = 2.8*sqrt((4*E*I.*buoyedw.*sin(90*pi/180))./rc);
```

Critical Buckling Force in an inclined section @ 0-90 deg

```
varincl     = linspace(0,90,10);

% Sinusoidal buckling is defined by Dawson et. al (1984)
Fcsinvarincl = sqrt((4*E*I(5).*buoyedw(5).*sin(varincl*pi/180))./rc(5));
```

```matlab
% Minimum and maximum helical buckling is defined by Mitchell et. al (1996)
Fchelvarinclmin = 1.4*sqrt((4*E*I(5).*buoyedw(5).*sin(varincl*pi/180))./rc(5));
Fchelvarinclmax = 2.8*sqrt((4*E*I(5).*buoyedw(5).*sin(varincl*pi/180))./rc(5));
```

Plotting

```matlab
% Plot radial clearance vs. critical buckling force

figure(1)
plot(rc,Fcsinincl,'ko',rc,Fchelinclmax,'k*','markersize',10)
grid minor
legend('\fontsize{16}Sinusoidal buckling','\fontsize{16}Helical buckling')
title('\fontsize{16}Effect of radial clearance on critical buckling limit')
xlabel('\fontsize{16}Radial clearance [in]');
ylabel('\fontsize{16}Critical buckling limit [lb]');

% Plot weight vs. critical buckling force

figure(2)
plot(buoyedw,Fcsinincl,'ko',buoyedw,Fchelinclmax,'k*','markersize',10)
grid minor
legend('\fontsize{16}Sinusoidal buckling','\fontsize{16}Helical buckling' ...
    , 'location', 'northwest')
title('\fontsize{16}Effect of weight on critical buckling limit')
xlabel('\fontsize{16}Weight [lb/in]');
ylabel('\fontsize{16}Critical buckling limit [lb]');

% Plot D/t-ratio vs. critical buckling force
figure(3)
plot(dtratio,Fchelinclmax,'ko', ...
    dtratio,Fchelhormax,'k*','markersize',10);
grid minor
legend('\fontsize{16}Inclined well','\fontsize{16}Horizontal well','location','northwest');
title('\fontsize{16}The effect of D/t-ratio on critical buckling limit');
xlabel('\fontsize{16}D/t-ratio');
ylabel('\fontsize{16}Critical buckling limit [lb]');

% Critical Buckling Ratio

% Ratio1 is the critical buckling ratio for a vertical well.
% Index 5 corresponds to a 3 1/2" #9.2 tubing.
ratio1 = Fchelv/Fchelv(5);

% Ratio2 is the critical buckling ratio for deviated well.
% Index 5 corresponds to a 3 1/2" #9.2 tubing.
ratio2 = Fchelinclmax/Fchelinclmax(5);

% Plot of moment of inertia vs. critical buckling ratio

figure(4)
plot(I,ratio1,'ko',I,ratio2,'k*','markersize',10);
xL = xlim;
line(xL, [1 1],'color','black','linestyle','--');  %x-axis
grid minor
legend('\fontsize{16}Vertical well','\fontsize{16}Inclined/Horizontal well','location','nor
thwest');
title('\fontsize{16}Effect of I on critical buckling ratio');
xlabel('\fontsize{16}Moment of inertia [in4]');
```

```
ylabel('\fontsize{16}Fcr*');

% Plot of radial clearance vs. critical buckling ratio

figure(5)
plot(rc,ratio1,'ko',rc,ratio2,'k*','markersize',10);
xL = xlim;
line(xL, [1 1],'color','black','linestyle','--');  %x-axis
grid minor
legend('\fontsize{16}Vertical well','\fontsize{16}Inclined/Horizontal well','location','nor
theast');
title('\fontsize{16}Effect of radial clearance on critical buckling ratio');
xlabel('Radial clearance [in]');
ylabel('\fontsize{16}Fcr*');

% Plot of inclination vs. critical buckling limit

figure(6)
plot(varincl,Fcsinvarincl,'ko',varincl,Fchelvarinclmin,'k*',varincl,Fchelvarinclmax,'kx','m
arkersize',10);
grid minor
legend('\fontsize{16}Sinusoidal buckling','\fontsize{16}Min helical buckling','\fontsize{16
}Max helical buckling','location','northwest');
title('\fontsize{16}Effect of inclination on critical buckling limit');
xlabel('Inclination [deg]');
ylabel('\fontsize{16}Critical buckling limit [lb]');
```

Effect of I on critical buckling ratio

Effect of radial clearance on critical buckling ratio

Published with MATLAB® R2016a
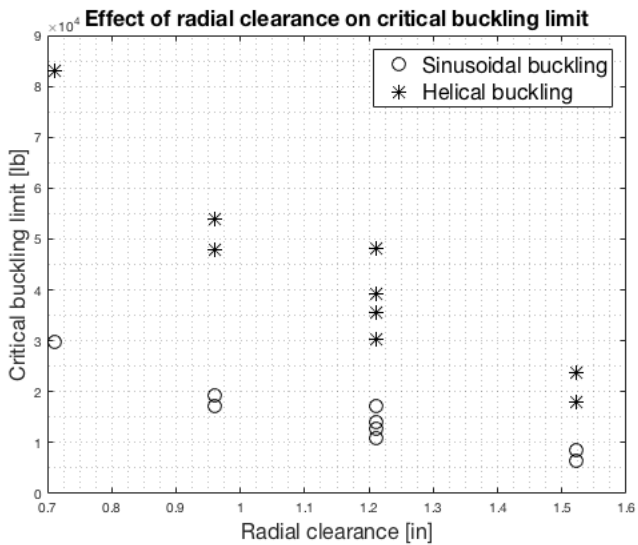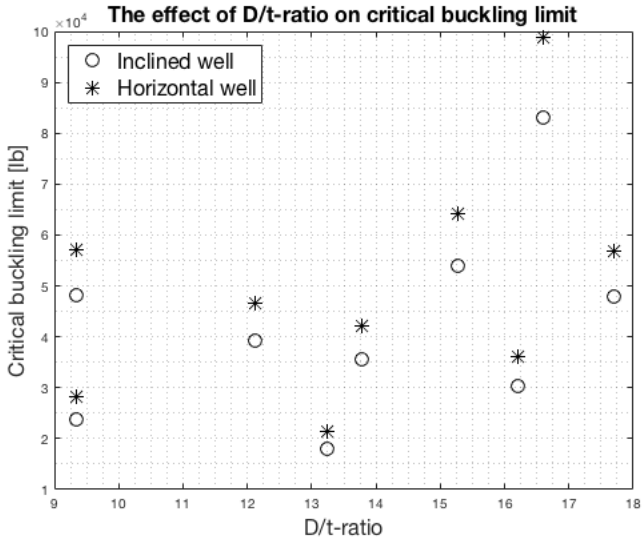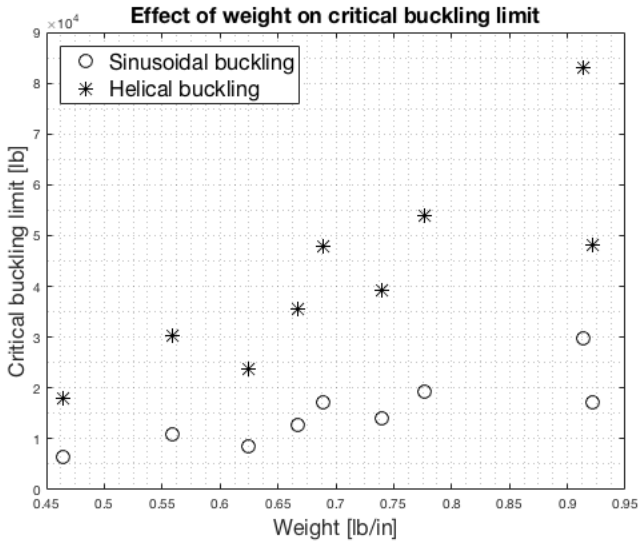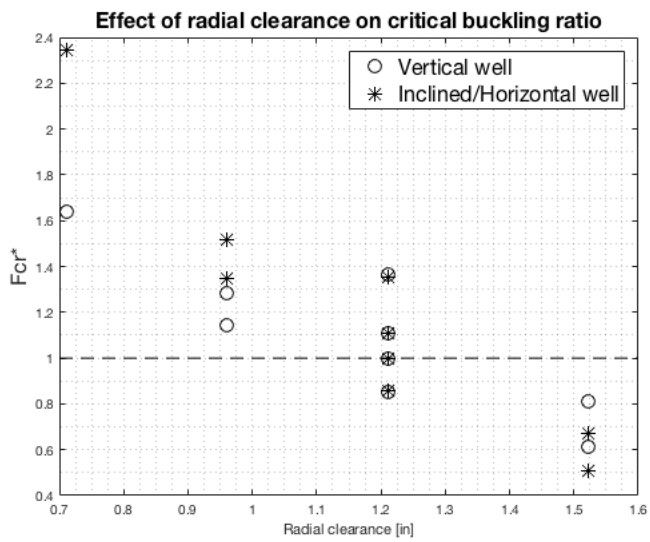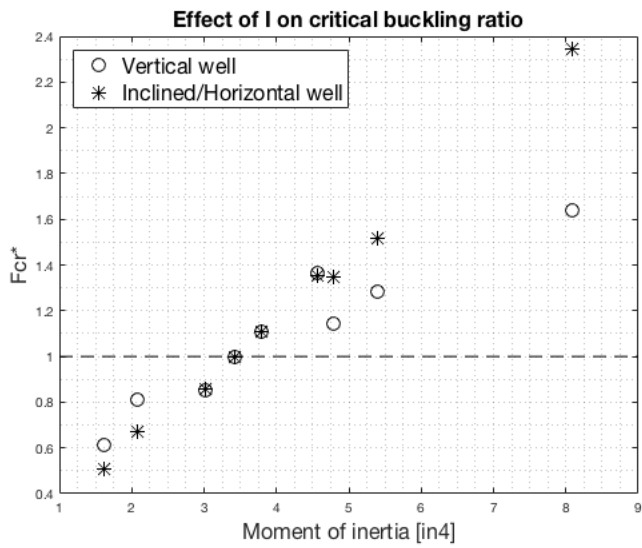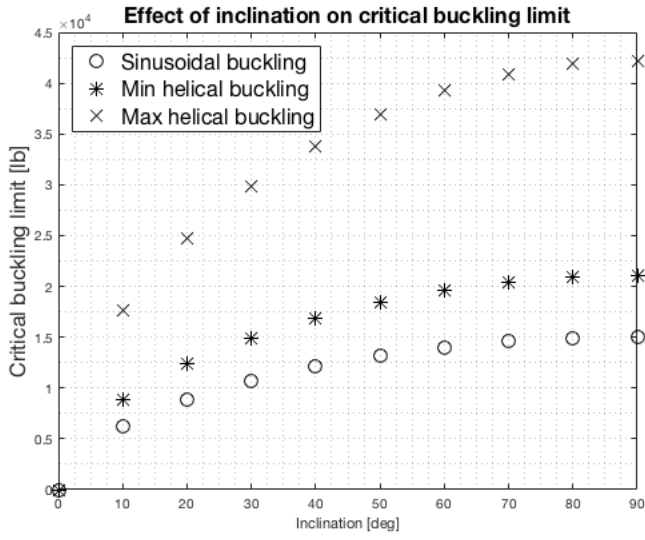
Appendix C

Buckling During Installation

This appendix includes the MatLab scripts used for constructing well paths and performing drag calculation with a variation of friction factors.

The first script constructs the ideal well path. The technique described in section 4.3.1 is used to calculate the build section length. Drag calculations are performed using the traditional method: one section at the time, using one subscript for each section.

The second script imports data from Compass, and constructs the real well path. Drag calculations are performed by creating 99 index points, thus including dog leg variations.

The third and last script uses the real well path, and implements the critical buckling limits.

Contents

```
clc
clear all
```

INPUTS

```
MW        = 1.1;                        % mud weight [sg]
rhosteel  = 65.5/8.33;                  % density of steel [sg]
BF        = 1-MW/rhosteel;              % buoyancy factor [sg]
wDP       = 0.1343;                     % weight of 3 1/2" tbg [kN/m]

% Wellpath Calculations

TVD       = [669.62 667 660 650 450 0]; % total vertical depth [m]
incl      = [89.9 89.9 85 85 0 0];      % well inclination [deg]
incl      = incl*pi/180;                % well inclination [rad]

h         = [0 ...                      % height of each cross-section [m]
              TVD(1)-TVD(2) ...
              TVD(2)-TVD(3) ...
              TVD(3)-TVD(4) ...
              TVD(4)-TVD(5) ...
              TVD(5)-TVD(6)];

R         = [0 ...                      % radius of curvature [m]
              0 ...
              h(3)/(sin(incl(2))-sin(incl(3))) ...
              0 ...
              h(5)/(sin(incl(4))-sin(incl(5))) ...
              0];

L         = [0 ...                      % total well length [m]
              1503.11 ...
              R(3)*abs(incl(3)-incl(2)) ...
              h(4)/cos(incl(4)) ...
              R(5)*abs(incl(5)-incl(4)) ...
              h(6)];

MD        = [sum(L) ...                 % measured depth [m]
              sum(L)-L(2) ...
              sum(L)-L(2)-L(3) ...
              sum(L)-L(2)-L(3)-L(4) ...
              sum(L)-L(2)-L(3)-L(4)-L(5) ...
              sum(L)-L(2)-L(3)-L(4)-L(5)-L(6)];

% To investigate for different friction factors
my        = linspace(0.00,1.0,11);      % friction factor
azi       = [0 0 0 0 0 0];              % azimuth [rad]
WOB       = 0;                          % weight on bit

% Calculate dogleg angle
```

```
DL        = zeros(1,length(L));

for i=1:(length(L)-1)
   DL(i+1) = acos (sin(incl(i))*sin(incl(i+1))*cos(azi(i)-azi(i+1)) ...
            + cos(incl(i))*cos(incl(i+1)));
end

% Equations Lowering String

% If the static hook load equals the axial force with no friction,
% then the code is correct.

staticweight = zeros(1,length(TVD));
statichookload = zeros(1,length(TVD));

for i = 1:length(TVD)
    staticweight(i)  = TVD(i)*BF*wDP;
    statichookload(i)  = staticweight(1)-staticweight(i);
end

statichookload = statichookload*224.8089; % kN to lb
```

Three-dimensional model by Bernt S. Aadnoy

```
F        = zeros(1,length(L));
hookload = zeros(1,length(my));

F(1)     = WOB;

%This friction factor is currently being evaluated
my = 0.5;
for j=1:length(my)
    for i=2:length(L)
        if incl(i)-incl(i-1) == 0
            % the section is straight
            F(i) = F(i-1) + BF*wDP*L(i)*(cos(incl(i))-my(j)*sin(incl(i)));
        else % the section is curved
            F(i) = F(i-1)*exp(-my(j)*abs(DL(i)-DL(i-1)))+ BF*L(i)*wDP*( sin(incl(i))-sin(in
cl(i-1)) )/(incl(i)-incl(i-1));
        end
    end
    hookload(j)=F(6);
    hookload(j)=hookload(j)*224.8089;


    % Plot Axial Force vs. TVD

    figure(j)
    plot(F*224.8089,MD,'k',statichookload,MD,'k-.')   % convert from [kN] to [lb]
    xL = xlim;
    yL = ylim;
    line([0 0], yL,'color','black');  %y-axis
    set(gca,'YDir','reverse')
    axis([-20000 20000 0 MD(1)])
    grid minor
    title('\fontsize{16}Axial Force when lowering String')
    legend(['\fontsize{12}Dynamic Hook Load \mu =' num2str(my(j))] ...
```

```matlab
            ,'\fontsize{12}Static Hook Load', 'location','southeast');
    xlabel('\fontsize{16}F [lb]')
    ylabel('\fontsize{16}MD [m]')


end
```
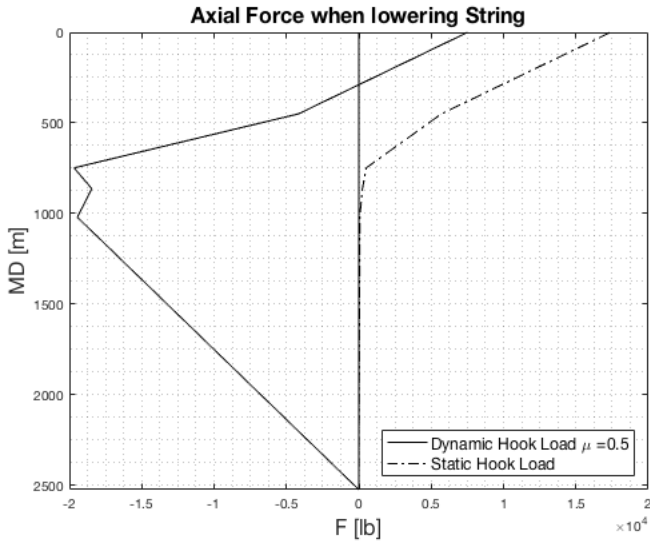

Ideal Wellpath

```matlab
% TVD is plotted on the y-axis

y       = flip([669.62 667 660 650 450 0]);

% Horizontal departure is plotted on the x-axis

x1      = 0;
x2      = 0;
x3      = R(5)-sqrt(R(5)^2-(TVD(4)-TVD(5))^2);
x4      = x3 + (cos(pi/2-incl(3))*L(4));
x5      = x4 + sqrt(R(3)^2-(R(3)-(TVD(2)-TVD(3)))^2);
x6      = x5+cos(pi/2-incl(1))*L(2);

x       = [x1 x2 x3 x4 x5 x6];

% Vertical section

verticalsection   = linspace(TVD(6),TVD(5),10);

for i = 1:length(verticalsection)
    xv(i) = 0;
    yv(i) = verticalsection(i);
end
```

```matlab
% Build section

build1 = linspace(TVD(5),TVD(4),10);
inclb = linspace(incl(5),incl(4),10);

for i = 1:length(build1)
    yb(i) = TVD(5)-R(5)*sin(pi+inclb(i));
    xb(i) = R(5)+R(5)*cos(pi+inclb(i));
end

% Tangent section

tangentsection = linspace(0,L(4),10);

for i = 1:length(tangentsection)
    xt(i) = x(3) + tangentsection(i)*cos(-5*pi/180);
    yt(i) = TVD(4) - tangentsection(i)*sin(-5*pi/180);
end

% Build section

build2 = linspace(TVD(3),TVD(2),10);
inclb2 = linspace(incl(3),incl(2),10);

for i = 1:length(build2)
    yb2(i) = (TVD(2)-R(3))-R(3)*sin(pi+inclb2(i));
    xb2(i) = x(5)+R(3)*cos(pi+inclb2(i));
end

% Horizontal section

horizontalsection = linspace(0,L(2),10);
inclh = acos((TVD(1)-TVD(2))/L(2));
for i = 1:length(horizontalsection)
    xh(i) = x(5) + horizontalsection(i)*cos(-pi/2+inclh);
    yh(i) = TVD(2) - horizontalsection(i)*sin(-pi/2+inclh);
end

% Plot well path

figure(2)
plot(x,y,'ko',xv,yv,'k',xb,yb,'k',xt,yt,'k',xb2,yb2,'k',xh,yh,'k','markersize',10)
set(gca,'YDir','reverse')
legend('\fontsize{16}Section markers','\fontsize{16}Ideal well path')
axis([-100 2000 0 700])
grid minor
xlabel('\fontsize{16}Horizontal departure [m]')
ylabel('\fontsize{16}Total vertical depth [m]')
title('\fontsize{16}Ideal well path')
hold on
```
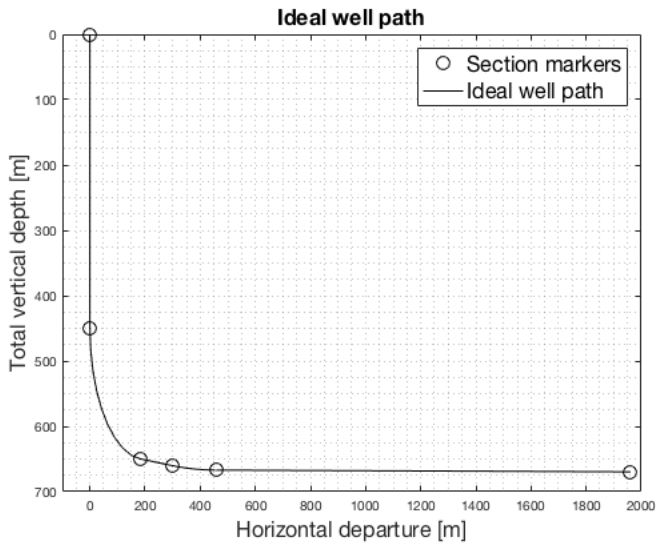
Contents

```
clc
clear all
```

INPUTS

```matlab
% Load Data from Compass

load('TVD.txt')
TVD=TVD';
load('MD.txt')
MD=MD';
load('incl.txt')
incl=incl'*pi/180;


MW       = 1.1;                      % mud weight [sg]
rhosteel = 65.5/8.33;               % density of steel [sg]
BF       = 1-MW/rhosteel;           % buoyancy factor [sg]
wDP      = 0.1343;                  % weight of 3 1/2" tbg [kN/m]
OD       = 0.0889;                  % outer diameter [m]
ID       = 0.0759968;              % inner diameter [m]
Ai       = pi/4 * ID^2;            % inner area [m2]
Ao       = pi/4 * OD^2;            % outer area [m2]


% Pressure Calculations
g        = 9.81;                    % gravity [m/s2]

for i = 1:length(TVD)
    Pi(i) = MW*g*TVD(i);            % hydrostatic inner pressure [Pa]
    Po(i) = Pi(i);                  % hydrostatic outer pressure [Pa]
end

% Wellpath Calculations

h = zeros(0,length(TVD));
R = zeros(0,length(TVD));

for i = 2:length(TVD)
    h(i) = TVD(i-1)-TVD(i);         % height of sections [m]
end

for i = 2:length(TVD)
    if incl(i)==incl(i-1)
         % the section is straight
        R(i) = 0;                   % radius of curvature [m]
    else
        % the section is curved
        R(i)=h(i)/(sin(incl(i-1))-sin(incl(i)));
    end
end
```

```matlab
L = zeros(1,length(TVD));

for i = 2:length(TVD)
    L(i) = MD(i-1)-MD(i) ;              % total well length [m]
end

% To investigate for different friction factors
my        = linspace(0.00,1.0,11);      % friction factor
WOB       = 0;                          % weight on bit

azi = zeros(1,length(TVD));

% Calculate dogleg angle

DL = zeros(1,length(L));  % rad
for i=1:(length(L)-1)
   DL(i+1) = acos (sin(incl(i))*sin(incl(i+1))*cos(azi(i)-azi(i+1)) ...
            + cos(incl(i))*cos(incl(i+1)));
end

% Equations Lowering String

% If the static hook load equals the axial force with no
% friction, then the code is correct.

staticweight = zeros(1,length(TVD));
statichookload = zeros(1,length(TVD));

for i = 1:length(TVD)
    staticweight(i)  = TVD(i)*BF*wDP;
    statichookload(i)  = staticweight(1)-staticweight(i);
end

statichookload = statichookload*224.8089; % kN to lb
```

Three-dimensional model by Bernt S. Aadnoy

```matlab
F = zeros(1,length(L));
hookload = zeros(1,length(my));
Feff = zeros(1,length(L));

F(1) = WOB;

my = 0.5;
for j=1:length(my)
    for i=2:length(L)
        if incl(i)-incl(i-1) == 0
             % the section is straight
            F(i) = F(i-1) + BF*wDP*L(i)*(cos(incl(i))-my(j)*sin(incl(i)));
        else % the section is curved
            F(i) = F(i-1)*exp(-my(j)*abs(DL(i)-DL(i-1)))+ BF*L(i)*wDP*( sin(incl(i))-sin(in
cl(i-1)) )/(incl(i)-incl(i-1));
        end
    end


    % Plot Axial Force vs. TVD
```

```matlab
    figure(j)
    plot(F*224.8089,MD,'k',statichookload,MD,'k-.')   % convert from [kN] to [lb]
    xL = xlim;
    yL = ylim;
    line([0 0], yL,'color','black');   %y-axis
    set(gca,'YDir','reverse')
    axis([-20000 20000 0 MD(1)])
    grid minor
    title('\fontsize{16}Axial Force when lowering String')
    legend(['\fontsize{12}Dynamic Hook Load \mu =' num2str(my(j))] ...
        ,'\fontsize{12}Static Hook Load', 'location','southeast');
    xlabel('\fontsize{16}F [lb]')
    ylabel('\fontsize{16}MD [m]')

end
```


Axial Force when lowering String
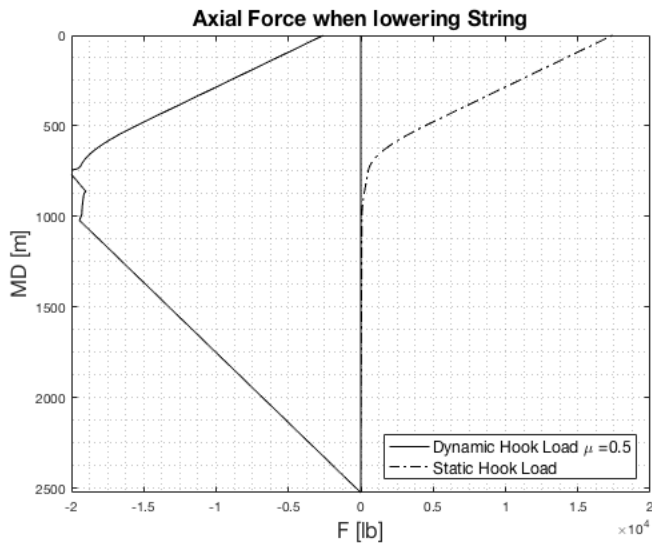
Real well path

```matlab
% Load horizontal departure from Compass

load('HD.txt')
HD=HD';

markersx = [HD(1) HD(53) HD(59) HD(64) HD(84) HD(99)];
markersy = [TVD(1) TVD(53) TVD(59) TVD(64) TVD(84) TVD(99)];

figure(2)
plot(markersx,markersy,'r*',HD,TVD,'r','markersize',10)
legend('\fontsize{16}Section markers','\fontsize{16}Real well path')
set(gca,'YDir','reverse')
axis([-100 2000 0 700])
grid minor
```

```matlab
xlabel('\fontsize{16}Horizontal departure [m]')
ylabel('\fontsize{16}Total vertical depth [m]')
title('\fontsize{16}Real well path')
```
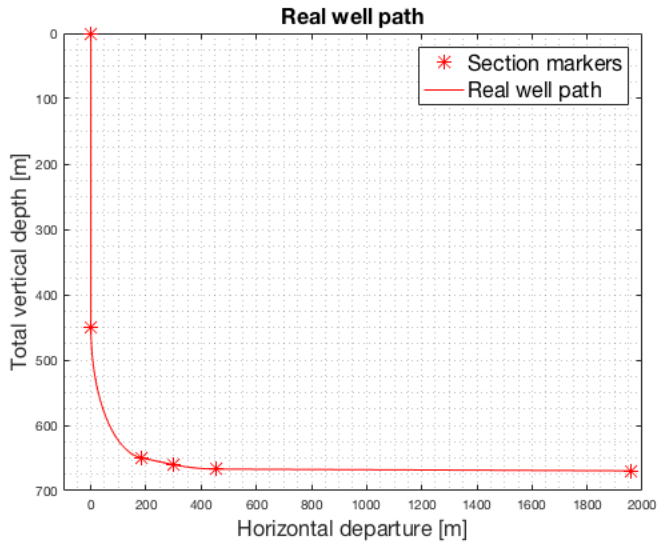
Contents

```
clc
clear all
```

INPUTS

```matlab
% Load Data from Compass

load('TVD.txt')
TVD=TVD';
load('MD.txt')
MD=MD';
load('incl.txt')
incl=incl'*pi/180;

% Inputs for drag model in SI units

MW       = 1.1;                    % mud weight [sg]
rhosteel = 65.5/8.33;             % density of steel [sg]
BF       = 1-MW/rhosteel;         % buoyancy factor [sg]
wDP      = 0.1343;                % weight of 3 1/2" tbg [kN/m]
OD       = 0.0889;               % outer diameter [m]
ID       = 0.0759968;            % inner diameter [m]
Ao       = pi/4 * OD^2;          % outer diameter [m2]
Ai       = pi/4 * ID^2;          % inner diameter [m2]

% Pressure Calculations in SI
g        = 9.81;                 % gravity [m/s2]

Pi = zeros(1,length(TVD));
Po = zeros(1,length(TVD));

for i = 1:length(TVD)
    Pi(i) = MW*g*TVD(i);          % hydrostatic inner pressure [kPa]
    Po(i) = Pi(i);                % hydrostatic outer pressure [kPa]
end

% Wellpath Calculations

h = zeros(0,length(TVD));
R = zeros(0,length(TVD));

for i = 2:length(TVD)
    h(i) = TVD(i-1)-TVD(i);       % height of sections [m]
end

for i = 2:length(TVD)
    if incl(i)==incl(i-1)
        % the section is straight
        R(i) = 0;                 % radius of curvature [m]
```

```matlab
    else
        % the section is curved
        R(i)=h(i)/(sin(incl(i-1))-sin(incl(i)));
    end
end


L = zeros(1,length(TVD));


for i = 2:length(TVD)
    L(i) = MD(i-1)-MD(i);                % total well length [m]
end

% To investigate for different friction factors
my        = linspace(0.00,1.0,11);      % friction factor
WOB       = 0;                           % weight on bit

azi = zeros(1,length(TVD));

% Calculate dogleg angle

DL = zeros(1,length(L));
for i=1:(length(L)-1)
   DL(i+1) = acos (sin(incl(i))*sin(incl(i+1))*cos(azi(i)-azi(i+1)) ...
            + cos(incl(i))*cos(incl(i+1)));
end

% Equations Lowering String

F = zeros(1,length(L));
hookload = zeros(1,length(my));

F(1) = WOB;
Fcsin = zeros(1,length(L));
Fcmin = Fcsin;
Fcmax = Fcsin;
Feff  = zeros(1,length(L));
```

Three-dimensional model by Bernt S. Aadnoy

```matlab
my = 0.45;
for j=1:length(my)
```

```matlab
    for i=2:length(L)
        if incl(i)-incl(i-1) == 0
             % the section is straight
            F(i) = F(i-1) + BF*wDP*L(i)*(cos(incl(i))-my(j)*sin(incl(i)));
        else % the section is curved
            F(i) = F(i-1)*exp(-my(j)*abs(DL(i)-DL(i-1)))+ BF*L(i)*wDP*( sin(incl(i))-sin(in
cl(i-1)) )/(incl(i)-incl(i-1));
        end
        Fa(1) = F(1) + Pi(1)*Ai - Po(1)*Ao;
        Fa(i) = F(i) + Pi(1)*Ai - Po(1)*Ao;
        Feff(1) = Fa(1) - Pi(1)*Ai + Po(1)*Ao;
        Feff(i) = Fa(i) - Pi(i)*Ai + Po(i)*Ao;
    end
    hookload(j)=F(6);
```

Buckling Limits

```matlab
% Inputs for Buckling Limit in oil field units

buoyedw  = 9.2*BF;                      % buoyed weight [lb/ft]
buoyedw  = buoyedw/12;                  % buoyed weight [lb/in]
OD       = 3.5;                         % outer diameter [in]
ID       = 2.992;                       % inner diameter [in]
I        = (pi/64)*(OD.^4-ID.^4);       % moment of inertia [in4]
E        = 30*10^6;                     % Young's modulus psi
csgID    = 5.921;                         % casing inner diameter [in]

% Test for bigger casing

%csgID = 9.063;

% Radial clearance

rc       = csgID/2-OD/2;

% Sinusoidal Buckling Limit
    for i = 1:length(TVD)
        if incl(i) == 0
            % Vertical section
            Fcsin(i) = -1.94*(E*I.*buoyedw.^2).^(1/3);          %lb
        else
            % Deviated sail section
            Fcsin(i) = -sqrt(4*E*I.*buoyedw.*sin(incl(i))./rc);    %lb
        end
    end

% Minimum Helical Buckling Limit
    for i = 1:length(TVD)
        if incl(i) == 0
            % Vertical section
            Fcmin(i) = -5.55*(E*I.*buoyedw.^2).^(1/3);          %lb
        else
            % Deviated sail section
            Fcmin(i) = -1.4*sqrt(4*E*I.*buoyedw.*sin(incl(i))./rc); %lb
        end
    end

% Maximum Helical Buckling Limit
    for i = 1:length(TVD)
        if incl(i)==0
            % Vertical section
            Fcmax(i)  = -5.55*(E*I.*buoyedw.^2).^(1/3);         %lb
        else
            % Deviated sail section
            Fcmax(i) = -2.8*sqrt(4*E*I.*buoyedw.*sin(incl(i))./rc); %lb
        end
    end

    % Plot drag force mot TVD
    figure(j)
    plot(F*224.8089,MD,'k',Feff*224.8089,MD,'k--',Fcsin,MD,'g',...
        Fcmin,MD,'b',Fcmax,MD,'r')
    axis([-45000 40000 0 MD(1)])
    xL = xlim;
    line(xL,[450 450],'color','black','linestyle',':');  %x-axis
```

```matlab
    line(xL,[MD(53) MD(53)],'color','black','linestyle',':');
    line(xL,[MD(64) MD(64)],'color','black','linestyle',':');
    line(xL,[MD(84) MD(84)],'color','black','linestyle',':');
    line(xL,[862.58 862.58],'color','black','linestyle',':');  %x-axis
    yL = ylim;
    line([0 0], yL,'color','black');  %y-axis
    set(gca,'YDir','reverse')

    grid minor
    title('\fontsize{16}Axial Force when lowering string')
    legend(['\fontsize{12}Dynamic Hook Load \mu =' num2str(my(j))],...
    '\fontsize{12}Effective Axial Load','\fontsize{12}Sinusoidal',...
    '\fontsize{12}Minimum Helical', ...
    '\fontsize{12}Maximum Helical','location','southeast');
    xlabel('\fontsize{16}F [lb]')
    ylabel('\fontsize{16}MD [m]')
```



```matlab
end
```
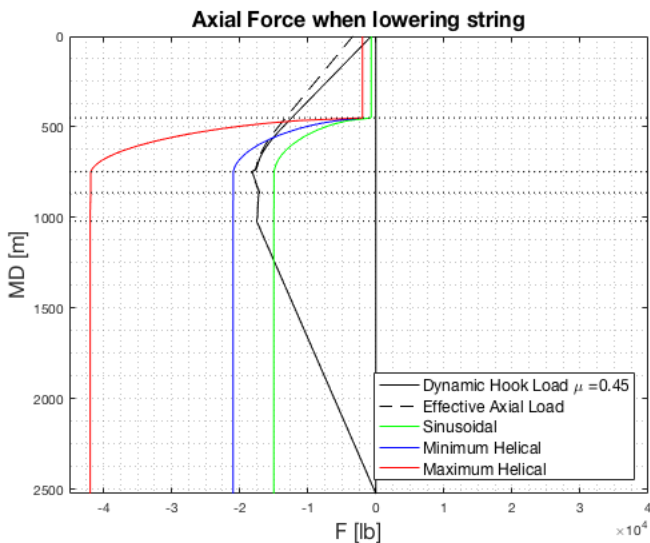
Permanent Corkscrewing

```matlab
grades    = [40 55 75 80 105]*1e3;       %psi

%Feff = 224.8089*Feff; %kN to lb

Feff = linspace(-150000,150000,100);

% so is the initial slack-off
so = zeros(1,length(F));
```

```matlab
% pressure from Pa to psi
Pi = Pi*0.145037738;

for i = 1:length(Feff)
    if Feff(i) < 0
        % compression
        so(i) = abs(OD*rc*(-Feff(i))./(4*I));
    else
        % tension
        so(i) = 0;
    end
end

% Maximum effective axial force
Feffmax = -grades(1)*4*I/(OD*rc);

figure(2)
plot(Feff(1:50),so(1:50),'b',Feffmax,grades(1),'ko','markersize',10)
hold on
xlim([-150000 150000])
ylim([0 140000])
xL = xlim;
yL = ylim;
line(xL, [grades(1) grades(1)],'color','black','linestyle','--');  %x-axis
line(xL, [grades(2) grades(2)],'color','black','linestyle','--');  %x-axis
line(xL, [grades(3) grades(3)],'color','black','linestyle','--');  %x-axis
line(xL, [grades(4) grades(4)],'color','black','linestyle','--');  %x-axis
line(xL, [grades(5) grades(5)],'color','black','linestyle','--');  %x-axis
line([0 0],yL,'color','black')
hold on
grid minor

xlabel('\fontsize{16}Effective axial force [lb]')
ylabel('\fontsize{16}Triaxial stress (reduced to bending stress) [psi]')
title('\fontsize{16}Permanent Corkscrewing')
legend('\fontsize{16}Sigmao Initial','\fontsize{16}Max Effective Axial Force', ...
    '\fontsize{16}Grades')
```

Published with MATLAB® R2016a
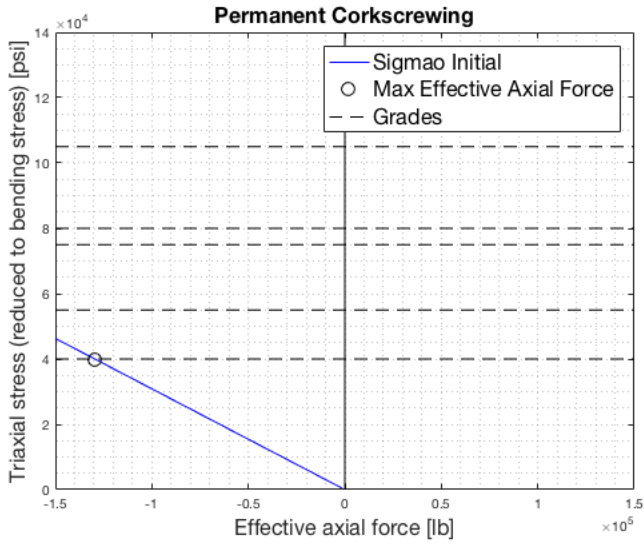
Appendix D

Buckling During Operations

This appendix includes the MatLab scripts used for compiling results from the method proposed by Lubinski et al. (1962) and Mitchell et al. (1999).

The first script is a pure reproduction of the model presented in the paper "Helical buckling of tubing sealed in packers" by Lubinski et al. (1962).

The second script is an implementation of the correlations for buckling strain and buckling length change presented by Mitchell et al. (1999). The script compares the buckling strain and buckling length change in the model presented by Lubinski et al. (1962) and Mitchell et al. (1999).

The third script is used for compiling results. The script is modified to apply for the well investigated, but the procedure of calculation is similar to the first script.

The fourth script is used for a subsea field with wet x-tree. The script is modified by adding a sea level, and hydrostatic pressure due to seawater.

Contents

```
clc
clear all

tic
```

INPUTS

```
% Tubing Inputs
OD      = 2.875;                    %in    outer diameter
weight  = 6.5;                      %lb/ft dry weight
ID      = 2.441;                    %in    inner diameter
grades  = 10^3.*[40 55 75 80 105];  %psi   yield strength
E       = 30*10^6;                  %psi   Young's modulus
poisson = 0.3;                      %      Poisson's ratio
Ct      = 6.9*10^(-6);              %/F    coeff. of thermal expansion
Lp      = 10000*12;                 %in    tubing length
Dp      = 3.25;                     %in    packer bore diameter

Ao      = pi/4*OD.^2;               %in2   outer area
Ai      = pi/4*ID.^2;               %in2   inner area
As      = Ao-Ai;                    %in2   cross-sectional area
Ap      = pi/4*Dp^2;                %in2   packer bore area
R       = OD./ID;                   %ratio OD/ID-ratio
ws      = weight./12;               %lb/in dry weight of tubing
I       = (pi/64)*(OD.^4-ID.^4);    %in4   moment of inertia

% Casing Inputs
csgOD     = 7;                      %in    outer diameter
csgweight = 32;                     %lb/ft dry weight
csgID     = 6.094;                  %in    inner diameter
rc        = (csgID-OD)/2;           %in    radial clearance

% Fluid Properties
rhot    = 1/231*[7.297 15];         %psi/in tubing initial-final
rhoa    = 1/231*[7.297 7.297];      %psi/in annulus initial-final
drhot   = rhot(2)-rhot(1);          %psi/in tubing change in density
drhoa   = rhoa(2)-rhoa(1);          %psi/in annulus change in density
wi      = rhot.*Ai;                 %lb/in  tubing initial-final
wo      = rhoa.*Ao;                 %lb/in  annulus initial-final
w       = ws + wi - wo;             %lb/in  total initial-final

% Pressures
pi      = [0 5000];                 %psi    surface initial-final
po      = [0 1000];                 %psi    surface initial-final
Pi      = pi+rhot*Lp;               %psi    packer initial-final
Po      = po+rhoa*Lp;               %psi    packer initial-final
```

```
dp        = [pi(2)-pi(1) po(2)-po(1)];  %psi    change in surface pressure
dP        = [Pi(2)-Pi(1) Po(2)-Po(1)];  %psi    change in packer pressure


% Temperature
dT        = -20;                        %F      avg. change in temperature

% Calculate Forces as if the tubing is free to move
Fa        = (Ap-Ao)*Po-(Ap-Ai)*Pi;     %lb     true axial force
Ff        = Ap*(Po-Pi);                 %lb     effective axial force

% Calculate length change associated with Ff
dLf       = Lp/(E*As).*Ff(2)-rc^2/(8*E*I*w(2)).*Ff(2).^2; %in

disp(['The length change related to Ff is ', num2str(dLf), ' in'])

% Critical Buckling Limit (Paslay Dawson)
Fcr = sqrt((4*E*I.*w(2))./rc);
```

```
The length change related to Ff is -192.6254 in
```

Length Changes: Packers Permitting Free Motion

```
% All length changes are in inches

% The first length change is deformation due to the true axial force acting
% on the bottom of the tubing. Hooke's law is used:
dL1       = Lp/(E*As)*((Ap-Ao)*dP(2)-(Ap-Ai)*dP(1));

% The second length change occurs due to helical buckling. If the change in
% outer pressure is higher than the change in inner pressure, there will be
% no helical buckling (Lubinski et. al (1962)), hence:

if dP(2)>dP(1)
    % No helical buckling
    dL2   = 0;
else
    % Helical buckling. Calculate length change with a non-linear equation.
    dL2   = -rc^2*Ap^2*(dP(2)-dP(1)).^2/(8*E*I*w(2));
    % Sinusoidal buckling length change by Mitchell:
    % Ff(2) = -Ff(2); % Change signs for Mitchells equation
    %dL2 = -(rc)^2/(4*E*I*w(2))*(Ff(2)-Fcr)*(0.3771*Ff(2)-0.3668*Fcr);
    % Ff(2) = -Ff(2); % Change back for the remaining model
end

% Calculate length change due to radial pressure due to ballooning
% and fluid flow
delta     = 0; % Pressure drop per unit length
dL3       = -(poisson/E)* ...
            ((drhot-R^2*drhoa-(1+2*poisson)/(2*poisson)*delta)*Lp^2/(R^2-1))...
            -(2*poisson/E)*((dp(1)-R^2*dp(2))*Lp/(R^2-1));

% The fourth length change occurs due to temperature change, also known as
% thermal expansion or thermal contraction.
dL4       = Lp*Ct*dT;

% Total length change is then:
dL        = dL1+dL2+dL3+dL4;
```

```matlab
disp(['If the tubing is free to move, the total length change is ', ...
    num2str(dL),' in'])

% Neutral stability point if the tubing is free to move
nfree    = (Ff./w(2))/12; %ft

disp(['If the tubing is free to move, the neutral stability point is ', ...
    num2str(nfree),' ft from the bottom'])
```

```
If the tubing is free to move, the total length change is -165.32 in
If the tubing is free to move, the neutral stability point is 0     -8636.6248 ft from the
bottom
```

Length Changes: Packers Permitting Limited Motion

Define slack-off force

```matlab
Fso      = -20000; %lb
% Stick-up length is then
dL5      = - ((Lp/(E*As).*Fso-rc^2/(8*E*I*w(1)).*Fso.^2));
% Including stick-up length, the total length change is:
dL       = dL+dL5;

disp(['If the packer permits limited motion, the total length change is ',...
    num2str(dL), ' in'])
```

```
If the packer permits limited motion, the total length change is -115.6379 in
```

Length Changes: Packers Permitting No Motion

The packer will oppose to the desired length change "dLp".

```matlab
dLp      = dLf-dL;

% Plotting F vs. dL'
% Define F as a vector
F        = linspace(-80000,80000,10000);
% Make sure dL' is the same size vector as F
dLfnutt  = zeros(1,length(F));

% Make a loop to calculate dL' for every F.
for i = 1:length(F)
    if F(i) < 0
        % Compression
        dLfnutt(i) = Lp/(E*As).*F(i)-rc^2/(8*E*I*w(2)).*F(i).^2;
    else
        % Tension
        dLfnutt(i) = Lp/(E*As).*F(i);
    end
end

% Make a loop to calculate the roots of dL' when dL is known.
for i = 1:length(dLp)
```

```matlab
    if dLp(i) < 0
        % Compression
        % 'coeff' is the coefficients in the non-linear equation
            coeff = [-rc^2/(8*E*I*w(2)) Lp/(E*As) -dLp];
        % 'roots' calculates the F corresponding to dLp
            Ffstarroots = roots(coeff)';
        % 'Ffstar' is the effective axial force when the tubing is fixed
            Ffstar = Ffstarroots(2);
        % 'Fp' is the packer force
            Fp = Ffstar - Ff(2);
        % 'Fastar' is the true axial force when the tubing is fixed
            Fastar = Fa(2)+Fp;
            if Fp(i) > 0
              disp(['The tubing is shortening, and the packer' ...
                ' force is a tension: ',num2str(Fp(i)),'lb']);
            else
              disp(['The tubing is lengthening, and the packer' ...
                ' force is a compression: ',num2str(Fp(i)),'lb']);
            end
    else
        % Tension
        % 'coeff' is the coefficients in the linear eq: Hooke's law
            coeff = [0 Lp/(E*As) -dLp];
        % 'roots' calculates the F corresponding to dLp
            Ffstarroots = roots(coeff)';
            % 'Ffstar' is the effective axial force when the tubing is fixed
            Ffstar = Ffstarroots(2);
        % 'Fp' is the packer force
            Fp = Ffstar - Ff(2);
        % 'Fastar' is the true axial force when the tubing is fixed
            Fastar = Fa(2)+Fp;
            if Fp(i) > 0
                disp(['The tubing is shortening, and the packer' ...
                    ' force is a tension: ',num2str(Fp(i)),'lb']);
            else
                disp(['The tubing is lengthening, and the packer' ...
                    ' force is a compression: ',num2str(Fp(i)),'lb']);
            end
    end
end

disp(['The fictitious force when the tubing is fixed is ', ...
    num2str(Ffstar),' lb'])
```

```
The tubing is shortening, and the packer force is a tension: 35904.4633lb
The fictitious force when the tubing is fixed is -30474.61 lb
```

Plotting

```matlab
figure(1)
plot(F,dLfnutt,'r',Ffstar,dLp,'r*',Ff(2),dLf,'ro','markersize',10)
hold on
xL = xlim;
yL = ylim;
line([0 0], yL,'color','black');  %y-axis
line(xL, [0 0],'color','black');  %x-axis
hold on
line([Ff(2) Ff(2)],yL,'color','black','linestyle','-.')
```

```matlab
line(xL, [dLf dLf],'color','black','linestyle','-.')
hold on
line([Ffstar Ffstar],yL,'color','black','linestyle','--')
line(xL, [dLp dLp],'color','black','linestyle','--')
grid minor
xlabel('\fontsize{16}Axial Force [lb]')
ylabel('\fontsize{16}dL [in]')
title('\fontsize{16}Axial Force vs. Length Change')
legend('\fontsize{16}Axial Force vs. Length Change','\fontsize{16}Ff*', ...
    '\fontsize{16}Ff','location','northwest')
```


Neutral stability point if the tubing is fixed

```matlab
n         = (Ffstar./w(2))/12;                    %ft
disp(['If the tubing is fixed, the neutral stability point is ', ...
    num2str(n),' ft from the bottom'])

toc
```

```
If the tubing is fixed, the neutral stability point is -3965.0715 ft from the bottom
Elapsed time is 2.553992 seconds.
```

Contents

```
clc
clear all
```

INPUTS

```
% Tubing Inputs
OD       = 2.875;                    %in     outer diameter
weight   = 6.5;                      %lb/ft  dry weight
ID       = 2.441;                    %in     inner diameter
grades   = 10^3.*[40 55 75 80 105];  %psi    yield strength
E        = 30*10^6;                  %psi    Young's modulus
poisson  = 0.3;                      %       Poisson's ratio
Ct       = 6.9*10^(-6);              %/F     coeff. of thermal expansion
Lp       = 10000*12;                 %in     tubing length
Dp       = 3.25;                     %in     packer bore diameter

Ao       = pi/4*OD.^2;               %in2    outer area
Ai       = pi/4*ID.^2;               %in2    inner area
As       = Ao-Ai;                    %in2    cross-sectional area
Ap       = pi/4*Dp^2;                %in2    packer bore area
R        = OD./ID;                   %ratio  OD/ID-ratio
ws       = weight./12;               %lb/in  dry weight in lb/in
I        = (pi/64)*(OD.^4-ID.^4);    %in4    moment of inertia

incl = linspace(0,pi/3,100);         %rad, well inclination

% Figure (9) in "Buckling Analysis in Deviated Wells: A Practical Method"
% by Mitchell et al. KOP = 2000 ft
TVD = (2000 + 8000*cos(incl))*12;    %in

% Casing Inputs
csgOD     = 7;                       %in     outer diameter
csgweight = 32;                      %lb/ft  dry weight
csgID     = 6.094;                   %in     inner diameter
rc        = (csgID-OD)/2;            %in     radial clearance

% Fluid Properties
rhot      = 1/231*[7.297 15];        %psi/in tubing initial-final
rhoa      = 1/231*[7.297 7.297];     %psi/in annulus initial-final
drhot     = rhot(2)-rhot(1);         %psi/in tubing change in density
drhoa     = rhoa(2)-rhoa(1);         %psi/in annulus change in density
wi        = rhot.*Ai;                %lb/in  tubing initial-final
wo        = rhoa.*Ao;                %lb/in  annulus initial-final
w         = ws + wi - wo;            %lb/in  total initial-final
```

```matlab
pi = 3.1416;

% Dawson Paslay Equation
% Dawson Paslay limit is defined with 0 inclination.
% This is a conservative assumption.
Fcr = sqrt((4*E*I.*w(2))./rc);

% Fictitious Force
% For the general case of arbitrary variation of F (Mitchell et al)
Feff = Fcr*linspace(0,4.50,1000);
```

Lubinski Buckling Strain

The buckling strain is defined as a vector.

```matlab
epsilonLUB = zeros(1,length(Feff));
for i = 1:length(Feff)
    if Feff(i) > 0
        % Helical buckling when the fictitious force is in compression (+)
        epsilonLUB(i) = -(rc)^2/(4*E*I)*Feff(i);
    else
        % No buckling
        epsilonLUB(i) = 0;
    end
end
```

Mitchell Buckling Strain

The buckling strain is defined as a vector.

```matlab
epsilonMIT = zeros(1,length(Feff));
for i = 1:length(Feff)
    if Feff(i) < Fcr
        % No buckling
        epsilonMIT(i) = 0;
    elseif Feff(i) < 2.8*Fcr
        % Sinusoidal Buckling
        epsilonMIT(i) = -0.7285*(rc)^2/(4*E*I)*(Feff(i)).^(0.08)*(Feff(i)-Fcr)^(.92);
    else
        % Helical Buckling
        epsilonMIT(i) = -(rc)^2/(4*E*I)*Feff(i);

    end
end
```

Plotting

```matlab
figure(1)
plot(Feff/Fcr,-epsilonLUB*4*E*I/rc^2,'k--',...
    Feff/Fcr,-epsilonMIT*4*E*I/rc^2,'k')
legend('\fontsize{16}Lubinski',...
    '\fontsize{16}Mitchell Correlation','location','northwest')
grid minor
xlabel('\fontsize{16}F/Fcr')
ylabel('\fontsize{16}4EIe/r2')
title('\fontsize{16}Buckling Strain Comparison')
```

```
yL = ylim;
% Define PD-limit
line([1 1],yL,'color','black','linestyle',':');
% Define helical buckling limit (Mitchell)
line([2.8 2.8],yL,'color','black','linestyle',':');
```
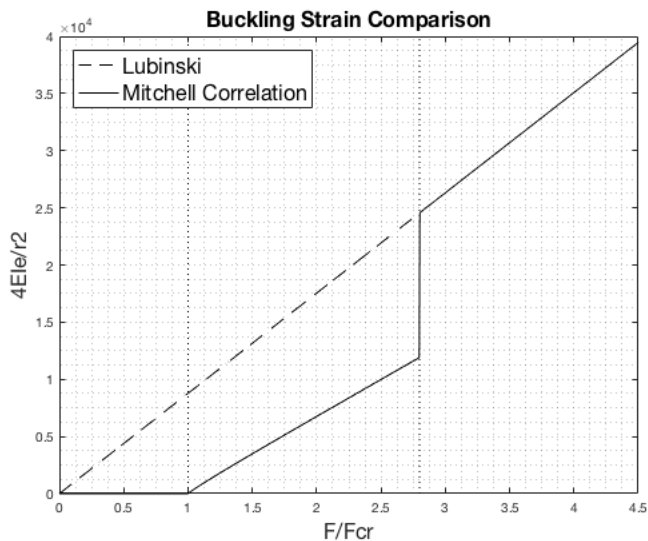

Lubinski Buckling Length Change

The buckling length change is defined as a vector.

```
dLbLUB = zeros(1,length(Feff));
for i = 1:length(Feff)
    if Feff(i) > 0
        % Helical buckling when the fictitious force is in compression (+)
        dLbLUB(i) = -(rc)^2/(8*E*I*w(2))*Feff(i)^2;
    else
        % No buckling
        dLbLUB(i) = 0;
    end
end
```

Mitchell Buckling Length Change

The buckling length change is defined as a vector.

```
dLbMIT = zeros(1,length(Feff));
for i = 1:length(Feff)
    if Feff(i) < Fcr
        % No buckling
        dLbMIT(i) = 0;
```

```matlab
    elseif Feff(i) < 2.8*Fcr
        % Sinusoidal Buckling
        dLbMIT(i) = -(rc)^2/(4*E*I*w(2))*(Feff(i)-Fcr)*(0.3771*Feff(i)-0.3668*Fcr);
    else
        % Helical Buckling
        dLbMIT(i) = -(rc)^2/(8*E*I*w(2))*(Feff(i)^2);

    end
end
```

Plotting

```matlab
figure(2)
plot(Feff/Fcr,-dLbLUB*8*E*I*w(2)/rc^2,'k--',...
    Feff/Fcr,-dLbMIT*8*E*I*w(2)/rc^2,'k')
legend('\fontsize{16}Lubinski',...
    '\fontsize{16}Mitchell Correlation','location','northwest')
grid minor
xlabel('\fontsize{16}F/Fcr')
ylabel('\fontsize{16}-8EIwdLb/r2')
title('\fontsize{16}Buckling Length Change Comparison')
yL = ylim;
% Define PD-limit
line([1 1],yL,'color','black','linestyle',':');
% Define helical buckling limit (Mitchell)
line([2.8 2.8],yL,'color','black','linestyle',':');
```


Published with MATLAB® R2016a

Contents

```
clc
clear all
```

INPUTS

```
tic
% Tubing Inputs
OD      = 3.5;                   %in     outer diameter
weight  = 9.2;                   %lb/ft  dry weight
ID      = 2.992;                 %in     inner diameter
grades  = 10^3.*[40 55 75 80 105];   %psi   yield strength
E       = 30*10^6;               %psi    Young's modulus
poisson = 0.3;                   %       Poisson's ratio
Ct      = 6.9*10^(-6);           %/F     coeff. of thermal expansion
% Total length of well
Lp      = 2523.1;                %m      value from Compass
Lp      = Lp*39.37;              %in     converting from m to in
% Total vertical depth
TVD     = 669.62;                %m      value from Compass
TVD     = TVD*39.37;             %in     converting from m to in
% Tubing calculations
Ao      = pi/4*OD.^2;            %in2    outer area
Ai      = pi/4*ID.^2;            %in2    inner area
As      = Ao-Ai;                 %in2    cross-sectional area
Ap      = Ai;                    %in2    packer bore area PBR
R       = OD./ID;                %ratio  OD/ID-ratio
ws      = weight./12;            %lb/in  dry weight of tubing
I       = (pi/64)*(OD.^4-ID.^4); %in4    moment of inertia
% Casing Inputs
csgID   = 5.921;                 %in     inner diameter
rc      = (csgID-OD)/2;          %in     radial clearance
```

```
% Fluid Properties
rhosw    = 1/231*8.68;                 %psi/in sea water density
rhog     = 1/231*1;                    %psi/in gas density
rhoo     = 1/231*7.68;                 %psi/in oil density
% Pressures
Pr       = 1015.3;                     %psi    70 bar reservoir pressure
Pg       = rhog*TVD;                   %psi    gas-filled well
SIWHP    = Pr - Pg;                    %psi    shut-in wellhead pressure
WDP      = SIWHP + 508;                %psi    35 bar safety margin
Ppacker  = 4278.6;                     %psi    295 bar set packer pressure
```

Length changes and packer forces

```
 % Load case: Set packer
rhot     = [rhosw rhosw];              %psi/in initial-final
rhoa     = [rhosw rhosw];              %psi/in initial-final
pi       = [0 Ppacker-rhot(2)*TVD];    %psi    surface initial-final
po       = [0 0];                      %psi    surface initial-final
dT       = 0;                          %C      avg. change in temperature
dT       = dT*1.8;                     %F
%
% % Load case: Start bullheading (gas filled well)
% rhot     = [rhosw rhog];             %psi/in initial-final
% rhoa     = [rhosw rhosw];            %psi/in initial-final
% pi       = [0 WDP];                  %psi    surface initial-final
% po       = [0 0];                    %psi    surface initial-final
% dT       = 3;                        %C      avg. change in temperature
% dT       = dT*1.8;                   %F

% % Load case: Start bullheading (oil filled well)
% rhot     = [rhosw rhoo];             %psi/in initial-final
% rhoa     = [rhosw rhosw];            %psi/in initial-final
% pi       = [0 WDP];                  %psi    surface initial-final
% po       = [0 0];                    %psi    surface initial-final
% dT       = 3;                        %C      avg. change in temperature
% dT       = dT*1.8;                   %F
%
% % Load case: Shut-in
% rhot     = [rhosw rhog];             %psi/in tubing initial-final
% rhoa     = [rhosw rhosw];            %psi/in annulus initial-final
% pi       = [0 SIWHP];                %psi    surface initial-final
% po       = [0 0];                    %psi    surface initial-final
% dT       = -4;                       %C      avg. change in temperature
% dT       = dT*1.8;                   %F

% Density calculations
drhot    = rhot(2)-rhot(1);            %psi/in change in density
drhoa    = rhoa(2)-rhoa(1);            %psi/in change in density
wi       = rhot.*Ai;                   %lb/in  tubing initial-final
wo       = rhoa.*Ao;                   %lb/in  annulus initial-final
w        = ws + wi - wo;               %lb/in  total initial-final

% Pressure calculations
Pi       = pi+rhot*TVD;                %psi    packer initial-final
Po       = po+rhoa*TVD;                %psi    packer initial-final
dp       = [pi(2)-pi(1) po(2)-po(1)];  %psi    change in surface pressure
dP       = [Pi(2)-Pi(1) Po(2)-Po(1)];  %psi    change in packer pressure

% Calculate Forces as if the tubing is free to move
```

```matlab
Fa        = (Ap-Ao)*Po-(Ap-Ai)*Pi;      %lb     true axial force
Ff        = Ap*(Po-Pi);                  %lb     effective axial force

% Calculate length change associated with Ff
dLf       = Lp/(E*As).*Ff(2)-rc^2/(8*E*I*w(2)).*Ff(2).^2; %in

disp(['The length change related to this force is ', num2str(dLf), ' in'])
```

```
The length change related to this force is -30.9725 in
```

Critical buckling limits

Critical buckling for vertical well

```matlab
Fcr       = (E*I.*w(2)^2).^(1/3); %lb
% Sinusoidal buckling is defined by Lubinski et. al (1950)
Fcsinv    = 1.94*Fcr; %lb
% Helical buckling is defined by Wu et. al (1995)
Fchelv    = 5.55*Fcr; %lb
% Critical buckling for deviated section (Paslay Dawson)
incl      = linspace(0,85*3.1416/180,100); % build from 0 to 85 degrees
TVDbuild  = linspace(450,650,100);         % vertical depth of build section
% Sinusoidal buckling is defined by Dawson and Paslay (1984)
Fcrsindev = sqrt((4*E*I.*w(2)*sin(incl))./rc);
% Helical buckling is defined by Mitchell et. al (1999)
Fcrheldev = 1.4*Fcrsindev;
% Critical buckling for horizontal section
Fcrsinhor = sqrt((4*E*I.*w(2)*sin(3.1416/2))./rc);
Fcrhelhor = 1.4*Fcrsinhor;
```

Length Changes: Packers Permitting Free Motion

All length changes are in inches

```matlab
% The first length change is deformation due to the true axial force acting
% on the bottom of the tubing. Hooke's law is used:
dL1       = Lp/(E*As)*((Ap-Ao)*dP(2)-(Ap-Ai)*dP(1));
% The second length change occurs due to helical buckling. If the change in
% outer pressure is higher than the change in inner pressure, there will be
% no helical buckling (Lubinski et. al (1962)), hence:
if dP(2)>dP(1)
    % No helical buckling
    dL2   = 0;
else
    % Helical buckling. Calculate length change with a non-linear equation.
     dL2  = -rc^2*Ap^2*(dP(2)-dP(1)).^2/(8*E*I*w(2));
    % Sinusoidal buckling length change by Mitchell:
    % Ff(2) = -Ff(2); % Change signs for Mitchells equation
    % dL2   = -(rc)^2/(4*E*I*w(2))*(Ff(2)-Fcr(2))*(0.3771*Ff(2)-0.3668*Fcr(2));
    % Ff(2) = -Ff(2); % Change back for the remaining model
end
% Calculate radial pressure due to ballooning and fluid flow
%delta    = 0; % Pressure drop per unit length
%dL3      = -(poisson/E)*((drhot-R^2*drhoa-(1+2*poisson)/(2*poisson)*delta)*Lp^2/(R^2-1)).
..
%           -(2*poisson/E)*((dp(1)-R^2*dp(2))*Lp/(R^2-1));
```

```matlab
% Ballooning equation from Jonathan Bellarby "Well Completion Design"
avgdpi    = (dp(1)+dP(1))/2;   %psi, average pressure change
avgdpo    = (dp(2)+dP(2))/2;   %psi, average pressure change
dL3       = -(2*poisson/E)*(avgdpi*Ai-avgdpo*Ao)*(1/(Ao-Ai))*Lp;

% The fourth length change occurs due to temperature change, also known as
% thermal expansion or thermal contraction.
dL4       = Lp*Ct*dT;

% Total length change is then:
dL        = dL1+dL2+dL3+dL4;

disp(['If the tubing is free to move, the total length change is ', ...
    num2str(dL),' in'])


% Neutral stability point if the tubing is free to move
nfree     = (Ff./w)/12;        %ft
disp(['If the tubing is free to move, the neutral stability point is ', ...
    num2str(nfree(2)),' ft from the bottom'])
```

```
If the tubing is free to move, the total length change is -19.1516 in
If the tubing is free to move, the neutral stability point is -2878.1739 ft from the bottom
```

Length Changes: Packers Permitting Limited Motion

Define slack-off force

```matlab
Fso       = 0; %lb

% Variation of initial slack-off/pick-up
% Fso       = linspace(-10000,10000,100); %lb

%Length change due to slack-off or pick-up
dL5       = - ((Lp/(E*As).*Fso-rc^2/(8*E*I*w(1)).*Fso.^2));

% Including stick-up length, the total length change is:
dL        = dL+dL5;

disp(['If the packer permits limited motion, the total length change is ',...
    num2str(dL), ' in'])
```

```
If the packer permits limited motion, the total length change is -19.1516 in
```

Length Changes: Packers Permitting No Motion

The packer will oppose to the desired length change "dLp".

```matlab
dLp       = dLf-dL;

% Plotting F vs. dL'
% Define F as a vector
F         = linspace(-40000,40000,10000);
```

```matlab
% Make sure dL' is the same size vector as F
dLfnutt = zeros(1,length(F));

% Make a loop to calculate dL' for every F.
for i = 1:length(F)
    if F(i) < 0 && F(i) > -Lp*w(2)
        % Compression
        dLfnutt(i) = Lp/(E*As).*F(i)-rc^2/(8*E*I*w(2)).*F(i).^2;
    else
        % Tension
        dLfnutt(i) = Lp/(E*As).*F(i);
    end
end

% Define vectors
Ffstar = zeros(1,length(Fso));
Fp     = zeros(1,length(Fso));
Fastar = zeros(1,length(Fso));

for i = 1:length(dLp)
    if dLp(i) < 0
        % Compression
        % 'coeff' is the coefficients in the non-linear equation
          coeff = [-rc^2/(8*E*I*w(2)) Lp/(E*As) -dLp(i)];
        % 'roots' calculates the F corresponding to dLp
          Ffstarroots = roots(coeff)';
        % 'Ffstar' is the effective axial force when the tubing is fixed
          Ffstar(i) = Ffstarroots(2);
        % 'Fp' is the packer force
          Fp(i) = Ffstar(i) - Ff(2);
        % 'Fastar' is the true axial force when the tubing is fixed
          Fastar(i) = Fp(i)+Fa(2);
          if Fp(i) > 0
            disp(['The tubing is shortening, and the packer' ...
              ' force is a tension: ',num2str(Fp(i)),'lb']);
          else
            disp(['The tubing is lengthening, and the packer' ...
              ' force is a compression: ',num2str(Fp(i)),'lb']);
          end
    else
        % Tension
        % 'coeff' is the coefficients in the linear eq: Hooke's law
          coeff = [0 Lp/(E*As) -dLp(i)];
        % 'roots' calculates the F corresponding to dLp
          Ffstarroots = roots(coeff);
        % 'Ffstar' is the effective axial force when the tubing is fixed
          Ffstar(i) = Ffstarroots;
        % 'Fp' is the packer force
          Fp(i) = Ffstar(i) - Ff(2);
        % 'Fastar' is the true axial force when the tubing is fixed
          Fastar(i) = Fp(i)+Fa(2);
          if Fp(i) > 0
              disp(['The tubing is shortening, and the packer' ...
              ' force is a tension: ',num2str(Fp(i)),'lb']);
          else
              disp(['The tubing is lengthening, and the packer' ...
              ' force is a compression: ',num2str(Fp(i)),'lb']);
          end
    end
end
```

```matlab
disp(['The fictitious force when the tubing is fixed is ', ...
    num2str(Ffstar),' lb'])
```

```
The tubing is shortening, and the packer force is a tension: 14041.8376lb
The fictitious force when the tubing is fixed is -9075.8233 lb
```

Plotting with constant slack-off/pick-up

```matlab
figure(1)
plot(F,dLfnutt,'r',Ffstar,dLp,'r*',Ff(2),dLf,'ro',Ffstar,dLf,'b>',...
    'markersize',10)
hold on
xL = xlim;
yL = ylim;
line([Ff(2) Ffstar],[dLf dLf],'linestyle','-')
line([0 0], yL,'color','black');  %y-axis
line(xL, [0 0],'color','black');  %x-axis
hold on
line([Ff(2) Ff(2)],yL,'color','black','linestyle','-.')
line(xL, [dLf dLf],'color','black','linestyle','-.')
hold on
line([Ffstar Ffstar],yL,'color','black','linestyle','--')
line(xL, [dLp dLp],'color','black','linestyle','--')
grid minor
xlabel('\fontsize{16}Axial Force [lb]')
ylabel('\fontsize{16}dL [in]')
title('\fontsize{16}Axial Force vs. Length Change')
legend('\fontsize{16}Axial Force vs. Length Change' ...
, '\fontsize{16}Ff*','\fontsize{16}Ff','\fontsize{16}Fp', ...
    'location','northwest')
```

Plotting with variating slack-off/pick-up

figure(1) plot(F,dLfnutt,'r',Ffstar,dLp,'r*',Ff(2),dLf,'ro','markersize',10) hold on xL = xlim; yL = ylim; grid minor

line([0 0], yL,'color','black'); %y-axis line(xL, [0 0],'color','black'); %x-axis hold on line([Ff(2) Ff(2)],yL,'color','black','linestyle','-.') line(xL, [dLf dLf],'color','black','linestyle','-.') hold on grid minor xlabel('\fontsize{16}Axial Force [lb]') ylabel('\fontsize{16}dL [in]') title('\fontsize{16}Axial Force vs. Length Change') legend('\fontsize{16}Axial Force vs. Length Change' ... , '\fontsize{16}Ff*','\fontsize{16}Ff', ... 'location','northwest')

Neutral Stability Point

```
% Neutral Point when the tubing is fixed
n        = ([0 Ffstar]/w(2))/12;              %ft

% True vs. Effective Axial Load
% Capital P is the pressure at packer level, and lowercase p is the
% pressure at surface. Note how the pressures are used in each equation.

% Initial Conditions

% Surface (z=0)
% True Axial Load
Fas(1) = TVD*ws  + Po(1)*(Ap-Ao) - Pi(1)*(Ap-Ai);
% Effective Axial Load
Ffs(1) = Fas(1) - pi(1)*Ai + po(1)*Ao;

% Packer (z=zshoe)
% True Axial Load
Fap(1) = Po(1)*(Ap-Ao) - Pi(1)*(Ap-Ai);
% Effective Axial Load
% Assumes that the pressure is bled of after setting the packer, hence Fp=0
Ffp(1) = Fap(1) - Pi(1)*Ai + Po(1)*Ao;
```

```matlab
% After Load Case

% Surface (z=0)
% The packer force will adjuct the true axial load, and this effect will
% also be included when calculating the effective axial load. Lubinski used
% a star "*" to describe these loads when the tubing is anchored.
% True Axial Load
Fas(2) = TVD*ws  + Po(2)*(Ap-Ao) - Pi(2)*(Ap-Ai) + Fp;
% Effective Axial Load
Ffs(2) = Fas(2) - pi(2)*Ai + po(2)*Ao;
% Packer (z=zshoe)
% True Axial Load
Fap(2) = Po(2)*(Ap-Ao) - Pi(2)*(Ap-Ai) + Fp;
% Effective Axial Load
Ffp(2) = Fap(2) - Pi(2)*Ai + Po(2)*Ao;
```

Plotting axial loads and neutral stability point

```matlab
figure(2)
plot([Fas(1) Fap(1)],[0 TVD]/12,'k', ...
     [Ffs(1) Ffp(1)],[0 TVD]/12,'r', ...
     [Fas(2) Fap(2)],[0 TVD]/12,'k--', ...
     [Ffs(2) Ffp(2)],[0 TVD]/12,'r--', ...
     0, TVD/12+n,'ro')
ylim([0 TVD/12]);
yL = [0 TVD/12];
xL = xlim;
line([0 0], yL,'color','black');
line(xL,[0 0],'color','black');
line(xL,[TVD/12 TVD/12],'color','black');
legend('\fontsize{16}Fa Initial Conditions', ...
    '\fontsize{16}Feff Initial Conditions', ...
    '\fontsize{16}Fa Load Case', ...
    '\fontsize{16}Feff Load Case', ...
    '\fontsize{16}NSP','location','northwest')
set(gca,'YDir','reverse')
grid minor
ylabel('\fontsize{16}Depth [ft]')
yyaxis right
ylim([0 670])
line(xL,[450 450],'color','black','linestyle',':');
line(xL,[650 650],'color','black','linestyle',':');
set(gca,'YDir','reverse')
xlabel('\fontsize{16}Force [lb]')
ylabel('\fontsize{16}Depth [m]')
title('\fontsize{16}True vs. Effective Axial Force')
```

Permanent Corkscrewing

```
% Initial Conditions after slack-off but before changing P and T

% 'soinitial' is the stress at outer wall after slack-off
soinitial = zeros(1,length(Fso));

for i = 1:length(Fso)
    if Fso(i) < 0
        soinitial(i) = abs(Fso(i)/As + OD*rc*Fso(i)./(4*I));
    end
end

% Permanent Corkscrewing after changing P and T

% 'so' is stress at the outer wall
so = zeros(1,length(Ffstar));
% 'si' is stress at the inner wall
si = so;

% Change signs of effecti
Ffstar = -Ffstar;
Fastar = -Fastar;

for i = 1:length(Ffstar)

    if Ffstar(i) < 0
        % No buckling
        sigmab = 0;
        % elseif Ffstar(i) < 5.55*Fcr && Ffstar(i) > 1.94*Fcr
        % Sinusoidal Buckling
        % sigmab = 0.3151*OD*rc/I*Ffstar(i).^(0.08)*(Ffstar(i)-Fcr).^(0.92);
        % elseif Ffstar(i) > 5.55*Fcr
```

```matlab
    else
        % Helical Buckling
        sigmab = OD*rc/(4*I).*Ffstar(i);
    end

    sigmaa = Fastar(i)/As;

        soplus   = sqrt(3*((Pi(2)-Po(2))/(R^2-1))^2 + ...
                    ((Pi(2)-R^2*Po(2))/(R^2-1)+sigmaa+sigmab)^2);
        sominus  = sqrt(3*((Pi(2)-Po(2))/(R^2-1))^2 + ...
                    ((Pi(2)-R^2*Po(2))/(R^2-1)+sigmaa-sigmab)^2);
        so(i)    = max(soplus,sominus);

        siplus   = sqrt(3*(R^2*(Pi(2)-Po(2))/(R^2-1))^2 + ...
                    ((Pi(2)-R^2*Po(2))/(R^2-1)+sigmaa+sigmab./R)^2);
        siminus  = sqrt(3*(R^2*(Pi(2)-Po(2))/(R^2-1))^2 + ...
                    ((Pi(2)-R^2*Po(2))/(R^2-1)+sigmaa-sigmab./R)^2);
        si(i)    = max(siplus,siminus);

end
```

Plotting with constant slack-off/pick-up

```matlab
figure(3)
plot(Fso,soinitial,'bo',Fso,so,'ro',Fso,si,'yo','markersize',10)
hold on
xL = xlim;
line(xL, [grades(1) grades(1)],'color','black','linestyle','--');  %x-axis
line(xL, [grades(2) grades(2)],'color','black','linestyle','--');  %x-axis
line(xL, [grades(3) grades(3)],'color','black','linestyle','--');  %x-axis
line(xL, [grades(4) grades(4)],'color','black','linestyle','--');  %x-axis
line(xL, [grades(5) grades(5)],'color','black','linestyle','--');  %x-axis
%yL = [0 120000];
yL = ylim;
line([0 0], yL,'color','black');  %y-axis
hold on
grid minor
xlabel('\fontsize{16}Initial Slack-Off and Pick-Up Force [lb]')
ylabel('\fontsize{16}Triaxial Stress [psi]')
title('\fontsize{16}Permanent Corkscrewing')
legend('\fontsize{16}Sigmao Initial','\fontsize{16}Sigmao',...
    '\fontsize{16}Sigmai','location','southeast')
```

Plotting with variating slack-off/pick-up

```
% figure(3)
% plot(Fso(1:50),soinitial(1:50),'b',Fso,so,'r',Fso,si,'y','markersize',10)
% hold on
% xL = xlim;
% % line(xL, [grades(1) grades(1)],'color','black','linestyle','--');  %x-axis
% % line(xL, [grades(2) grades(2)],'color','black','linestyle','--');  %x-axis
% % line(xL, [grades(3) grades(3)],'color','black','linestyle','--');  %x-axis
% % line(xL, [grades(4) grades(4)],'color','black','linestyle','--');  %x-axis
% % line(xL, [grades(5) grades(5)],'color','black','linestyle','--');  %x-axis
% %yL = [0 120000];
% yL = ylim;
% line([0 0], yL,'color','black');  %y-axis
% hold on
% grid minor
% xlabel('\fontsize{16}Initial Slack-Off and Pick-Up Force [lb]')
% ylabel('\fontsize{16}Triaxial Stress [psi]')
% title('\fontsize{16}Permanent Corkscrewing')
% legend('\fontsize{16}Sigmao Initial','\fontsize{16}Sigmao',...
% '\fontsize{16}Sigmai','location','southeast')
```

Plotting axial loads and neutral stability point with critical buckling

```
figure(4)
plot([Fas(1) Fap(1)],[0 TVD]/12,'k', ...
     [Ffs(1) Ffp(1)],[0 TVD]/12,'r', ...
     [Fas(2) Fap(2)],[0 TVD]/12,'k--', ...
     [Ffs(2) Ffp(2)],[0 TVD]/12,'r--', ...
     0, TVD/12+n(2),'ro', ...
     -[Fcsinv Fcsinv],[0 450*39.37]/12,'g', ...
```

```
        -[Fchelv Fchelv],[0 450*39.37]/12,'b', ...
        -Fcrsindev,TVDbuild*39.37/12,'g', ...
        -Fcrheldev,TVDbuild*39.37/12,'b', ...
        [-Fcrsinhor -Fcrsinhor],[650 669.62]*39.37/12,'g', ...
        [-Fcrhelhor -Fcrhelhor],[650 669.62]*39.37/12,'b')
ylim([0 TVD/12]);
yL = [0 TVD/12];
xL = xlim;
line([0 0], yL,'color','black');
line(xL,[0 0],'color','black');
line(xL,[TVD/12 TVD/12],'color','black');
legend('\fontsize{12}Fa Initial Conditions', ...
    '\fontsize{12}Feff Initial Conditions', ...
    '\fontsize{12}Fa Load Case', ...
    '\fontsize{12}Feff Load Case', ...
    '\fontsize{12}NSP', ...
    '\fontsize{12}Sinusoidal buckling', ...
    '\fontsize{12}Helical buckling', ...
    'location','northwest')
set(gca,'YDir','reverse')
grid minor
ylabel('\fontsize{16}Depth [ft]')
yyaxis right
ylim([0 670])
line(xL,[450 450],'color','black','linestyle',':');
line(xL,[650 650],'color','black','linestyle',':');
set(gca,'YDir','reverse')
xlabel('\fontsize{16}Force [lb]')
ylabel('\fontsize{16}Depth [m]')
title('\fontsize{16}True vs. Effective Axial Force')
```


Including locally imposed bending loads on axial loads

```matlab
TVDvector = linspace(0,TVD/12,1000);
Favector  = linspace(Fas(2),Fap(2),1000);
Feffvector = linspace(Ffs(2),Ffp(2),1000);
% Define compression as positive
Favector  = -Favector;
Feffvector = -Feffvector;
Fbendvector = zeros(1,length(Favector));

for i = 1:length(Feffvector)
    if TVDvector(i) < 450*39.37/12
        if Feffvector(i) < Fcsinv
            % No  buckling
            Fbendvector(i) = Favector(i);
        elseif Feffvector(i) < Fchelv
            % Sinusoidal buckling
            if Favector(i) < 0
                % Tubing is in tension
                Fbendvector(i) = Favector(i) ...
                - 0.3151*OD*rc/I*Feffvector(i).^(0.08)*(Feffvector(i)-Fcsinv).^(0.92);

            else
                % Tubing is in compression
                Fbendvector(i) = Favector(i) ...
                + 0.3151*OD*rc/I*Feffvector(i).^(0.08)*(Feffvector(i)-Fcsinv).^(0.92);
            end
        else
            % Helical buckling
            if Favector(i) < 0
                % Tubing is in tension
                Fbendvector(i) = Favector(i) - OD*rc/(4*I).*Feffvector(i);
            else
                % Tubing is in compression
                Fbendvector(i) = Favector(i) + OD*rc/(4*I).*Feffvector(i);
            end
        end
    else
        Fbendvector(i) = Favector(i);
    end
end


% Define compression as negative:
Fbendvector = -Fbendvector;
```

Plotting bending stress

```matlab
figure(5)
plot([Fas(2) Fap(2)],[0 TVD]/12,'k--', ...
    [Ffs(2) Ffp(2)],[0 TVD]/12,'r--', ...
    Fbendvector,TVDvector,'k-.',...
    0, TVD/12+n(2),'ro', ...
    -[Fcsinv Fcsinv],[0 450*39.37]/12,'g', ...
    -[Fchelv Fchelv],[0 450*39.37]/12,'b', ...
    -Fcrsindev,TVDbuild*39.37/12,'g', ...
    -Fcrheldev,TVDbuild*39.37/12,'b', ...
    [-Fcrsinhor -Fcrsinhor],[650 669.62]*39.37/12,'g', ...
    [-Fcrhelhor -Fcrhelhor],[650 669.62]*39.37/12,'b')
ylim([0 TVD/12]);
yL = [0 TVD/12];
```

```matlab
xL = xlim;
line([0 0], yL,'color','black');
line(xL,[0 0],'color','black');
line(xL,[TVD/12 TVD/12],'color','black');
legend('\fontsize{16}Fa Load Case', ...
    '\fontsize{16}Feff Load Case', ...
    '\fontsize{16}Fa with Bending', ...
    'location','northwest') %, ...
%     '\fontsize{12}Fa Load Case', ...
%     '\fontsize{12}Feff Load Case', ...
%     '\fontsize{12}NSP', ...
%     '\fontsize{12}Sinusoidal buckling', ...
%     '\fontsize{12}Helical buckling', ...
%     'location','northwest')
set(gca,'YDir','reverse')
grid minor
ylabel('\fontsize{16}Depth [ft]')
yyaxis right
ylim([0 670])
line(xL,[450 450],'color','black','linestyle',':');
line(xL,[650 650],'color','black','linestyle',':');
set(gca,'YDir','reverse')
xlabel('\fontsize{16}Force [lb]')
ylabel('\fontsize{16}Depth [m]')
title('\fontsize{16}True vs. Effective Axial Force')

toc
```

```
Elapsed time is 6.661067 seconds.
```

Contents

```
clc
clear all
```

INPUTS

```
tic
% Tubing Inputs
OD        = 3.5;                    %in     outer diameter
weight    = 9.2;                    %lb/ft  dry weight
ID        = 2.992;                  %in     inner diameter
grades    = 10^3.*[40 55 75 80 105]; %psi    yield strength
E         = 30*10^6;                %psi    Young's modulus
poisson   = 0.3;                    %       Poisson's ratio
Ct        = 6.9*10^(-6);            %/F     coeff. of thermal expansion
% Total vertical depth
TVDsw     = 400;                    %m      sea water depth
TVDsw     = TVDsw*39.37;            %in     converting from m to in
TVD       = 269.62;                 %m      vertical well depth
TVD       = TVD*39.37;              %in     converting from m to in
% Total length of well
Lp        = 2523.1-TVDsw;           %m      value from Compass minus
                                    %       sea water depth
Lp        = Lp*39.37;               %in     converting from m to in
% Tubing calculations
Ao        = pi/4*OD.^2;             %in2    outer area
Ai        = pi/4*ID.^2;             %in2    inner area
As        = Ao-Ai;                  %in2    cross-sectional area
Ap        = Ai;                     %in2    packer bore area PBR
R         = OD./ID;                 %ratio  OD/ID-ratio
ws        = weight./12;             %lb/in  dry weight of tubing
I         = (pi/64)*(OD.^4-ID.^4);  %in4    moment of inertia
% Casing Inputs
```

```
csgID    = 5.921;                    %in    inner diameter
rc       = (csgID-OD)/2;             %in    radial clearance

% Fluid Properties
rhosw    = 1/231*8.68;               %psi/in sea water density
rhog     = 1/231*1;                  %psi/in gas density
rhoo     = 1/231*7.68;               %psi/in oil density
% Pressures
Pr       = 1015.3;                   %psi    70 bar reservoir pressure
Pg       = rhog*TVD;                 %psi    gas-filled well
SIWHP    = Pr - Pg;                  %psi    shut-in wellhead pressure
WDP      = SIWHP + 508;              %psi    35 bar safety margin
Ppacker  = 4278.6;                   %psi    295 bar set packer pressure
Psw      = rhosw*TVDsw;              %psi    sea water pressure
```

Length changes and packer forces

```
% Load case: Set packer
rhot     = [rhosw rhosw];            %psi/in initial-final
rhoa     = [rhosw rhosw];            %psi/in initial-final
pi       = [Psw Ppacker-rhot(2)*TVD]; %psi   surface initial-final
po       = [Psw Psw];                %psi    surface initial-final
dT       = 0;                        %C      avg. change in temperature
dT       = dT*1.8;                   %F

% %Load case: Start bullheading (gas filled well)
% rhot     = [rhosw rhog];            %psi/in initial-final
% rhoa     = [rhosw rhosw];           %psi/in initial-final
% pi       = [Psw WDP];               %psi    surface initial-final
% po       = [Psw Psw];               %psi    surface initial-final
% dT       = 3;                       %C      avg. change in temperature
% dT       = dT*1.8;                  %F
%
% % Load case: Start bullheading (oil filled well)
% rhot     = [rhosw rhoo];            %psi/in initial-final
% rhoa     = [rhosw rhosw];           %psi/in initial-final
% pi       = [Psw WDP];               %psi    surface initial-final
% po       = [Psw Psw];               %psi    surface initial-final
% dT       = 3;                       %C      avg. change in temperature
% dT       = dT*1.8;                  %F
%
% % Load case: Shut-in
% rhot     = [rhosw rhog];            %psi/in tubing initial-final
% rhoa     = [rhosw rhosw];           %psi/in annulus initial-final
% pi       = [Psw SIWHP];             %psi    surface initial-final
% po       = [Psw Psw];               %psi    surface initial-final
% dT       = -4;                      %C      avg. change in temperature
% dT       = dT*1.8;                  %F

% Density calculations
drhot    = rhot(2)-rhot(1);          %psi/in change in density
drhoa    = rhoa(2)-rhoa(1);          %psi/in change in density
wi       = rhot.*Ai;                 %lb/in  tubing initial-final
wo       = rhoa.*Ao;                 %lb/in  annulus initial-final
w        = ws + wi - wo;             %lb/in  total initial-final

% Pressure calculations
Pi       = pi+rhot*TVD;              %psi    packer initial-final
Po       = po+rhoa*TVD;              %psi    packer initial-final
```

```
dp        = [pi(2)-pi(1) po(2)-po(1)];  %psi    change in surface pressure
dP        = [Pi(2)-Pi(1) Po(2)-Po(1)];  %psi    change in packer pressure

% Calculate Forces as if the tubing is free to move
Fa        = (Ap-Ao)*Po-(Ap-Ai)*Pi;      %lb      true axial force
Ff        = Ap*(Po-Pi);                  %lb      effective axial force

% Calculate length change associated with Ff
dLf       = Lp/(E*As).*Ff(2)-rc^2/(8*E*I*w(2)).*Ff(2).^2; %in

disp(['The length change related to this force is ', num2str(dLf), ' in'])
```

```
The length change related to this force is 153.4786 in
```

Critical buckling limits

Critical buckling for vertical well

```
Fcr       = (E*I.*(w(2)).^2).^(1/3); %lb
% Sinusoidal buckling is defined by Lubinski et. al (1950)
Fcsinv    = 1.94*Fcr; %lb
% Helical buckling is defined by Wu et. al (1995)
Fchelv    = 5.55*Fcr; %lb
% Critical buckling for deviated section (Paslay Dawson)
incl      = linspace(0,85*3.1416/180,100); % build from 0 to 85 degrees
TVDbuild  = linspace(50,250,100);          % vertical depth of build section
% Sinusoidal buckling is defined by Dawson and Paslay (1984)
Fcrsindev = sqrt((4*E*I.*w(2)*sin(incl))./rc);
% Helical buckling is defined by Mitchell et. al (1999)
Fcrheldev = 1.4*Fcrsindev;
% Critical buckling for horizontal section
Fcrsinhor = sqrt((4*E*I.*w(2)*sin(3.1416/2))./rc);
Fcrhelhor = 1.4*Fcrsinhor;
```

Length Changes: Packers Permitting Free Motion

All length changes are in inches

```
% The first length change is deformation due to the true axial force acting
% on the bottom of the tubing. Hooke's law is used:
dL1       = Lp/(E*As)*((Ap-Ao)*dP(2)-(Ap-Ai)*dP(1));
% The second length change occurs due to helical buckling. If the change in
% outer pressure is higher than the change in inner pressure, there will be
% no helical buckling (Lubinski et. al (1962)), hence:
if dP(2)>dP(1)
    % No helical buckling
    dL2   = 0;
else
    % Helical buckling. Calculate length change with a non-linear equation.
     dL2  = -rc^2*Ap^2*(dP(2)-dP(1)).^2/(8*E*I*w(2));
    % Sinusoidal buckling length change by Mitchell:
    % Ff(2) = -Ff(2); % Change signs for Mitchells equation
    % dL2   = -(rc)^2/(4*E*I*w(2))*(Ff(2)-Fcr(2))*(0.3771*Ff(2)-0.3668*Fcr(2));
    % Ff(2) = -Ff(2); % Change back for the remaining model
end
% Calculate radial pressure due to ballooning and fluid flow
```

```
%delta     = 0; % Pressure drop per unit length
%dL3       = -(poisson/E)*((drhot-R^2*drhoa-(1+2*poisson)/(2*poisson)*delta)*Lp^2/(R^2-1))...
%           -(2*poisson/E)*((dp(1)-R^2*dp(2))*Lp/(R^2-1));

% Ballooning equation from Jonathan Bellarby "Well Completion Design"
avgdpi     = (dp(1)+dP(1))/2;    %psi, average pressure change
avgdpo     = (dp(2)+dP(2))/2;    %psi, average pressure change
dL3        = -(2*poisson/E)*(avgdpi*Ai-avgdpo*Ao)*(1/(Ao-Ai))*Lp;

% The fourth length change occurs due to temperature change, also known as
% thermal expansion or thermal contraction.
dL4        = Lp*Ct*dT;

% Total length change is then:
dL         = dL1+dL2+dL3+dL4;

disp(['If the tubing is free to move, the total length change is ', ...
    num2str(dL),' in'])


% Neutral stability point if the tubing is free to move
nfree      = (Ff./w)/12;         %ft
disp(['If the tubing is free to move, the neutral stability point is ', ...
    num2str(nfree(2)),' ft from the bottom'])
```

```
  If the tubing is free to move, the total length change is 91.5191 in
  If the tubing is free to move, the neutral stability point is -2878.1739 ft from the bottom
```

Length Changes: Packers Permitting Limited Motion

Define slack-off force

```
Fso        = 0; %lb

% Variation of initial slack-off/pick-up
% Fso      = linspace(-10000,10000,100); %lb

%Length change due to slack-off or pick-up
dL5        = - ((Lp/(E*As).*Fso-rc^2/(8*E*I*w(1)).*Fso.^2));

% Including stick-up length, the total length change is:
dL         = dL+dL5;

disp(['If the packer permits limited motion, the total length change is ',...
    num2str(dL), ' in'])
```

```
  If the packer permits limited motion, the total length change is 91.5191 in
```

Length Changes: Packers Permitting No Motion

The packer will oppose to the desired length change "Lp".

```
dLp        = dLf-dL;
```

```matlab
% Plotting F vs. dL'
% Define F as a vector
F        = linspace(-40000,40000,10000);
% Make sure dL' is the same size vector as F
dLfnutt = zeros(1,length(F));

% Make a loop to calculate dL' for every F.
for i = 1:length(F)
    if F(i) < 0 && F(i) > -Lp*w(2)
        % Compression
        dLfnutt(i) = Lp/(E*As).*F(i)-rc^2/(8*E*I*w(2)).*F(i).^2;
    elseif F(i)<-Lp*w(2)
        % Equation (26) in "Helical buckling of tubing sealed in packers"
        % by Lubinski et. al (1962)
        dLfnutt(i) = Lp/(E*As).*F(i)-rc^2/(8*E*I*w(2)).*F(i).^2*(-Lp*w(2)/F(i)*(2+Lp*w(2)/F
(i)));
    else
        % Tension
        dLfnutt(i) = Lp/(E*As).*F(i);
    end
end


Ffstar = zeros(1,length(Fso));
Fp    = zeros(1,length(Fso));
Fastar = zeros(1,length(Fso));

for i = 1:length(dLp)
    if dLp(i) < 0
        % Compression
        % 'coeff' is the coefficients in the non-linear equation
          coeff = [-rc^2/(8*E*I*w(2)) Lp/(E*As) -dLp(i)];
        % 'roots' calculates the F corresponding to dLp
          Ffstarroots = roots(coeff)';
        % 'Ffstar' is the effective axial force when the tubing is fixed
          Ffstar(i) = Ffstarroots(2);
        % 'Fp' is the packer force
          Fp(i) = Ffstar(i) - Ff(2);
        % 'Fastar' is the true axial force when the tubing is fixed
          Fastar(i) = Fp(i)+Fa(2);
          if Fp(i) > 0
            disp(['The tubing is shortening, and the packer' ...
              ' force is a tension: ',num2str(Fp(i)),'lb']);
          else
            disp(['The tubing is lengthening, and the packer' ...
              ' force is a compression: ',num2str(Fp(i)),'lb']);
          end
    else
        % Tension
        % 'coeff' is the coefficients in the linear eq: Hooke's law
          coeff = [0 Lp/(E*As) -dLp(i)];
        % 'roots' calculates the F corresponding to dLp
          Ffstarroots = roots(coeff);
        % 'Ffstar' is the effective axial force when the tubing is fixed
          Ffstar(i) = Ffstarroots;
        % 'Fp' is the packer force
          Fp(i) = Ffstar(i) - Ff(2);
        % 'Fastar' is the true axial force when the tubing is fixed
          Fastar(i) = Fp(i)+Fa(2);
          if Fp(i) > 0
```

```
            disp(['The tubing is shortening, and the packer' ...
                ' force is a tension: ',num2str(Fp(i)),'lb']);
        else
            disp(['The tubing is lengthening, and the packer' ...
                ' force is a compression: ',num2str(Fp(i)),'lb']);
        end
    end
end
disp(['The fictitious force is ', ...
    num2str(Ffstar),' lb'])
```
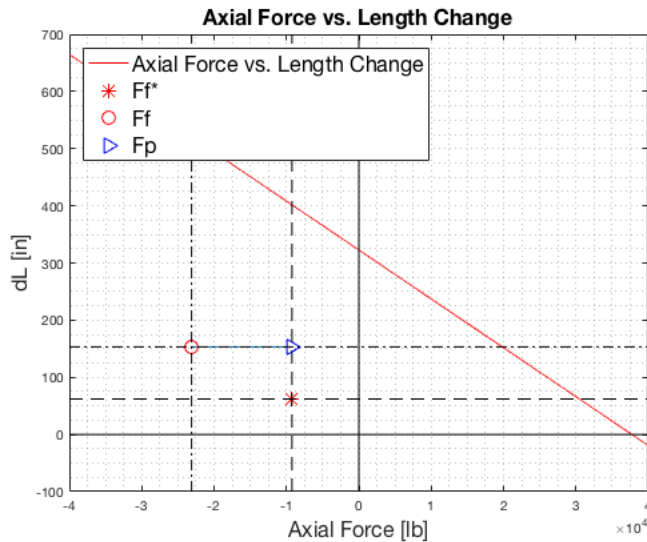
```
The tubing is shortening, and the packer force is a tension: 13870.5965lb
The fictitious force is -9247.0644 lb
```

Plotting with constant slack-off/pick-up

```
figure(1)
plot(F,dLfnutt,'r',Ffstar,dLp,'r*',Ff(2),dLf,'ro',Ffstar,dLf,'b>',...
    'markersize',10)
hold on
xL = xlim;
yL = ylim;
line([Ff(2) Ffstar],[dLf dLf],'linestyle','-')
line([0 0], yL,'color','black');   %y-axis
line(xL, [0 0],'color','black');   %x-axis
hold on
line([Ff(2) Ff(2)],yL,'color','black','linestyle','-.')
line(xL, [dLf dLf],'color','black','linestyle','-.')
hold on
line([Ffstar Ffstar],yL,'color','black','linestyle','--')
line(xL, [dLp dLp],'color','black','linestyle','--')
grid minor
xlabel('\fontsize{16}Axial Force [lb]')
ylabel('\fontsize{16}dL [in]')
title('\fontsize{16}Axial Force vs. Length Change')
legend('\fontsize{16}Axial Force vs. Length Change' ...
, '\fontsize{16}Ff*','\fontsize{16}Ff','\fontsize{16}Fp', ...
    'location','northwest')
```

Plotting with variating slack-off/pick-up

figure(1) plot(F,dLfnutt,'r',Ffstar,dLp,'r*',Ff(2),dLf,'ro','markersize',10) hold on xL = xlim; yL = ylim; grid minor

line([0 0], yL,'color','black'); %y-axis line(xL, [0 0],'color','black'); %x-axis hold on line([Ff(2) Ff(2)],yL,'color','black','linestyle','-.') line(xL, [dLf dLf],'color','black','linestyle','-.') hold on grid minor xlabel('\fontsize{16}Axial Force [lb]') ylabel('\fontsize{16}dL [in]') title('\fontsize{16}Axial Force vs. Length Change') legend('\fontsize{16}Axial Force vs. Length Change' ... , '\fontsize{16}Ff*','\fontsize{16}Ff', ... 'location','northwest')

Neutral Stability Point

```
% Neutral Point when the tubing is fixed
n        = ([0 Ffstar]/w(2))/12;              %ft

% True vs. Effective Axial Load
% Capital P is the pressure at packer level, and lowercase p is the
% pressure at surface. Note how the pressures are used in each equation.

% Initial Conditions

% Surface (z=0)
% True Axial Load
Fas(1) = TVD*ws  + Po(1)*(Ap-Ao) - Pi(1)*(Ap-Ai);
% Effective Axial Load
Ffs(1) = Fas(1) - pi(1)*Ai + po(1)*Ao;

% Packer (z=zshoe)
% True Axial Load
Fap(1) = Po(1)*(Ap-Ao) - Pi(1)*(Ap-Ai);
% Effective Axial Load
% Assumes that the pressure is bled of after setting the packer, hence Fp=0
Ffp(1) = Fap(1) - Pi(1)*Ai + Po(1)*Ao;
```

```
% After Load Case

% Surface (z=0)
% The packer force will adjuct the true axial load, and this effect will
% also be included when calculating the effective axial load. Lubinski used
% a star "*" to describe these loads when the tubing is anchored.
% True Axial Load
Fas(2) = TVD*ws  + Po(2)*(Ap-Ao) - Pi(2)*(Ap-Ai) + Fp;
% Effective Axial Load
Ffs(2) = Fas(2) - pi(2)*Ai + po(2)*Ao;
% Packer (z=zshoe)
% True Axial Load
Fap(2) = Po(2)*(Ap-Ao) - Pi(2)*(Ap-Ai) + Fp;
% Effective Axial Load
Ffp(2) = Fap(2) - Pi(2)*Ai + Po(2)*Ao;
```
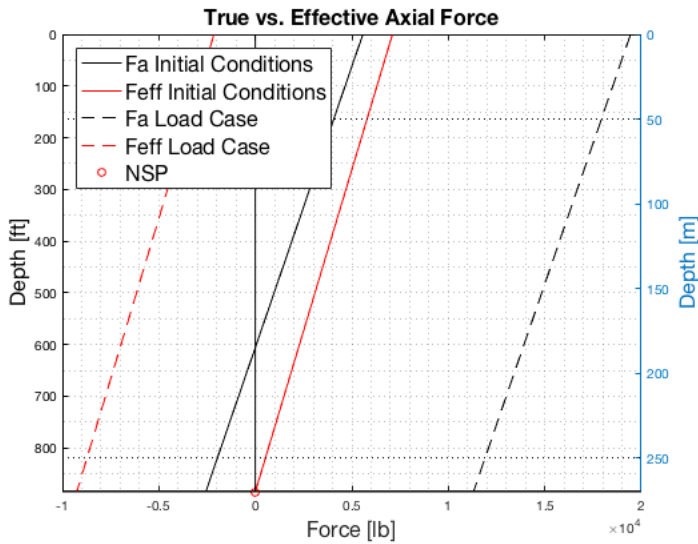
Plotting axial loads and neutral stability point

```
figure(2)
plot([Fas(1) Fap(1)],[0 TVD]/12,'k', ...
     [Ffs(1) Ffp(1)],[0 TVD]/12,'r', ...
     [Fas(2) Fap(2)],[0 TVD]/12,'k--', ...
     [Ffs(2) Ffp(2)],[0 TVD]/12,'r--', ...
     0, TVD/12+n,'ro')
ylim([0 TVD/12]);
yL = [0 TVD/12];
xL = xlim;
line([0 0], yL,'color','black');
line(xL,[0 0],'color','black');
line(xL,[TVD/12 TVD/12],'color','black');
legend('\fontsize{16}Fa Initial Conditions', ...
    '\fontsize{16}Feff Initial Conditions', ...
    '\fontsize{16}Fa Load Case', ...
    '\fontsize{16}Feff Load Case', ...
    '\fontsize{16}NSP','location','northwest')
set(gca,'YDir','reverse')
grid minor
ylabel('\fontsize{16}Depth [ft]')
yyaxis right
ylim([0 270])
line(xL,[50 50],'color','black','linestyle',':');
line(xL,[250 250],'color','black','linestyle',':');
set(gca,'YDir','reverse')
xlabel('\fontsize{16}Force [lb]')
ylabel('\fontsize{16}Depth [m]')
title('\fontsize{16}True vs. Effective Axial Force')
```

Permanent Corkscrewing

```matlab
% Initial Conditions after SO but before changing P and T

soinitial = zeros(1,length(Fso));

for i = 1:length(Fso)
    if Fso(i) < 0
        soinitial(i) = abs(Fso(i)/As + OD*rc*Fso(i)./(4*I));
    end
end

% Permanent Corkscrewing after changing P and T

so = zeros(1,length(Ffstar));
si = so;

Ffstar = -Ffstar;
Fastar = -Fastar;

for i = 1:length(Ffstar)

    if Ffstar(i) < 0
        % No buckling
        sigmab = 0;
        % elseif Ffstar(i) < 5.55*Fcr && Ffstar(i) > 1.94*Fcr
        % Sinusoidal Buckling
        % sigmab = 0.3151*OD*rc/I*Ffstar(i).^(0.08)*(Ffstar(i)-Fcr).^(0.92);
        % elseif Ffstar(i) > 5.55*Fcr
    else
        % Helical Buckling
        sigmab = OD*rc/(4*I).*Ffstar(i);
    end
```

```matlab
    sigmaa = Fastar(i)/As;

        soplus   = sqrt(3*((Pi(2)-Po(2))/(R^2-1))^2 + ...
                     ((Pi(2)-R^2*Po(2))/(R^2-1)+sigmaa+sigmab)^2);
        sominus  = sqrt(3*((Pi(2)-Po(2))/(R^2-1))^2 + ...
                     ((Pi(2)-R^2*Po(2))/(R^2-1)+sigmaa-sigmab)^2);
        so(i)    = max(soplus,sominus);

        siplus   = sqrt(3*(R^2*(Pi(2)-Po(2))/(R^2-1))^2 + ...
                     ((Pi(2)-R^2*Po(2))/(R^2-1)+sigmaa+sigmab./R)^2);
        siminus  = sqrt(3*(R^2*(Pi(2)-Po(2))/(R^2-1))^2 + ...
                     ((Pi(2)-R^2*Po(2))/(R^2-1)+sigmaa-sigmab./R)^2);
        si(i)    = max(siplus,siminus);

end
```
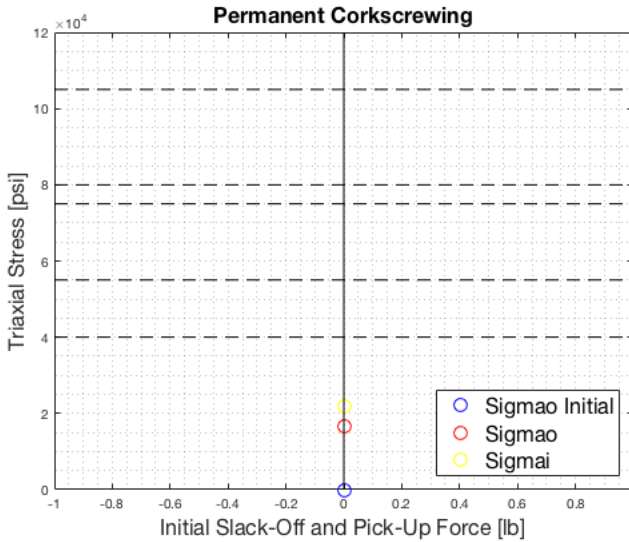
Plotting with constant slack-off/pick-up

```matlab
figure(3)
plot(Fso,soinitial,'bo',Fso,so,'ro',Fso,si,'yo','markersize',10)
hold on
xL = xlim;
line(xL, [grades(1) grades(1)],'color','black','linestyle','--');  %x-axis
line(xL, [grades(2) grades(2)],'color','black','linestyle','--');  %x-axis
line(xL, [grades(3) grades(3)],'color','black','linestyle','--');  %x-axis
line(xL, [grades(4) grades(4)],'color','black','linestyle','--');  %x-axis
line(xL, [grades(5) grades(5)],'color','black','linestyle','--');  %x-axis
%yL = [0 120000];
yL = ylim;
line([0 0], yL,'color','black');  %y-axis
hold on
grid minor
xlabel('\fontsize{16}Initial Slack-Off and Pick-Up Force [lb]')
ylabel('\fontsize{16}Triaxial Stress [psi]')
title('\fontsize{16}Permanent Corkscrewing')
legend('\fontsize{16}Sigmao Initial','\fontsize{16}Sigmao',...
    '\fontsize{16}Sigmai','location','southeast')
```

Plotting with variating slack-off/pick-up

```
% figure(3)
% plot(Fso(1:50),soinitial(1:50),'b',Fso,so,'r',Fso,si,'y','markersize',10)
% hold on
% xL = xlim;
% % line(xL, [grades(1) grades(1)],'color','black','linestyle','--');  %x-axis
% % line(xL, [grades(2) grades(2)],'color','black','linestyle','--');  %x-axis
% % line(xL, [grades(3) grades(3)],'color','black','linestyle','--');  %x-axis
% % line(xL, [grades(4) grades(4)],'color','black','linestyle','--');  %x-axis
% % line(xL, [grades(5) grades(5)],'color','black','linestyle','--');  %x-axis
% %yL = [0 120000];
% yL = ylim;
% line([0 0], yL,'color','black');  %y-axis
% hold on
% grid minor
% xlabel('\fontsize{16}Initial Slack-Off and Pick-Up Force [lb]')
% ylabel('\fontsize{16}Triaxial Stress [psi]')
% title('\fontsize{16}Permanent Corkscrewing')
% legend('\fontsize{16}Sigmao Initial','\fontsize{16}Sigmao',...
% '\fontsize{16}Sigmai','location','southeast')
```

Plotting axial loads and neutral stability point with critical buckling
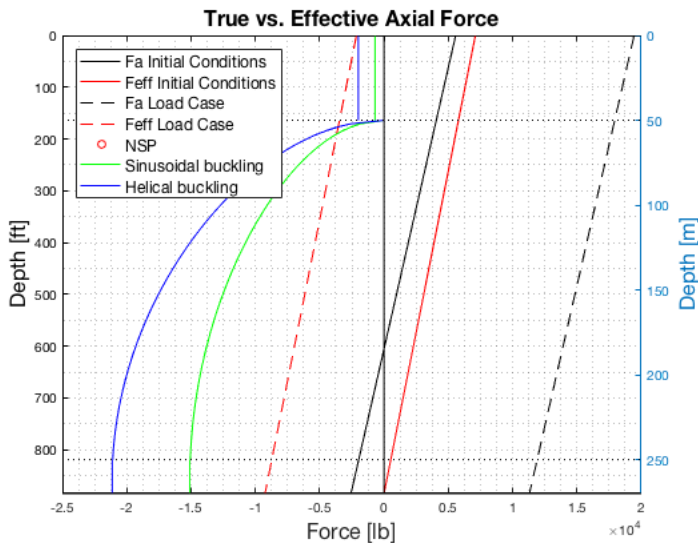
```
figure(4)
plot([Fas(1) Fap(1)],[0 TVD]/12,'k', ...
     [Ffs(1) Ffp(1)],[0 TVD]/12,'r', ...
     [Fas(2) Fap(2)],[0 TVD]/12,'k--', ...
     [Ffs(2) Ffp(2)],[0 TVD]/12,'r--', ...
     0, TVD/12+n(2),'ro', ...
     -[Fcsinv Fcsinv],[0 50*39.37]/12,'g', ...
```

```
    -[Fchelv Fchelv],[0 50*39.37]/12,'b', ...
    -Fcrsindev,TVDbuild*39.37/12,'g', ...
    -Fcrheldev,TVDbuild*39.37/12,'b', ...
    [-Fcrsinhor -Fcrsinhor],[250 269.62]*39.37/12,'g', ...
    [-Fcrhelhor -Fcrhelhor],[250 269.62]*39.37/12,'b')
ylim([0 TVD/12]);
yL = [0 TVD/12];
xL = xlim;
line([0 0], yL,'color','black');
line(xL,[0 0],'color','black');
line(xL,[TVD/12 TVD/12],'color','black');
legend('\fontsize{12}Fa Initial Conditions', ...
    '\fontsize{12}Feff Initial Conditions', ...
    '\fontsize{12}Fa Load Case', ...
    '\fontsize{12}Feff Load Case', ...
    '\fontsize{12}NSP', ...
    '\fontsize{12}Sinusoidal buckling', ...
    '\fontsize{12}Helical buckling', ...
    'location','northwest')
set(gca,'YDir','reverse')
grid minor
ylabel('\fontsize{16}Depth [ft]')
yyaxis right
ylim([0 270])
line(xL,[50 50],'color','black','linestyle',':');
line(xL,[250 250],'color','black','linestyle',':');
set(gca,'YDir','reverse')
xlabel('\fontsize{16}Force [lb]')
ylabel('\fontsize{16}Depth [m]')
title('\fontsize{16}True vs. Effective Axial Force')
```


Including locally imposed bending loads on axial loads

```matlab
TVDvector = linspace(0,TVD/12,1000);
Favector  = linspace(Fas(2),Fap(2),1000);
Feffvector = linspace(Ffs(2),Ffp(2),1000);
% Define compression as positive
Favector  = -Favector;
Feffvector = -Feffvector;
Fbendvector = zeros(1,length(Favector));

for i = 1:length(Feffvector)
    if TVDvector(i) < 50*39.37/12
        if Feffvector(i) < Fcsinv
            % No  buckling
            Fbendvector(i) = Favector(i);
        elseif Feffvector(i) < Fchelv
            % Sinusoidal buckling
            if Favector(i) < 0
                % Tubing is in tension
                Fbendvector(i) = Favector(i) ...
                - 0.3151*OD*rc/I*Feffvector(i).^(0.08)*(Feffvector(i)-Fcsinv).^(0.92);

            else
                % Tubing is in compression
                Fbendvector(i) = Favector(i) ...
                + 0.3151*OD*rc/I*Feffvector(i).^(0.08)*(Feffvector(i)-Fcsinv).^(0.92);
            end
        else
            % Helical buckling
            if Favector(i) < 0
                % Tubing is in tension
                Fbendvector(i) = Favector(i) - OD*rc/(4*I).*Feffvector(i);
            else
                % Tubing is in compression
                Fbendvector(i) = Favector(i) + OD*rc/(4*I).*Feffvector(i);
            end
        end
    else
        Fbendvector(i) = Favector(i);
    end
end


% Define compression as negative:
Fbendvector = -Fbendvector;
```

Plotting bending stress

```matlab
figure(5)
plot([Fas(2) Fap(2)],[0 TVD]/12,'k--', ...
    [Ffs(2) Ffp(2)],[0 TVD]/12,'r--', ...
    Fbendvector,TVDvector,'k-.',...
    0, TVD/12+n(2),'ro', ...
    -[Fcsinv Fcsinv],[0 50*39.37]/12,'g', ...
    -[Fchelv Fchelv],[0 50*39.37]/12,'b', ...
    -Fcrsindev,TVDbuild*39.37/12,'g', ...
    -Fcrheldev,TVDbuild*39.37/12,'b', ...
    [-Fcrsinhor -Fcrsinhor],[250 269.62]*39.37/12,'g', ...
    [-Fcrhelhor -Fcrhelhor],[250 269.62]*39.37/12,'b')
ylim([0 TVD/12]);
yL = [0 TVD/12];
```
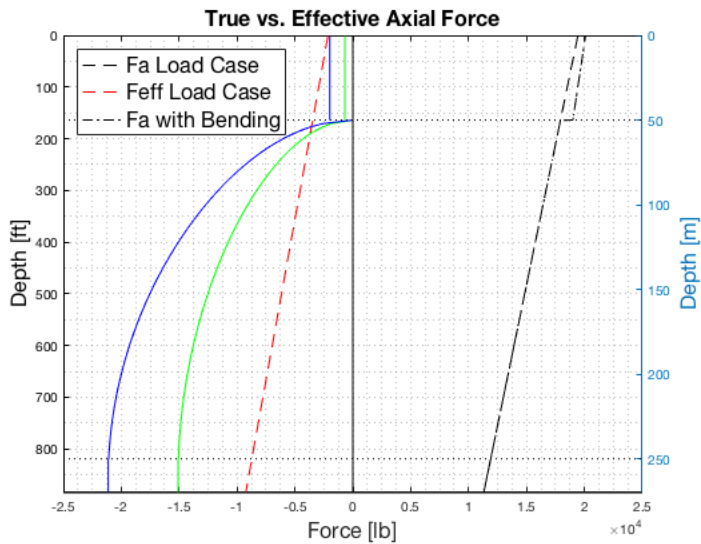
```matlab
xL = xlim;
line([0 0], yL,'color','black');
line(xL,[0 0],'color','black');
line(xL,[TVD/12 TVD/12],'color','black');
legend('\fontsize{16}Fa Load Case', ...
    '\fontsize{16}Feff Load Case', ...
    '\fontsize{16}Fa with Bending', ...
    'location','northwest') %, ...
%       '\fontsize{12}Fa Load Case', ...
%       '\fontsize{12}Feff Load Case', ...
%       '\fontsize{12}NSP', ...
%       '\fontsize{12}Sinusoidal buckling', ...
%       '\fontsize{12}Helical buckling', ...
%       'location','northwest')
set(gca,'YDir','reverse')
grid minor
ylabel('\fontsize{16}Depth [ft]')
yyaxis right
ylim([0 270])
line(xL,[50 50],'color','black','linestyle',':');
line(xL,[250 250],'color','black','linestyle',':');
set(gca,'YDir','reverse')
xlabel('\fontsize{16}Force [lb]')
ylabel('\fontsize{16}Depth [m]')
title('\fontsize{16}True vs. Effective Axial Force')
toc
```

Elapsed time is 7.038854 seconds.